École polytechnique de Louvain

Ecodesign of continuous glucose monitoring devices

Authors: **Chloé Renson, Lucie Van Roy**
Supervisor: **David Bol**
Readers: **Rémi Dekimpe, Jean-Pierre Raskin, Augustin Wattiez**
Academic year 2024-2025
Master [120] in Electrical Engineering

Abstract

Growing concerns about the healthcare footprint raise questions about the design of medical devices. This master's thesis focuses on a widely used and frequently replaced medical sensor for patients with diabetes, the CGM. As its user base grows, this device will generate increasing amounts of waste in the future.

Building on an existing LCA of CGM systems, particularly the Freestyle Libre 2, key environmental hotspots are identified: the single-use plastic applicator, ICs, and the battery, especially significant in MRD. These hotspots drive the implementation of ecodesign strategies, forming a roadmap. First, plastic usage is reduced and a reusable applicator is designed. Then, the focus shifts to the ICs and the battery with three parallel strategies: extending the lifetime, making the IC module reusable, and using a rechargeable battery. These implementations are supported through a battery power profiling, a reverse-engineered electrical schematic, and an analysis of an inductive charger. By normalising the environmental impact of each strategy against the reference LCA, the improvement in environmental burden is assessed.

One of the final possible designs in this roadmap shows the best results, with normalised values under 9% for all impact categories compared to the reference. This is the strategy that combines plastic reduction with a rechargeable NiMH battery. Despite this excellent result, it is not necessarily the best strategy across all considerations: the study is product-centered and does not account for manufacturer economic viability, patient willingness to pay or quality of life. Adopting a multilevel perspective could lead to a different conclusion regarding the relevance of the proposed strategies.

Acknowledgments

This thesis would not have been possible without the help, support, and kindness of many people, to whom we are very grateful.

First, we would like to thank our supervisor, David Bol, for giving us the opportunity to explore the fascinating topic of ecodesign in continuous glucose monitoring devices. Thank you for trusting us with this project, for sharing your knowledge and expertise, and for the regular monitoring of the progress of our work.

A special thanks to Augustin Wattiez for his time, patience and availability. Your advice, encouragement, and detailed feedback helped us see things more clearly and improve our work. We are also grateful for the time you spent proofreading several chapters of this manuscript. We would also like to thank Rémi Dekimpe for joining our meetings and offering his advice whenever we needed it. We also thank Jean-Pierre Raskin, along with our three other readers, for taking the time to read our thesis.

Then, we want to thank the WELCOME platform team, and especially Souley Djadjandi. Thank you for fixing what we broke, for teaching us how to solder (even though we ended up asking you to do it in the end), and for being a reassuring presence whenever we were lost in the lab. We are also grateful to Grégoire Le Brun and Ramy Moumneh for helping us with the PBS setup and for your advice on power profiling.

Finally, thank you to our friends, Julien and Camille from the Grojet, for the emotional support and the coffee breaks. Having you by our side during these years made everything more fun.

Chloé and Lucie

First and foremost, I would like to thank my parents, sisters, and boyfriend for their endless support, not only throughout this thesis but during the entire journey of the past five years. Thank you for your patience, encouragement, and constant belief in me. Your presence made all the difference.

I am also very grateful to my friends from both scouts and university. Thank you for the countless memories and shared laughter.

Finally, a very special thanks to Lucie for being an awesome thesis partner. Thank you for embarking on this ambitious project with me.

Chloé

I would also like to thank my family, my boyfriend, and my friends for their incredible support over the past five years and during this thesis. Your encouragement, kindness, and the fun moments we shared helped me make the most of these wonderful (though sometimes stressful) years.

Special thanks to my amazing thesis partner Chloé. You made this thesis a better journey, working with you turned it into a positive and memorable experience.

Lucie

Declaration of Generative AI and AI-assisted technologies in the writing process

During the preparation of this work, AI tools such as ChatGPT, Deepl and Grammarly were used only to improve readability and language in the text. All content generated with these tools was reviewed and edited as needed. We take full responsibility for the final content of this work.

Contents

Acronyms

AC acidification.

ADC analog to digital converter.

AFE analog front-end.

AID automated insulin delivery.

BLE Bluetooth Low Energy.

CC climate change.

CE Conformité Européenne.

CEl counter electrode.

CF characterisation factors.

CGM continuous glucose monitoring.

CTUe comparative toxic unit for ecosystems.

CTUh comparative toxic unit for human.

EC European Commission.

ECOTOX ecotoxicity, freshwater.

EF Environmental Footprint.

EF 3.1 Environmental Footprint 3.1.

EI Ecoinvent.

EoL end-of-life.

FDA Food and Drug Administration.

FEU freshwater eutrophication.

FL2 Freestyle Libre 2.

FL3 Freestyle Libre 3.

FU functional unit.

IC integrated circuit.

IDF International Diabetes Federation.

ISF interstitial fluid.

LCA life cycle assessment.

LCI life cycle inventory.

LCIA life cycle impact assessment.

LPM Low Power Mode.

LU land use.

MARD mean absolute relative difference.

MCU microcontroller.

MEU marine eutrophication.

MRD resource use (minerals and metals).

NFC near field communication.

NiMH nickel-metal hydride.

ODP ozone depletion potential.

OTC over-the-counter.

PA power amplifier.

PB planetary boundaries.

PBS phosphate buffered saline.

PCB printed circuit board.

PEF Product Environmental Footprint.

PGA programmable-gain amplifier.

PWB printed wiring board.

RE reference electrode.

RF radio frequency.

RFID radio frequency identification.

SMBG self-monitoring of blood glucose.

SoC System-on-Chip.

UN United Nations.

WE working electrode.

WPT wireless power transfer.

WSN wireless sensor node.

WU water use.

Introduction

Context

The International Diabetes Federation (IDF) estimates that approximately 589 million adults aged 20-79 worldwide are living with diabetes. This number is projected to increase by 46% by 2050, meaning 1 in 8 adults could be diabetic [1]. This rise is happening much faster than the 25% expected growth of the global population over the next 25 years. The principal factors contributing to this trend are the ageing of the population and the increased urbanisation across the globe [2]. If not managed correctly and in an advanced stage of the disease, diabetes encourages the appearance of heart or kidney disease, stroke, amputations, sometimes leading to premature death of the patient [3]. To prevent these conditions from occurring, diabetic patients are encouraged to frequently monitor their blood sugar concentration because an accurate measurement is required to receive the appropriate dose of insulin. They can then adjust their insulin levels accordingly, either with an insulin pump or by adapting their diet. Since the late 1970s, diabetes has conventionally been managed through self-monitoring of blood glucose (SMBG) using a finger-prick glucose meter [4]. However, these tests require a painful blood sample from fingertips and provide measurements only a few times a day. The introduction of the first FDA-approved continuous glucose monitoring (CGM) device in 1999 marked a significant advancement in diabetes care.

CGM devices monitor glucose levels in real-time and have become a standard method for managing both type 1 and type 2 diabetes [5]. They offer a clearer understanding of daily glucose fluctuations by providing continuous data to patients throughout the day. This ultimately reduces the risk of hypoglycemia and hyperglycemia events, as well as diabetes-related complications [6]. Moreover, CGM users have a better understanding of how factors such as stress, diet, exercise, and medication affect their glucose levels. With access to real-time data, patients feel more empowered to take control of their condition, encouraging healthier habits. Consequently, CGMs serve as an educational tool that improves patient adhesion to treatment [7]. The benefits are not only for patients but also for researchers who use those glucose trends to evaluate treatment efficacy and adapt it for personalised treatments [7]. This data-driven approach also enables future perspectives and extended applications to classical diabetes follow-up. For example, predictive modeling uses machine learning techniques to predict glycemic events and help with clinical decision. It enables more personalised and accurate glucose management by complementing real-time measurements with prediction from the machine learning model. In addition, CGMs enable early diagnostic of type 1 and 2 and prediabetes patients [7].

Motivations

As those devices are a reference tool for managing diabetes, there is a sharp rise in demand. Figure 1 shows the growth in CGM users since 2010, with the number of worldwide users exceeding 8.5 millions in the first quarter of 2024, a significant increase from the estimated 6.7 million users in the same period of 2023 [8]. Most devices currently on the market are single-use and need frequent replacement, and this combination of high demand and disposability results in a substantial volume of waste, which originates from the device design and its material composition. Thus, this widespread adoption of CGM raises concerns regarding their environmental impact.

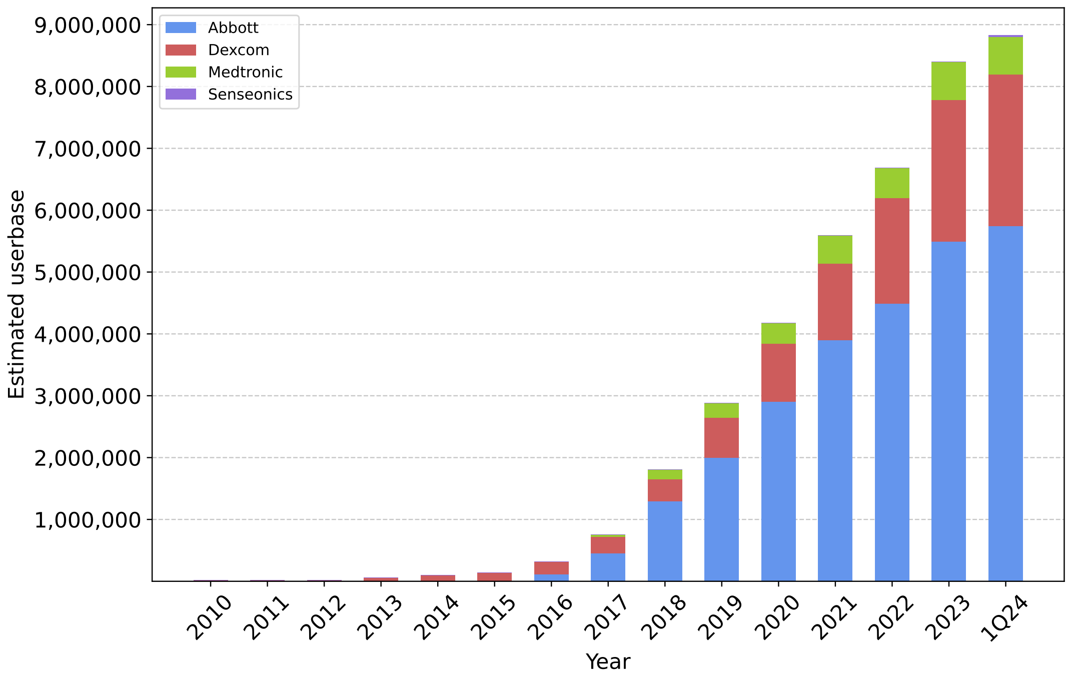

Figure 1: Estimated number of CGM users for the main manufacturers on the market from 2010 to the first quarter of 2024 (1Q24), adapted from [8]. Three transdermal CGM are approved by the Food and Drug Administration (FDA): Dexcom, Medtronic and Abbott [9]

Furthermore, each sensor is packaged in cardboard, which also contains an applicator. Surprisingly, the medical device itself represents only 10 % of the total mass. The remaining 90 %, including the cardboard and applicator, serves as support and is directly discarded [10]. Typically, most CGM devices last between 7 and 14 days depending on the model, which means that dozens of sensors are needed every year for each user. From a worldwide perspective, it has been estimated that over 230 million CGMs are used annually and then disposed of. A number that will continue to increase in the coming years with the expected increase of users [5].

Given the amount of waste generated by the widespread use of CGMs, it is important to consider how they fit into sustainability goals and climate policies. Indeed, climate change is affecting human health, threatening ecosystems and putting some populations at risk as extreme weather events and wildfires multiply [11]. Climate change and the environmental impacts of healthcare may form a detrimental feedback loop with climate-related events contributing to a rise in healthcare needs, which in turn, further increases environmental impacts [12]. To break this feedback loop and more generally to tackle climate change problems, the European Union has established policies and roadmaps. In 2015, COP21 resulted in the Paris Agreement, a legally binding treaty aimed at addressing climate change. The agreement seeks to limit the long-term global warming to well below 2°C, and to keep the temperature increase to 1.5°C. In 2021, this limit of 1.5°C of global temperature increase has been set and approved in Glasgow by the COP26. To achieve this goal, emissions need to be reduced by at least 55% from 1990 levels by 2030 [11]. Hence, the European Commission (EC) has adopted a new growth model called the European Green Deal [13]. One of the main building block of this model is the Circular Economy Action Plan adopted in 2020. It will ensure that products on the European market have a greater lifetime and are easier to reuse and recycle [14][15]. These measures focus on resource-intensive sectors with a high potential for circularity like electronics, batteries, plastics, and packaging [11]. However, CGM devices do not align with these sustainability goals as most of them are single-use and not recycled. There is therefore significant potential for improvement in their design.

Objectives

CGM is an essential technology for managing diabetes and it is necessary to address the significant amount of waste that will be generated by its growing number of users. This raises the question of **how to design CGM devices to be more environmentally sustainable**.

This work explores new CGM design approaches driven by environmental impact reduction objectives. This method, known as ecodesign, is defined as *"the integration of environmental aspects into the product development process, by balancing ecological and economic requirements. Ecodesign considers environmental aspects at all stages of the product development process, striving for products which make the lowest possible environmental impact throughout the product life cycle"* [16].

In the first place, we need to estimate the magnitude and main contributors of these impacts. This will be achieved by conducting a life cycle assessment (LCA), which involves compiling and evaluating the inputs, outputs, and potential environmental impacts associated with a product system throughout its life cycle [17]. Based on the results of this analysis, we can then identify environmental hotspots associated with CGMs and propose ecodesign strategies. This global approach helps us avoid the issue of burden shifting that occurs when efforts for lowering one type of environmental impact unintentionally increase other types of environmental impacts [17]. Ultimately, we intend to develop a complete ecodesign roadmap that incorporates the lessons learned from modeling the different ecodesign strategies.

Overview of the thesis

This master's thesis is structured in five chapters. Chapter 1 provides the background of CGM devices and an overview of the CGM devices available on the market. Chapter 2 describes the LCA methodology and applies it to the reference case. This reference case is based on the LCA results of the commercially available Freestyle Libre 2 CGM device.

It serves as a reference point and allows for a comparative analysis of the environmental impacts of each ecodesign strategy. Chapter 3 explains the ecodesign strategies proposed to reduce the impacts of the hotspots identified in the reference LCA. Chapter 4 presents the LCA results of the strategies compared to the reference LCA. Lastly, Chapter 5 discusses the limitations and possible future improvements of this work.

Chapter 1

Background

The purpose of this chapter is to introduce the fundamentals of CGM. First, the history of diabetes monitoring is reviewed, from urine tests to modern CGM systems. Next, the working principles of CGM devices are explained and the main technologies used to obtain real-time glucose measurements are described. Then, a comparison of the latest and most widely used devices on the market is made. Finally, environmental impact concerns are discussed, using global CGM waste mass as a starting point to motivate the need for a LCA study.

1.1 History of Diabetes Monitoring

Since its beginnings, diabetes monitoring has seen significant transformations due to technological innovation and the growing need for more accurate and user-friendly solutions. The earliest methods relied on urine testing, which remained the main diagnostic approach until the early 20th century. Chemical tests, like Benedict's solution introduced in 1908 [18], indicated the presence of sugar in urine. Unfortunately, these tests only provided a rough estimate of blood glucose levels as glucose had already been filtered by the kidneys. It was thus dependent on renal filtration, which can vary significantly among individuals and in certain physiological conditions, such as pregnancy [3].

A major advancement came in 1965 with the introduction of the first blood glucose test strip by Ames Laboratories, the Dextrostix. It used glucose oxidase to detect glucose levels in blood. A drop of blood was applied, washed off after 60 seconds, and the resulting color was compared to a reference chart [18]. Despite being more accurate than urine tests, it was still only intended for use in physician's offices and not suitable for home use.

Home blood glucose meters became available a few years later, around 1980. These devices rapidly improved throughout the 1980s and 1990s, requiring smaller blood samples and becoming more affordable. For diabetic patients, SMBG became the standard of care [18].

In parallel, biosensing technology based on electrochemical glucose detection was being developed. First described by Dr. Leland Clark in the 1960s, these systems used redox enzymes like glucose oxidase to catalyse reactions generating electrical currents proportional to glucose concentration [7].

In 1999, the first FDA-approved CGM system for physician use was launched: the MiniMed CGM. It provided detailed glucose profiles for clinical analysis, despite its 72-hour wear restriction and frequent calibration needs [7]. The sensor was physically connected to

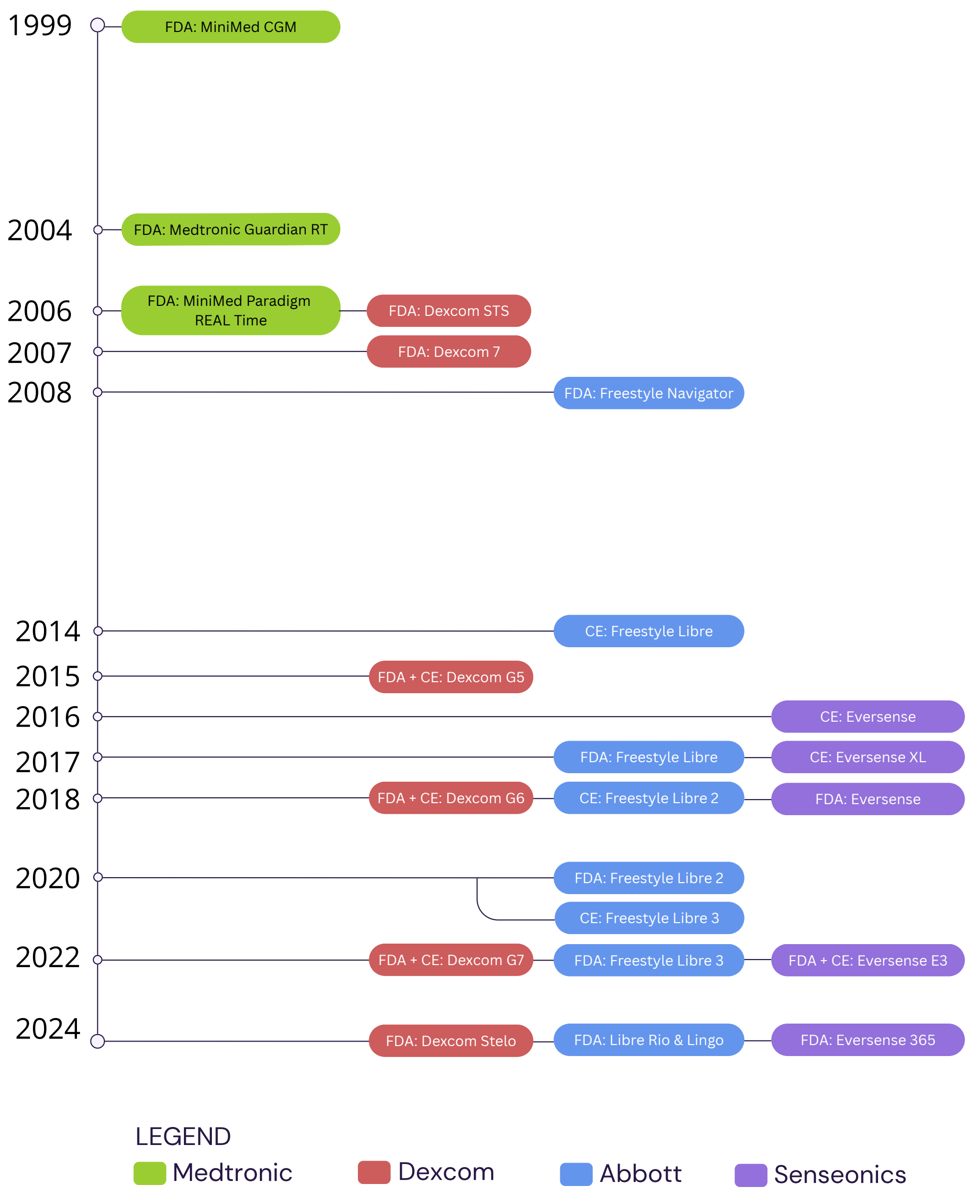

Figure 1.1: Evolution of CGM devices from the first FDA-approved CGM in 1999 to the first FDA-approved over-the-counter CGM in 2024.

the receiver by a cable [4].

In 2004, the Medtronic Guardian RT became the first CGM system approved for home use. It offered real-time, wireless data transmission for three days and included programmable alerts for high and low glucose levels, features that would become industry standards [7, 4]. Dexcom entered the market in 2006 with the STS (short term sensor) system, followed by the SEVEN in 2007, offering 72-hour and 7-day wear times, respectively [7].

Rapid development continued into the late 2000s as illustrated in Figure 1.1. The Medtronic MiniMed Paradigm REAL-Time, introduced in 2006, was the first integrated CGM-insulin pump system, marking a significant step toward automated insulin delivery (AID) [7]. Abbott joined the market in 2008 with the Freestyle Navigator, offering a 5-day sensor life [3].

Initially, all CGM systems required several blood glucose finger pricks for calibration [18]. However, this began to change with the launch of factory-calibrated systems. In 2016, Abbott released the Freestyle Libre Pro (for professional use), which required no finger pricks and had a 14-day wear period. The following year, the Freestyle Libre system became available to patients directly. Although it did not offer real-time readings, requiring users to scan the sensor to access data, it was significantly more affordable and accessible to a broader population. This sensor also had a warm-up period of only one hour and received Conformité Européenne (CE) approval in 2014 [4, 7].

At the same time, Dexcom continued to innovate with the G5 (2015), which allowed glucose monitoring through a smartphone app, and the G6 (2018), which eliminated the need for finger stick calibration and extended wear time to 10 days [7]. The G6 was also the first CGM to be FDA-approved for integration into AID systems [4].

Further advancements in sensor duration were introduced with the Eversense system by Senseonics. Approved by the FDA in 2018 (CE mark in 2016), it was the first fully implantable (subcutaneous) CGM with a lifespan of up to 90 days. The Eversense XL, released in 2019 (outside the U.S.), extended wear time to 180 days. In 2022, the Eversense E3 received FDA approval for 180 days, and more recently, the Eversense 365 became the first CGM approved for one-year wear [19].

The FDA's approval of the first over-the-counter (OTC) CGMs, the Dexcom Stelo and Abbott's Libre Rio and Lingo systems, in 2024 marked the most recent advancement in accessibility [7]. These devices target users not on insulin therapy or even non-diabetic people seeking insights into how diet and exercise affect their glucose levels.

Overall, CGM technology has evolved from basic chemical tests to sophisticated, implantable, real-time systems. It continues to expand its capabilities in accuracy, wear duration, and user accessibility, with a future likely dominated by integration into closed-loop and AI-driven insulin delivery systems.

1.2 Continuous Glucose Monitoring Working Principles

CGM devices represent progress for diabetes management because they offer (i) real-time measurements, (ii) short-term feedback on medication administration, and (iii) alarms for risky high or low glucose levels [20].

The main parts of the CGM product are the sensor, the applicator and the informational leaflet, packed in cardboard packaging [5]. As illustrated in Figure 1.2, the device consists of a battery and integrated circuits (ICs) soldered on a circuit board, protected by a plastic casing [5]. The sensor is usually worn on the upper arm and adheres to the skin with an adhesive patch. A thin filament, called the subcutaneous needle, is inserted through the skin to measure glucose levels in the interstitial fluid (ISF) [21]. Glucose measurements are sent to an external device, generally the user's smartphone, via wireless communication. The sensor is the transmitter, and the smartphone or dedicated reader is the receiver. The receiver device reads sensor measurements and keeps track of glucose levels. The specific reader can also save notes about what the user eats, its insulin injections and exercise sessions [20].

The typical use of a CGM begins with applying the sensor to the arm using the applicator. The Freestyle Libre 2 (FL2) (device used as reference in this study) has then a calibration period of 60 minutes [22]. After this, the first glucose measurements become available on the receiver without requiring finger pricks calibration (a feature specific to the FL2). Alarms for high or low glucose levels, and signal loss can be set on the smartphone. Abbott announces a lifespan for the FL2 of up to 14 days [22]. The sensor is automatically deactivated at the end of this period or earlier if a failure occurs [1], and must be replaced with a new one.

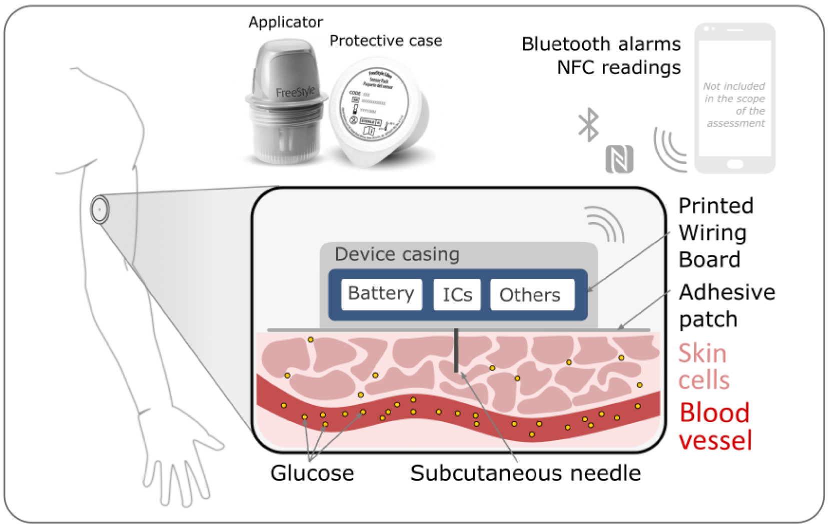

Figure 1.2: A CGM device along with the elements necessary for its use [23]. The sensor is applied on the arm using a dedicated applicator and secured by an adhesive patch. Glucose levels are measured in the ISF by the subcutaneous needle. The data are processed by ICs and transmitted wirelessly to the smartphone via near field communication (NFC) or Bluetooth Low Energy (BLE). The sensor is powered by a battery. 'Others' elements include passive electronic components. During transport, the subcutaneous needle is protected by the protective case.

Signal Processing

The CGM converts glucose sensor measurements into wirelessly transmitted data packets, as illustrated in Figure 1.3. Glucose levels are obtained through a biosensor that converts glucose concentration into an electrical signal. The glucose sensor is an amperometric sensor that generates a small current proportional to the glucose level. When this signal arrives in the analog front-end (AFE), it is amplified, filtered, and converted to a digital signal [24]. The microcontroller (MCU) then collects the data and packages it in data packets for transmission [24]. The device is battery-powered because it provides a reliable source of energy. However, research studies also explored power harvesting solutions for the CGM system [25].

Biosensor

In general, biosensors detect specific biological analytes, such as glucose, using electrochemical sensors [24]. The biosensor in a CGM is responsible for detecting glucose in the

[1]Information extracted from our experimental power profiling 3

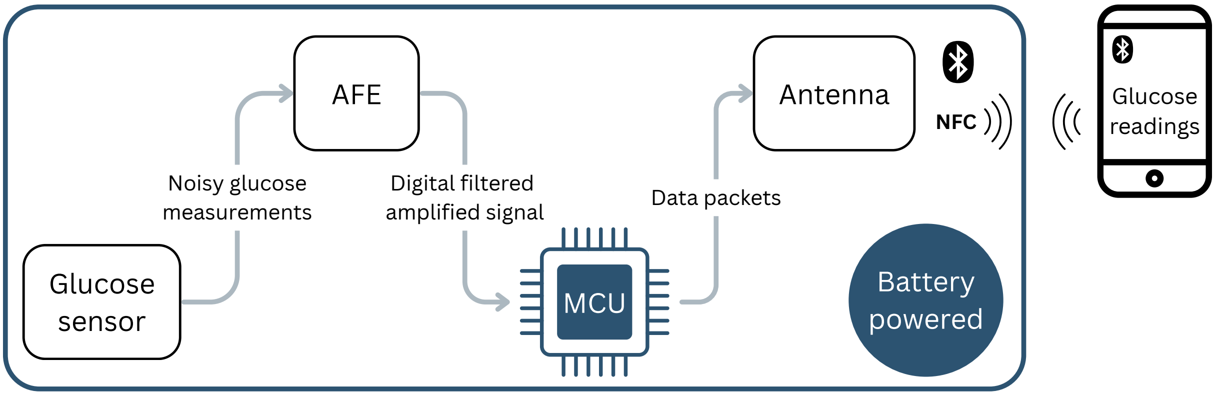

Figure 1.3: From the glucose measurements to the glucose reading on a smartphone, the path of the signal with an electronic point of view, inspired by [24]. The glucose measurements from the biosensor are noisy. The AFE circuitry filters and amplifies the signal. Next, data packets are prepared by the dedicated IC for transmission. An antenna provides the wireless link between the battery-powered device and the smartphone.

ISF. In 1962, Clark and Lyons developed the first glucose sensor with an amperometric electrode using the enzyme glucose oxidase to detect blood glucose [24].

Microelectrodes are coated with enzymes or materials that react with glucose molecules via oxidation or reduction reactions. These redox reactions generate an electrical signal proportional to the glucose concentration.

Typically, as illustrated in Figure 1.4, three microelectrodes are used [24]:

- **The working electrode (WE)**: catalyses redox reactions involving glucose.
- **The reference electrode (RE)**: stabilises the electrochemical potential.
- **The counter electrode (CEl)**: balances the current during measurements.

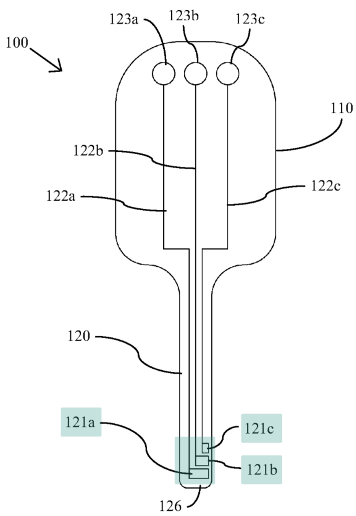

Figure 1.4: Analyte sensor with three microelectrodes (121 a,b,c) in a patent by Abbott [26]. There are probably one WE, one RE and one CEl.

In today's working electrodes, glucose oxidase is still the enzyme used to catalyse the redox reaction [9]. This redox reaction generates electrons that in turn produce a measurable current [9]. An amperometric sensor measures a current signal that, in this case, is proportional to the glucose level. A biocompatible membrane is coated on the electrode surface to minimise the immune response of the body [9].

In [24], the article explains how glucose measurements can be extracted from biofluids. Although blood samples are well understood and commonly used for glucose level measurements, other biological fluids offer less invasive alternatives. There is a linear correlation between blood glucose levels and glucose found in various biofluids such as sweat urine, interstitial fluid, tears, breath, and saliva, as shown in Figure 1.5. The linear correlation observed in ISF results from the diffusion of nutrients from the blood through the capillaries [24].

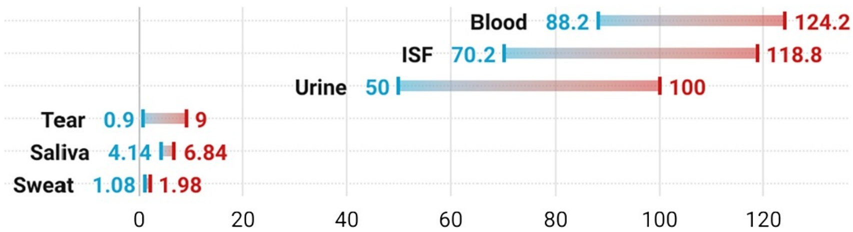

Figure 1.5: Glucose concentration in biofluids for healthy patients in [mg/dL] [24]. The ISF and blood glucose concentration present a linear relation due to the diffusion and nutrients exchange between those body fluids.

As explained above, monitoring glucose levels in ISF is preferred because it is painless and also offers better accuracy [27]. The microneedle is inserted into the dermis with minimal or no pain [28]. A hypodermic needle is used to insert the flexible sensing strips, approximately 6mm long, into the ISF [27]. In both FL2 and Freestyle Libre 3 (FL3), microneedles are used [22].

Wireless Communication

Wireless communication for CGM devices is often achieved using BLE or NFC [24].

In the FL2, communication is established between the smartphone and the sensor device over distances of up to six meters [22]. BLE fulfills these requirements by offering communication in a maximum range of several tens of meters. BLE operates at an ultrahigh frequency of 2.4 GHz. In this system, the CGM works as the slave, advertising packets and responding to requests from the master device, the smartphone [24].

NFC communication operates at 13.56 MHz and has a typical maximum range of a few centimeters. In the FL2, the sensor can be scanned through up to four centimeters of clothing [22]. This short-range communication is used primarily to activate the sensor[2]. Unlike BLE, NFC does not require pairing between the transmitter and the receiver. Data exchange can occur in either passive or active modes. In active mode, both the transmitter and receiver generate a radio frequency (RF) field, while in passive mode, only the transmitter produces the RF field [24].

[2]Information extracted from our experimental power profiling, see Chapter 3.

Performance and Challenges

The article [24] provides an overview of performance evaluations and limitations in CGM systems. The performance of a CGM is determined by various parameters, including accuracy, calibration, lifetime, stability and device standardisation. Accuracy, in particular, is affected by several external factors such as physical exercises, temperature variations, pH variations and nonspecific background offset currents in the sensor. Some devices require calibration using finger prick blood samples, which causes discomfort. In contrast, devices like the Freestyle Libre and Dexcom use self-calibration and do not require user intervention [9].

A limitation of real-time glucose monitoring is the delay between blood glucose levels and glucose concentration in ISF. This delay, typically between five and ten minutes, is due to diffusion. The diffusion is influenced by physical exercises, temperature and pH changes. While this delay is acceptable for daily diabetes management, it poses a risk in emergency situations like coma due to hypo or hyperglycemia. Fortunately, glucose level changes are generally gradual, not sudden, and can be anticipated by using data processing algorithms. Another measurement limitation is the presence of a non-specific background offset, commonly observed in glucose oxidase-based electrodes, although its exact cause remains unclear [9].

The foreign body response triggered by needle implantation also affects the device performance and longevity. When a foreign material is detected, the body initiates an inflammatory response involving:

- Recruitment of macrophage cells, which consume interstitial glucose near the sensor, resulting in inaccurate glucose readings.
- Recruitment of fibroblasts, which encapsulate the foreign body to isolate it from the surrounding tissue.

These reactions also lead to blood vessel regression. In turn, it reduces glucose diffusion and further affects measurements in the ISF [4].

In addition, the constant open wound caused by the insertion needle, combined with micro-movements of the sensor, contributes to tissue destruction at the implantation site. This damage can result in chronic inflammation (as explained above), further affecting sensor performance over time [4].

Another constraint on CGM lifetime is the limited capacity of the embedded battery. Since CGM systems must remain small and lightweight, their energy storage is restricted. One potential solution is energy harvesting technologies for self-powered glucose biosensors. However, these innovations are not yet commercially available [25].

Patient satisfaction is also a key factor in evaluating CGM performance. Barriers to user acceptance include: (i) high cost, (ii) discomfort during CGM insertion, (iii) poor adhesion to the skin, (iv) interferences with sports and physical activities, and (v) skin reaction, among others [9].

In the next section (1.3), Table 1.1 compares commercially available CGM devices, taking into account several of the performance characteristics discussed here.

Feature	Abbott		Dexcom		Medtronics	Senseonics	
	Freestyle Libre 2 (Plus)	Freestyle Libre 3 (Plus)	G6	G7	Guardian 4	Eversense E3	Eversense 365
Age indication (years)	≥ 4 (≥ 2)	≥ 4 (≥ 2)	≥ 2	≥ 2	≥ 7	≥ 18	≥ 18
Diabetes type	1&2	1&2	1&2	1&2	1	1&2	1&2
Sensor wear (days)	14 (15)	14 (15)	10	10.5	7	180	365
Warm up period (hours)	1	1	2	0.5	2	24	24
Requires finger prick calibration	no	no	no	no	no	1-2x/day	1x/week [3]
Time between readings (min.)	1	1	5	5	5	5	5
Insulin pump integration	no (yes)	no (yes)	yes	yes	yes	yes	yes
Active alarms/alerts	yes	yes	yes	yes	yes	yes	yes
Accuracy: MARD (%)	9.3 (8.2)	7.9	9	8.2	10.6	8.5	8.8
FDA approval year	2020	2022	2018	2022	2023	2022	2024
Type of device	flash [4]	real-time	real-time with predictive low alerts	real-time with predictive low alerts	part of insulin pump system	implant	implant

Table 1.1: Most popular CGM devices currently available on the market by Abbott, Dexcom, Medtronics and Senseonics [29, 30, 31, 32, 33, 34, 35].

[3] 1x/day for 13 days, then 1x/week

[4] The Freestyle Libre 2 CGM is said to be flash [29] but the device used for our study 3 was real-time, probably due to some improvements in the most recent versions

1.3 Devices Available on the Market

Table 1.1 presents a comparison of the latest and most widely used CGMs available on the market. It highlights key features such as sensor lifespan, calibration requirements, and measurement accuracy. Device accuracy is represented using the mean absolute relative difference (MARD), which quantifies the average deviation between CGM readings and reference blood glucose measurements at normal to high glucose levels. A lower MARD indicates higher accuracy.

1.4 Environmental Impacts

The environmental impacts of CGM devices are important to assess. Primarily, CGMs have a limited lifespan, up to 14 days for the FL2 [22]. The potential number of users is large and expected to rise. According to the IDF, approximately 589 million adults aged 20-79 currently have diabetes worldwide. Diabetes is projected to increase by 46% by 2050, affecting 1 in 8 adults [1]. This rise is driven by population ageing and the increased global urbanisation [2]. In short, the combination of limited device lifespan and a growing number of users is leading to the generation of tons of waste that is expected to increase in the coming years.

As shown in Figure 1, at the end of the first quarter of 2024, there were over 8.5 million CGM users worldwide [8]. This translates into hundreds of millions of sensors being used annually. Considering the maximum lifetime announced by the companies and no devices failures, we obtain more than 264.7 million sensors/year:

- Abbott (Libre 2 et 3): 5.7 million x 26 sensors/year = 148.2 million sensors
- Dexcom (G6 et G7): 2.3 million x 37 sensors/year = 85,2 million sensors
- Medtronic (Gardian 4): 600 000 x 52 sensors/year = 31,2 million sensors
- Senseonics (E3): 4000 x 2 sensors/year = 8000 sensors

According to [5], over 230 million sensors are thrown away each year globally, which is consistent with our calculations. A typical CGM system consists of the sensor itself, a cardboard packaging, a plastic applicator, and an informational leaflet [5]. The sensor consists of a circuit board, a battery and a plastic casing [5].

Tables 1.2 and 1.3 summarise the estimated mass of waste generated annually by three commonly used CGM models: Freestyle Libre 2, Freestyle Libre 3, and Dexcom G7.

	FL2	FL3	G7	Total (t)
Packaging (t)	1326.4	696.5	1455.2	3478.1
Applicator (t)	5305.6	3282.6	6076.1	14664.3
Leaflet (t)	289.0	318.6	1668.0	2275.6
Total (t)	6921.0	4297.7	9199.3	20418.0

Table 1.2: Annual quantities of cardboard packaging, plastic applicators, and paper leaflets waste generated by three globally used CGM systems [5].

	FL2	FL3	G7	Total (t)
Case (t)	140.0	37.8	165.1	342.9
Circuit board (t)	55.6	13.3	60.4	129.3
Battery (t)	27.4	26.7	54.5	108.6
Total (t)	223.3	77.8	280.0	580.8

Table 1.3: Annual quantities of plastic cases, electronic waste, and batteries generated by three globally used CGM systems [5].

In Table 1.2, we observe that the waste generated annually, excluding the sensor device itself, represent more than 20,000 tons of waste. 20,000 tons is equivalent to the mass of more than eight Atomium or over two Eiffel towers. In Table 1.3, assuming an average car mass of 1.5 tons, the total annual mass of discarded batteries, circuit boards, and casings is approximately equivalent to the mass of 387 cars.

In 2022, the average EU habitant generated 5 tons of waste annually [36]. Considering 8.6 million CGM users, each user contributes to around 2.37 kg of waste per year from packaging, applicators, and leaflets and also discards 67.5g per year of sensor casing, circuit board, and battery. Combined, this represents 0.049% of the total annual waste generated by a typical EU citizen.

The projections estimate an increase in diabetes of 46% by 2050, reaching 860 million people. Currently, CGM users represent 8.6 million out of 589 million people with diabetes worldwide, an adoption rate of approximately 1.46%. If this rate remains constant, an estimated 12.56 million people will be using CGMs in 2050. In terms of global waste, it would represent 29,820 tons of cardboard packaging, plastic applicators and paper leaflets annually, and 848 tons of casing and electronics mass annually.

However, waste mass alone does not reflect the full environmental impact of CGM devices. A complete environmental assessment must also include other life cycle stages, such as production, transportation, and usage phases to take into account the total environmental burden of the product.

Chapter 2

Reference LCA

As previously discussed, CGM systems generate significant amounts of waste due to their disposable components and frequent replacements. In order to rigorously assess the environmental impacts of these devices and identify improvement opportunities, a robust and comprehensive methodology is required, one that supports informed decision making aligned with the United Nations' Sustainable Development Goals (United Nations (UN) SDGs) [17].

Such decisions must be made from a systems perspective to avoid burden shifting that occurs when reducing impact in one area unintentionally increases it elsewhere. This requires considering the entire life cycle of the product as well as a wide range of environmental impacts. LCA is a standardised and widely recognised tool that meets these requirements [17].

This chapter introduces the fundamental principles and structure of LCA to provide the necessary context for its application. The reference case study is then presented: an LCA of a commercial CGM device, the FL2 by Abbott, as proposed by [23]. It serves as a basis for evaluating alternative ecodesign strategies later in the thesis.

The LCA methodology follows the international standards defined in ISO14040, which provides the general principles and framework, and ISO14044, which specifies the requirements and guidelines for its implementation [17].

An LCA is divided into four methodological phases, illustrated in Figure 2.1a. The **goal and scope definition** states the purpose of the study and defines the product system(s) to be assessed. It establishes the system boundaries (see Figure 2.1b) and methodological assumptions, providing the groundwork for the entire analysis. The **inventory analysis** is often the most time-consuming part and involves collecting and compiling data on all elementary flows, such as resource inputs and emissions, linked to the processes within the defined product system. The analysis is guided by the previously defined goal and scope and typically relies on multiple data sources. Once completed, this phase provides the list of elementary flows associated with the product system for the defined boundaries, also know as the **life cycle inventory (LCI)**. The **impact assessment** phase is where the inventory data is translated into environmental impact indicators through a structured process known as **life cycle impact assessment (LCIA)**. Finally, the **interpretation** phase synthesises the findings from all previous phases, analysing them in the context of data quality, uncertainties, and assumptions made throughout the study.

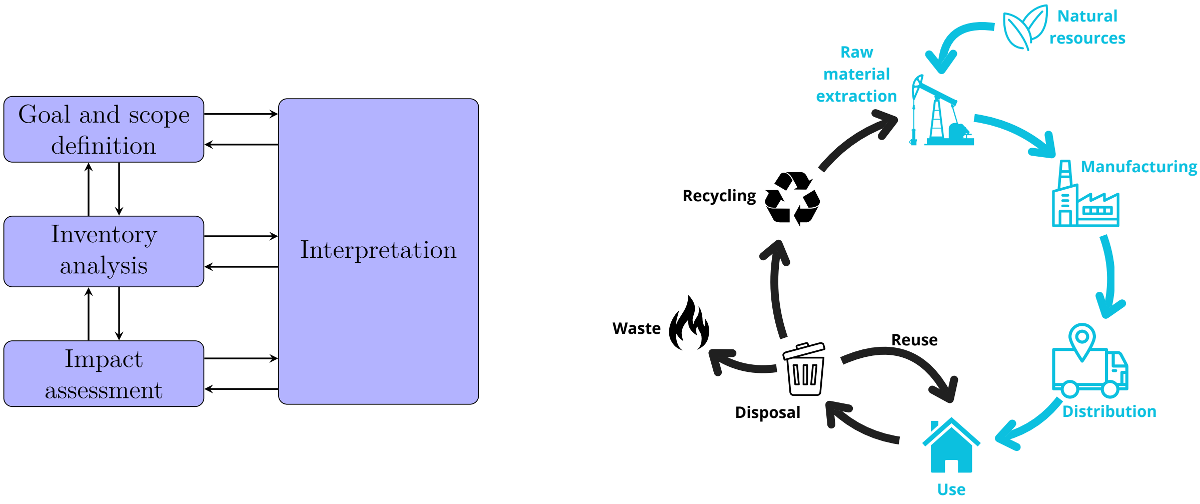

(a) LCA phases.

(b) Life-cycle stages.

Figure 2.1: An LCA entails 4 methodological phases (left), standardised and made mandatory by ISO standards 14040 and 14044. The construction of an LCA model is articulated around life-cycle stages (right), often represented in a circular pattern. In blue, we have indicated the stages considered in this work.

2.1 Goal and Scope

2.1.1 Goal Definition

The goal of an LCA defines in detail the purpose of the study. It establishes the context in which the assessment is carried out and specifies how and to whom the results will be communicated.

In accordance with ISO standards [37], the goal definition of the reference case includes several key elements. The **intended application of the results** is to identify the environmental hotspots of the FL2 CGM, i.e., the components or processes with the highest environmental burden. These are potential targets for ecodesign strategies. The study also aims to estimate the potential impact reductions associated with alternative design options. The **decision context** is driven by the significant waste generated by single-use CGM devices, which are frequently discarded and replaced.

The study is carried out under certain **methodological limitations**: it includes all life-cycle stages from raw material extraction to the use phase but excludes end-of-life (EoL) treatment. The **target audience** includes university students and teachers familiar with LCA, as well as electronic design engineers working on medical devices such as CGMs who may be seeking to integrate sustainability into their product development process [23]. This study is not intended to be a **comparative statement disclosed to the public**, and is conducted as part of a Master's program at UCLouvain, with no external commissioner.

2.1.2 Scope Definition

The scope, defined together with the goal, serves as a guiding framework to report how the analysis is conducted. It mainly consists of a detailed specification of the studied product system, its life cycle, and system boundaries [37].

The **product system under analysis** is the FL2 by Abbott [22], a CGM currently available on the market. The **system boundaries** encompass stages from raw material extraction to the use phase, excluding the EoL, as shown in Figure 2.1b.

The **functional unit (FU)** is defined as *one year of continuous glucose monitoring for a single diabetic patient (type 1 or 2) in Belgium* [23]. Based on this FU and the product's maximum lifespan of 14 days per sensor, the **reference flow** corresponds to 26 sensors per year, assuming continuous monitoring without interruption or premature failure.

This study employs an attributional **modeling approach**, following the guidance of the ILCD Handbook [38]. For the **impact assessment**, the **Environmental Footprint 3.1 (EF 3.1) method** [39] is selected, as recommended by the EC. This method has been updated recently, integrating the latest IPCC 2021 characterisation factors [40], and includes 16 midpoint categories. Among these, climate change (CC), resource use (minerals and metals) (MRD), water use (WU) are especially relevant for ICT devices [23]. A complete list of the impact categories is provided in Table 2.1, and a comparison to alternative LCIA methods in Table A.1.

Lastly, the Ecoinvent v3.9.1 **database** [41] is used for the LCI. It offers suitable granularity for modeling electronic components and is fully compatible with Brightway2, the open-source LCA software used for this study [42, 23].

2.2 Inventory Analysis

According to [17] : *"The inventory analysis collects information about the physical flows in terms of input of resources, materials, semi-products and products and the output of emissions, waste and valuable products for the product system"*. In other words, the inventory analysis is a phase of the LCA that collects all inputs and outputs of the processes within the product system. The LCI is the result of the inventory analysis and represents a compilation of all physical elementary flows required to fulfil the function of the product system, as defined by the FU [17].

A unit process is the smallest element of a LCI analysis [17]. It serves as a building block of the life-cycle model and is characterised by quantified input and output flows, as illustrated in Figure 2.2. Due to the complexity of product systems, generic data from a database is used to complete the life-cycle model [17].

LCI Database

The life-cycle model is primarily based on background data from Ecoinvent 3.9.1. However, since Ecoinvent is not exhaustive, some processes needed are not available. As a solution, specific flows from the database were grouped to create custom unit processes that completed the missing background data.

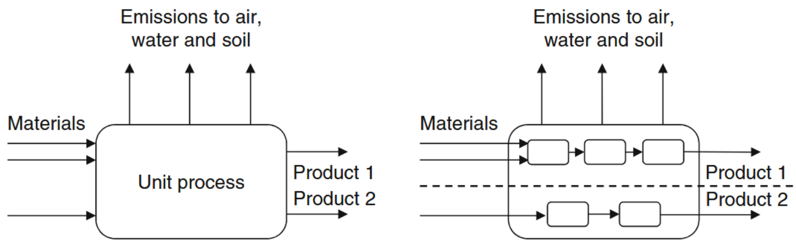

Figure 2.2: (Left) A unit process with the input and output flows. (Right) Breaking the unit process in smaller units, showing higher resolution modeling [17].

Ecoinvent offers four types of system model. In this analysis, the *cut-off by classification* approach is used. Within this framework, wastes are the responsibility of the producer. This means that recycled materials are burden-free for the next user, who is only assigned the impacts associated with the recycling process. Any valuable outputs, such as energy coming from waste incineration, are transferred without environmental burdens [36].

Data Collection

The product system contains two types of data: material and non-material.

All material components are included in the box and its content: the applicator, the sensor pack, and the instruction set, illustrated in Figure 2.3a. In the patents (Figures 2.3c and 2.3b), all components of the device itself and the elements of the applicator are detailed. With the addition of the packaging and instruction set, this represents the complete inventory of material data from the FL2.

The non-material inventory includes all transportation activities. Specifically, it covers the transport of materials for the final product assembly. The electronic components are assumed to be produced in Asia, while the applicator and wearable device are manufactured in the United States. The subcutaneous needle is produced in the United Kingdom and added to the product to be imported by a European distributor based in Germany. The final product, including the box, is then transported to the delivery warehouse in the Netherlands before reaching the end-user in Belgium, as illustrated in Figure 2.4 [23].

Life-Cycle Model

With the foreground and background processes, the complete life-cycle model is built. The foreground model in Figure 2.5 is a compilation of all unit processes specific to our product system. Both material and non-material processes are included. Each unit process is mapped either to an activity in the Ecoinvent database or to a custom process. A custom process is created by combining specific flows when the process is not available directly in the database. In opposition to the foreground model processes, background processes are not specific to the product system.

Product or waste flows within the foreground model are quantified to define the reference flow. The reference flow measures the outputs necessary to fulfil the function of the functional unit [17]. All unit processes in a life-cycle model belong to the technosphere, which includes everything that is *"intentionally man-made"* [17]. Unit processes leading to the reference flow are considered upstream processes, while those following it are classified as downstream processes.

(a) Each FL2 shipment includes a cardboard box and its content: an applicator, a sensor pack and an instruction set.

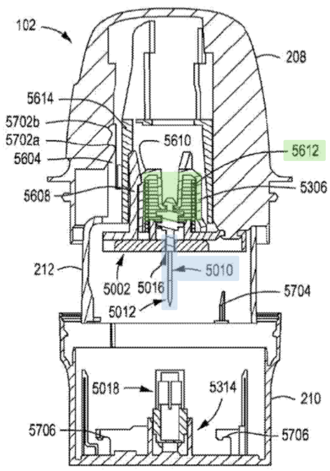

(b) Applicator from Figure 2.3a, with detailed components such as: a steel spring (5612), a hard needle (5010) and plastic parts [43].

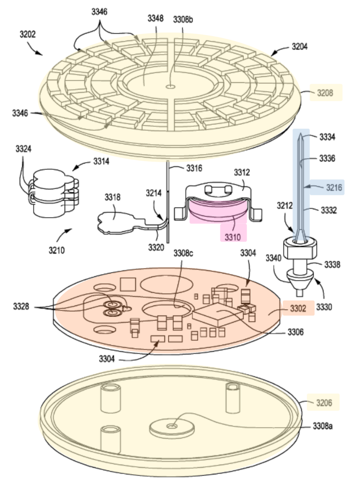

(c) CGM device and its components: the casing top and bottom (3208, 3206), the hard needle (3216), the battery (3310), and the printed circuit board (PCB) (3302) with the passive components and the two ICs [26].

Figure 2.3: Description of material parts for the CGM product system: content of a typical cardboard box delivered, applicator and CGM elements from Abbott patents.

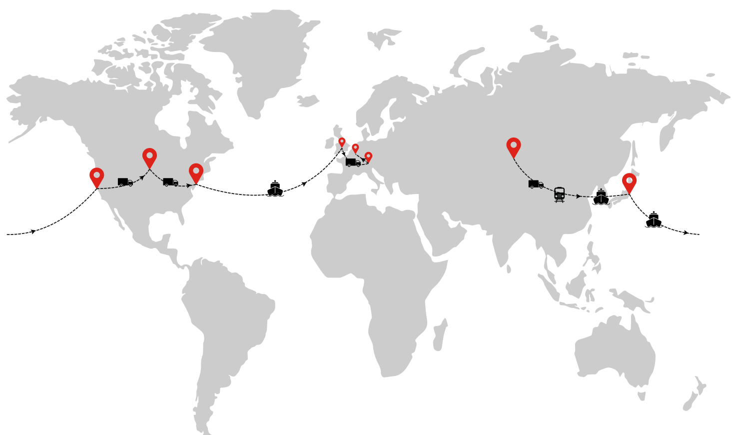

Figure 2.4: Transports of materials necessary to assemble the final product and deliver it in Belgium.

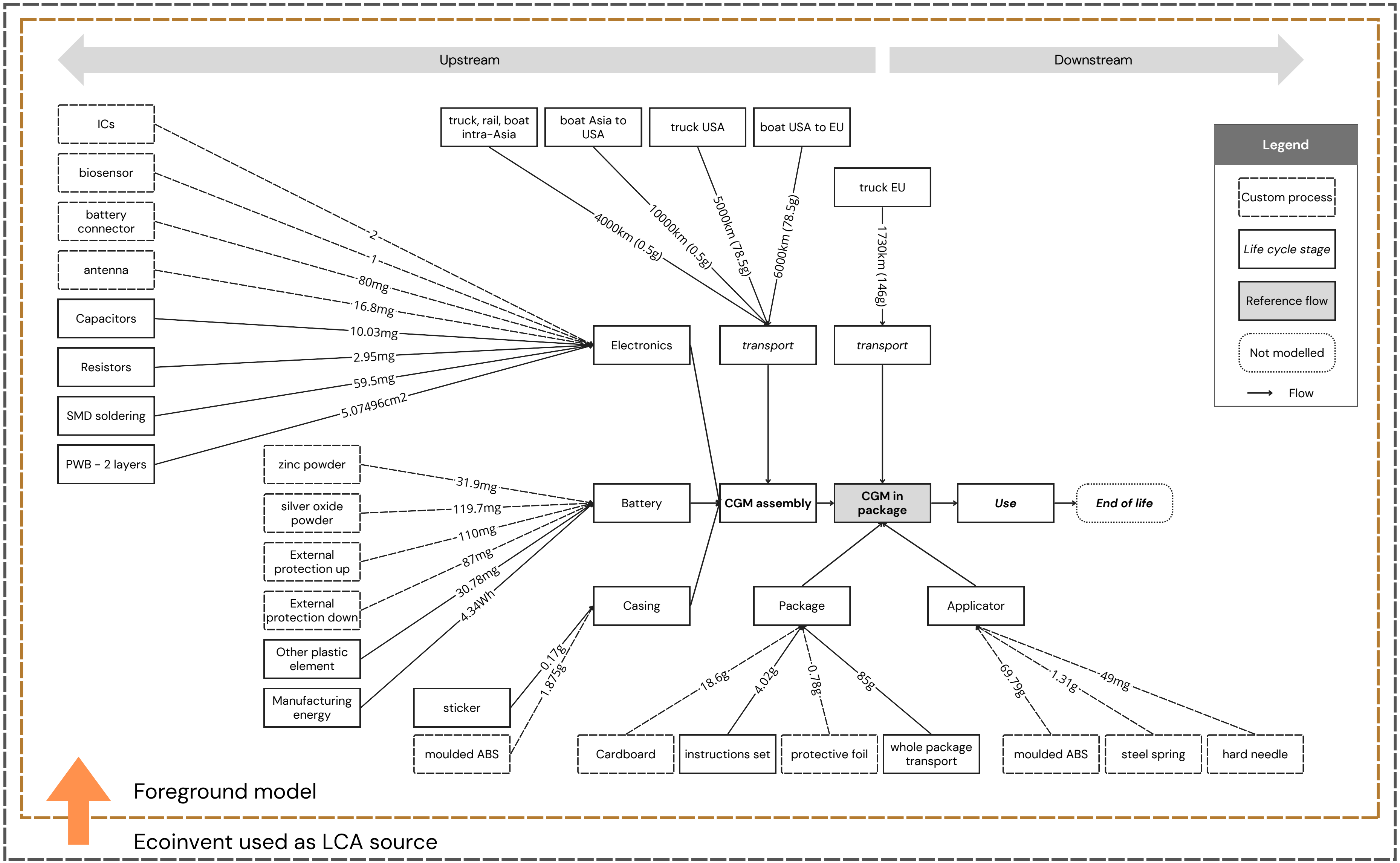

Figure 2.5: Foreground model of the reference LCA. All unit processes (material and non-material) specific to the product system are represented. Some are mapped to custom processes, created by grouping flows because they are not available in the Ecoinvent database. The remaining processes are mapped to background processes from Ecoinvent. The flows are quantified. The life cycle stages are written in italics.

2.3 LCIA

According to ISO 14040 standard, the LCIA phase consists of five steps, the first three being mandatory and the last two optional [44], as illustrated in Figure 2.6.

The first step is the **selection** and involves identifying relevant impact categories, the associated category indicators, and the appropriate characterisation models. These choices must be consistent with the goal and scope of the study. In practice, this selection is done implicitly by choosing the EF 3.1 method when defining the scope.

Next, we have the **classification** step, where each elementary flow from the LCI is assigned to the appropriate impact categories. This step is also automatically handled by the LCI software.

The third and final mandatory step is the **characterisation**, which calculates the indicator result for each impact category. This is done by multiplying the quantity of each elementary flow by its corresponding **characterisation factor**. This factor quantifies the relative contribution of a specific flow to a given environmental impact.

The **normalisation and weighting** steps are considered optional. The **normalisation** expresses each indicator result relatively to a reference value, such as the average annual impact of an individual. It facilitates interpretation by bringing results from different impact categories to a common scale. The **weighting** then applies (subjective) value-based factors to the normalised results to reflect the relative importance of each category.

For both the reference LCA and the alternative ecodesign strategies assessed in this study, the analysis is limited to the three mandatory steps, including the characterisation phase. The results for the 16 midpoint impact categories included in the EF 3.1 method [39] are presented in Table 2.1.

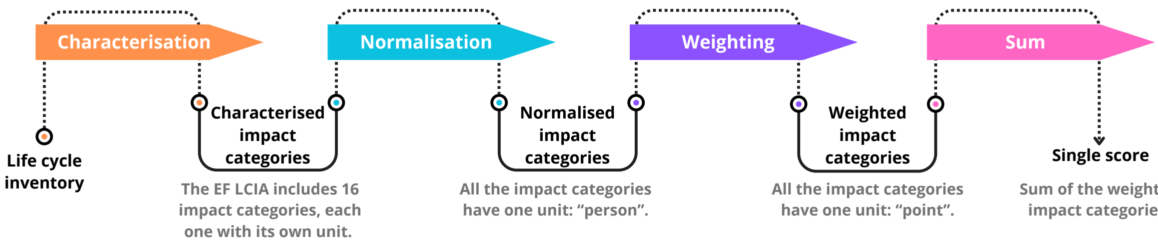

Figure 2.6: EF3.1 LCIA method. The inputs and outputs from the LCI are aggregated in 16 midpoint characterised impact categories. These impact categories can then be normalised and weighted (optional). The weighted impact categories can then be summed to obtain the EF single overall score. Adapted from [39].

2.3.1 Reference Results

The reference scenario provides the environmental performance of the FL2 CGM system and serves to identify the main environmental hotspots within the product system. Although the impact categories in Figure 2.7 cannot be compared due to different units and scales, it is still possible to determine which components have a significant contribution across several categories.

Two main hotspots appear in this analysis: the **applicator**, which is mainly made of plastic, and the **ICs**. These components contribute substantially across almost all

Impact category	Abbreviation	Value	Unit
climate change	CC	30.3	kg CO_{2eq}
ozone depletion	ODP	1.8e-06	kg CFC-11_{eq}
human toxicity: cancer	HTOX_c	2.4e-08	CTUh
human toxicity: non-cancer	HTOX_nc	5.3e-07	CTUh
particulate matter formation	PM	1.8e-06	disease incidences
ionising radiation, human health	IR	2.1	kBq U^{235}
photochemical ozone formation, human health	POF	0.12	kg $NMVOC_{eq}$
acidification	AC	0.15	mol H^+_{eq}
terrestrial eutrophication	TEU	0.35	mol N_{eq}
freshwater eutrophication	FEU	0.013	kg P_{eq}
marine eutrophication	MEU	0.037	kg N_{eq}
ecotoxicity, freshwater	ECOTOX	233	CTUe
land use	LU	172.2	dimensionless (pt)
Water use	WU	12.6	m^3 world eq. deprived
resource use, minerals and metals	MRD	2.3e-03	kg Sb_{eq}
Resource use, fossil	FRD	469.8	MJ

Table 2.1: LCIA results for the FL2 reference case in absolute values for the 16 midpoint impact categories included in the EF 3.1 method.

categories. The applicator accounts for **more than 20% of the impacts in 8 categories**, and **over more than 30% in 4 of them**. The ICs are even more impactful, representing **more than 20% of the impacts in 11 categories**, and **exceeding 47% in 3 of them**.

However, in the **MRD** category, the battery is by far the largest contributor, representing **86% of the total impact**, primarily due to the silver oxide cathode, as shown in Figure 2.8a. A similar pattern is observed in the **ECOTOX** category (Figure 2.8b), where the cathode alone contributes to **38.8%** of the total impact.

In contrast, other components such as the **casing**, **packaging** and **electronics** have a relatively low environmental impact across all categories. The packaging accounts for **less than 10%** of the impacts in 12 categories, the casing contributes **less than 2%** in every category, and the electronics remain **below 10%** in all categories except one.

Given these findings, the initial focus of our ecodesign strategies will be on the applicator as it has potential for substantial impact reductions with relatively simple design changes. Later efforts will concentrate on the ICs and battery.

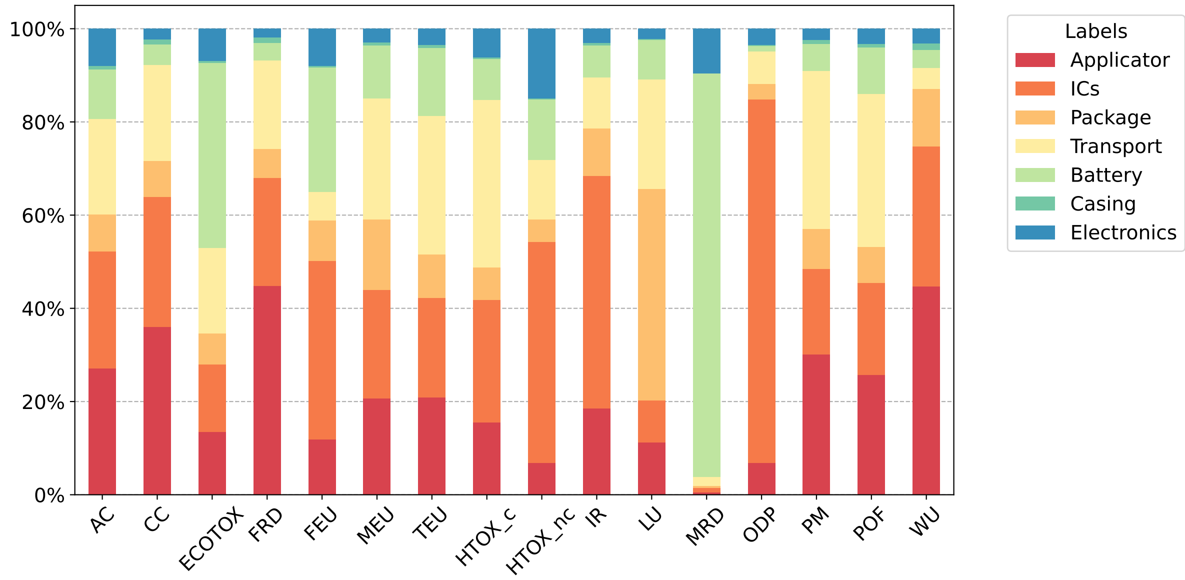

Figure 2.7: Impacts of the Freestyle Libre 2 normalised with the total characterisation result. The two main hotspots appearing are the ICs and the applicator. In the MRD category, the battery dominates largely.

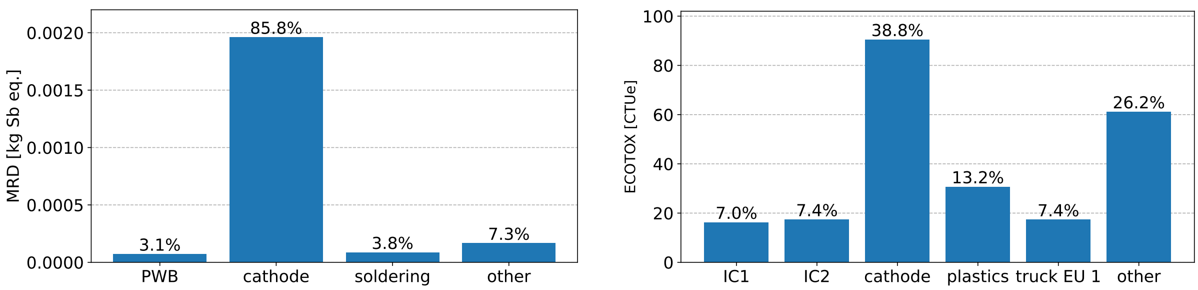

(a) MRD

(b) ecotoxicity, freshwater (ECOTOX)

Figure 2.8: Detailed MRD and ECOTOX impacts for hotspots identification. Only the main contributors to the total impact are detailed, the other contributors are included in the "other" category. In both Figures, the battery silver oxide appears dominant to a large extent.

Chapter 3

Ecodesign Strategies

Based on the hotspots identified in the previous chapter, we propose several strategies to reduce the environmental impact of CGM systems. We begin by hypothesising lower power consumption, allowing for a smaller battery capacity. Next, we address the plastic-related hotspot by eliminating the sensor pack and further reducing plastic use through a strategy that incorporates a reusable applicator.

We then focus on the electronics and battery hotspots and propose three strategies which are cumulative with the reusable applicator strategy: (i) We propose to extend the lifetime of the device from 14 days to over a month using a bigger battery, a strategy supported by CGM power profiling. (ii) We suggest reusing the ICs by dividing the CGM into a reusable and a single-use parts, a strategy supported by reverse engineering the electrical schematic of the device. (iii) We propose to implement a rechargeable CGM, supported by a comprehensive analysis of wireless charging technologies to select an appropriate commercial charger.

Each strategy is presented with a context, complementary research on relevant topics when necessary, and the hypothesis we made. Further technical details and parameter values necessary for implementation are provided in Appendix B.

3.1 Strategy 0: Smaller Battery Capacity and Consumption

An intuitive assumption might be that simply reducing the power consumption and replacing the battery with a smaller one, potentially using fewer materials and having a lower overall environmental burden, would result in significant environmental benefits. To test this idea, we implemented a first ecodesign strategy, called **Strategy 0**.

Hypothesis

The engineering team has managed to optimise the sensor power consumption, reducing it from 50μA to 30μA. This reduction in power consumption allows the use of a smaller battery with a lower capacity, while maintaining the same operating lifetime as the reference (14 days).

More specifically, the original battery is replaced with a 1.5V model with a standard discharge current of 30μA and a capacity of 16mAh. This corresponds to approximately

533 hours, or 22.2 days of operation (from which a security margin is taken ensuring 14 days of normal operation).

In this strategy, we made the strong and somewhat idealised assumption that consumption is reduced without any intervention. This means that only the battery is replaced with a smaller one, while all other aspects of the device, such as its design, electronic components, and usage conditions, remain unchanged. This simplification allows us to isolate and evaluate the environmental impact of the battery itself, without introducing additional variables. The modifications made in Strategy 0 are summarised in Figure 3.1, and the corresponding values are given in Table B.3.

The new battery (see Table B.1) is smaller and lighter, but this change in mass is considered too small to have a significant impact on the transport and is therefore neglected.

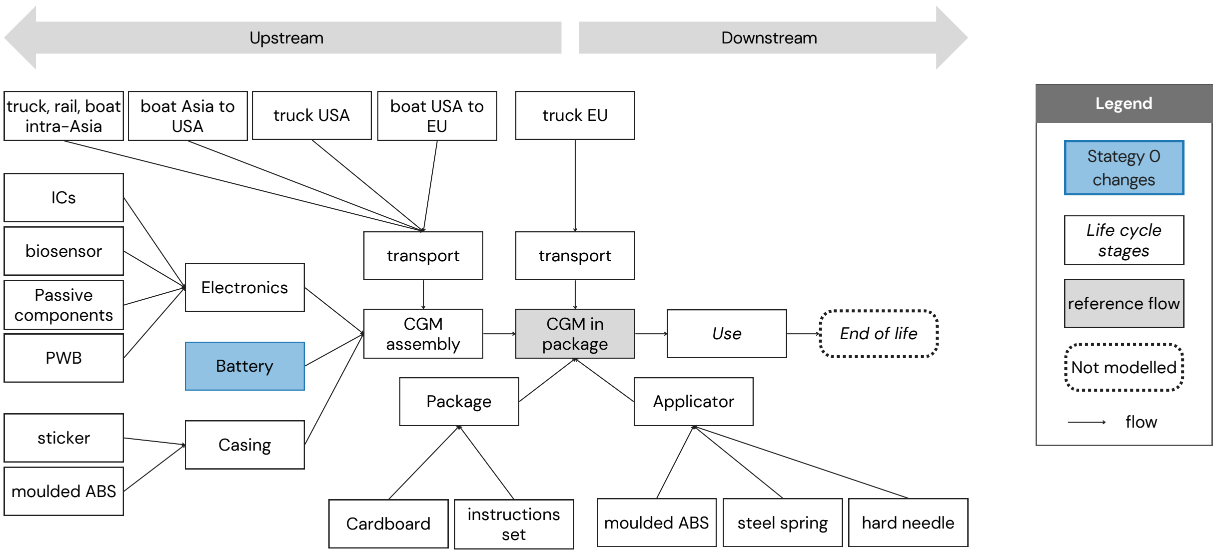

Figure 3.1: Strategy 0: foreground model with related changes. According to our hypothesis, only the battery changes for this strategy. The CGM lifetime remains 14 days and a smaller battery capacity allows to cover the reduced energy consumption.

3.2 Applicator Design

3.2.1 Strategy 1: Single-Piece Applicator

As part of the company's commitment to sustainability, Abbott has improved the design of the latest generation of its CGMs to reduce their environmental impact. As shown in Figure 3.2, the FL3 sensor is more compact than the previous model, achieving a 70% reduction in volume, including a 41% reduction in plastic use and a 43% reduction in cardboard packaging [31].

Strategy 1 is based on this approach and redesigns the FL2 applicator, while keeping the sensor itself unchanged. To reduce plastic use, this strategy focuses on eliminating the separate sensor pack by integrating the applicator into a single component.

Figure 3.2: Comparison between Abbott's FL2 and FL3 [45]. The applicator of the FL2 is in two pieces. Strategy 1 is inspired by the single-piece applicator of the FL3.

Hypothesis

The CGM is still the FL2 sensor, and no changes are made to the casing, electronics, or battery. The applicator is redesigned to be in one piece, which reduces the amount of plastic used. As a consequence, the package becomes smaller and lighter, which in turn affects the transport stage. Specifically, since the device and applicator are assembled in the United States before shipment, the lighter packaging results in lower transport-related environmental impacts.

All modifications considered in this strategy are illustrated in Figure 3.3, and the detailed numerical values are provided in Table B.4.

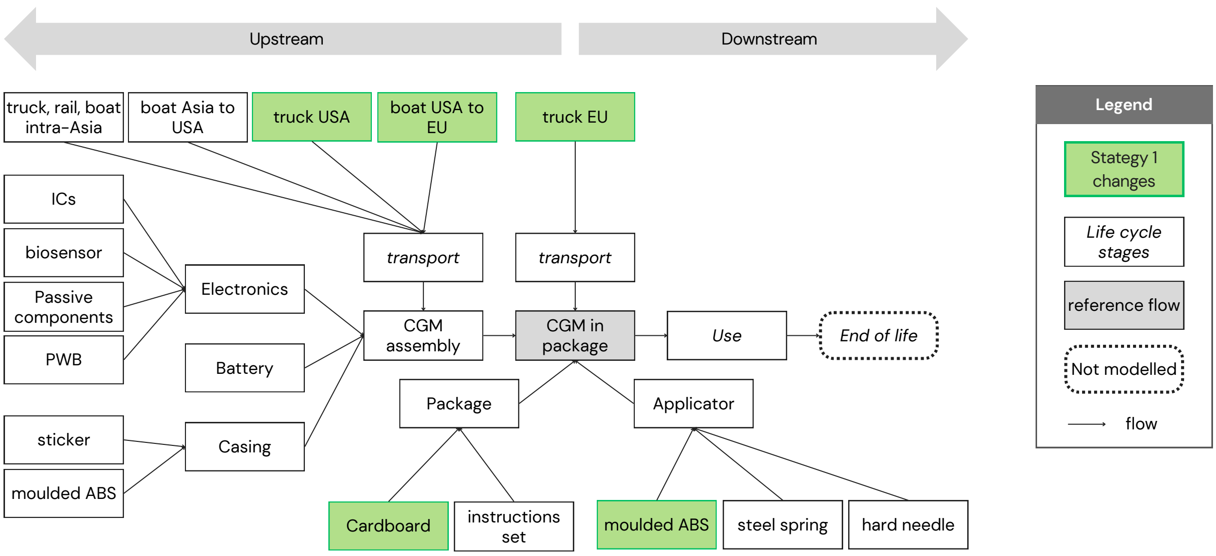

Figure 3.3: Strategy 1: foreground model with related changes. The sensor pack is removed so the applicator is in one piece. This reduces the amount of plastic (moulded ABS) in the applicator design. The cardboard packaging is smaller and lighter because of the reduced volume of the system and mass of plastic used.

3.2.2 Strategy 2: Reusable Applicator

When comparing Figure 4.4c with the reference (Figure 4.4a), it is clear that the applicator is no longer a hotspot but it still holds an accountable share of the total impacts. Moreover, plastic reduction is one of the easiest targets for our ecodesign lever as demonstrated by the FL3 design. While the current applicator does not contain components with a limited lifetime, it includes a needle that cannot be reused due to hygiene and safety standards. However, as reusable lancing devices already exist for SMBG, the possibility of a reusable CGM applicator should be investigated.

Strategy 2 proposes a new design with a reusable applicator and a single-use needle. Every two weeks, when a new CGM sensor is needed, a sterile disposable needle is also provided in the same box. The applicator is shipped only once and we hypothesise that it lasts for two years.

Figure 3.4 shows a comparison between the FL2 applicator design and an existing SMBG lancing device [46]. It suggests that almost all the necessary components, such as a spring and plastic mechanisms, are already present. Only small adjustments would be necessary to allow the needle to be detached and replaced. The new needle would be supplied with a protective plastic cover to ensure sterility like blood lancets used with lancing devices [47], as illustrated in Figure 3.5.

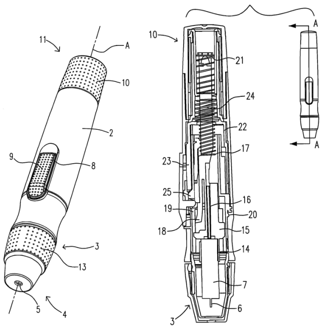

(a) SMBG lancing device [46]

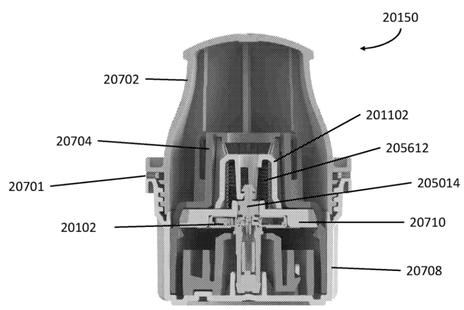

(b) FL2 applicator [43]

Figure 3.4: The compared designs for SMBG and FL2 shows that material components are similar: plastics, steel spring and needle. The objective of the FL2 applicator is similar to that of the SMBG lancing device: it triggers a spring to prick the skin with a needle. Therefore, it should be possible to design a reusable applicator for the FL2.

(a) Blood lancet with needle covered by a plastic casing [47].

(b) FL2 applicator needle [48].

Figure 3.5: The comparison of the single-use needles for SMBG and CGM technology shows that a protection can be added to guarantee a sterile needle. This would make it possible to replace the needle in the FL2 applicator and ship it with a protective casing to ensure safe usage.

Hypothesis

This strategy keeps the single-piece applicator from Strategy 1. The CGM device remains unchanged (still the FL2 sensor) meaning that no modifications are made to the casing, battery, or electronics. To ensure the reusability of the applicator over two years, it is assumed that additional plastic is required, with an estimated increase of 10% to 30% compared to the original applicator design. The reusable applicator is packaged separately and shipped once at the beginning of the two-year period. The size of the box may vary by ±20% relative to the original packaging.

Each disposable needle, protected by a plastic cover, is delivered together with the CGM sensor every two weeks, also in a box that may be slightly smaller or larger (±20%) than the original sensor packaging. An instruction leaflet continues to be included in every box. Lastly, all transport-related parameters are adjusted to take into account the less frequent shipment of the applicator and the delivery of needles with each sensor.

All the modifications associated with this strategy are illustrated in Figure 3.6, and the detailed numerical values are provided in Table B.5.

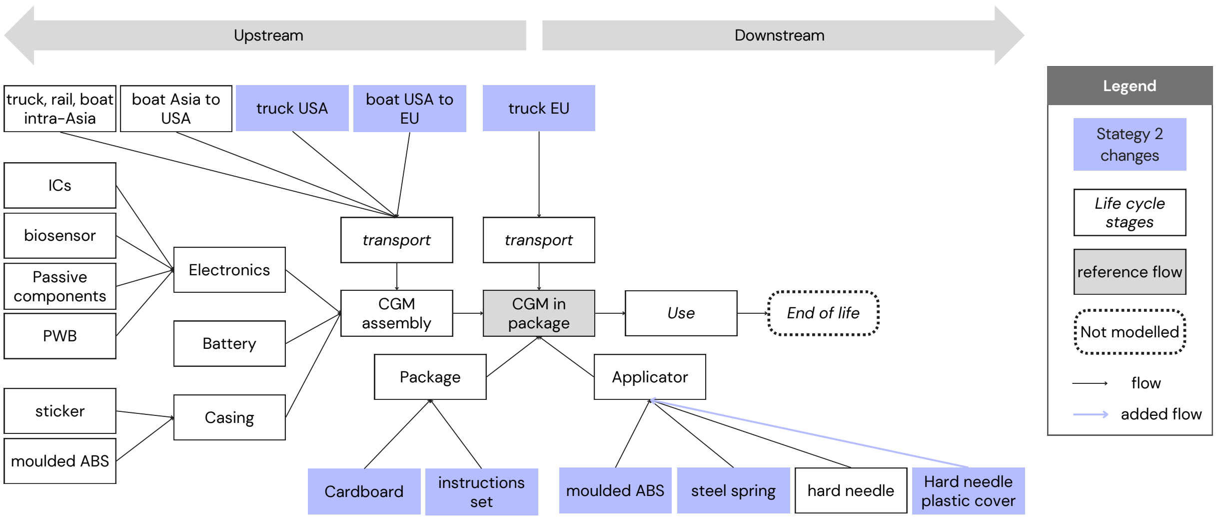

Figure 3.6: Strategy 2: foreground model with related changes. The applicator is single-piece and the plastic mass increases because of the new reusable design. The single-use hard needle is protected by a plastic cover to be replaced every two weeks in the applicator. The package and instructions set have been updated to allow the applicator to be transported separately from the CGM and single-use hard needle. The transports are adapted in consequence of the package changes.

3.3 Strategy 3: Extended Lifetime

The reusable applicator introduced in Strategy 2 greatly reduces the environmental burden of the applicator, as shown in Figure 4.4d. The next major contributors to the overall impact are the ICs and battery, which are part of the CGM device itself. One straightforward way to reduce their impact is to extend the device's lifetime, thereby reducing the number of times the battery and ICs need to be replaced. In order to determine how much the device's lifetime could be extended, it is necessary to identify which component is most likely to fail first. Although the enzyme-coated biosensor needle could be a limiting factor, for the purpose of this study we assume that it is not.

Given that ICs and electronics typically have long lifetimes, the battery is the next most likely limiting component and the one on which **Strategy 3** will focus. To extend the device usage period, we propose using a battery with a larger capacity. However, understanding the actual power consumption of the device is crucial to determine the required battery size.

3.3.1 Battery Power Profile

We perform a power profiling of the CGM with two main objectives: (i) to better understand the power consumption of the device in different modes of operation (sleep, calibration, and communication with the smartphone), and (ii) to identify the main sources of power consumption. This analysis will help determine the average power consumption and define the requirements for achieving an extended device lifetime.

First, we analyse the power consumption of the ICs to better understand our results. Then, we use power profiling data from the literature to complement and contextualise our own results. Next, we describe the measurement setup, which is based on the following studies [27, 28]. In these works, the CGM was placed in a solution that mimics interstitial fluid ISF in vitro to characterise amperometric glucose sensors for ISF measurements. Finally, we present our results and interpretations.

Power Consumption of the ICs

As detailed in Section 3.4.1, we identify that the sensor integrates two chips: the **RF430** [49] and the **EM9304** [50]. The RF430 is responsible for data processing and NFC communication, while the EM9304 handles BLE communication.

According to the datasheet [49], the RF430 operates at 1.5 V and supports multiple power modes. The power consumption varies depending on the memory in use (e.g. ROM or FRAM) and the clock frequency. Table 3.1 summarises its current consumption.

Operating Mode	Current Consumption / Time
Active (ROM, 1 MHz)	220 µA (typ.)
Active (FRAM, 2 MHz)	580 µA (max.)
Low Power Mode 0 (LPM0)	190 µA
Low Power Mode 3 (LPM3)	13 µA
Low Power Mode 4 (LPM4)	12 µA
Wake-up from LPM0	3 µs
Wake-up from LPM3/LPM4	up to 300 µs

Table 3.1: Summary of RF430 current consumption at 1.5 V for active and low-power modes. The maximum and minimum wake-up times from Low Power Mode (LPM) modes are also shown.

The EM9304 BLE chip has multiple power saving modes. The datasheet [50] lists the different current consumptions, as shown in Table 3.2, for an operating voltage of 3 V only.

These values (Tables 3.1, 3.2) represent theoretical current consumption under ideal conditions. In real operation, higher current may be observed due to custom modes of operation or simply non-ideal conditions.

To measure power consumption with high temporal resolution, we use the **Keithley DMM7510** digital multimeter, capable of sampling at up to 1Msample/sec (1 µs resolution) [51].

Operating Mode	Current Consumption
Chip Disabled	5 nA
Deep Sleep	650 nA (typ.)
Connected Sleep Mode	1 µA
Peak RX Current	3 mA
Peak TX Current (0.4 dBm)	5.2 mA
Max Battery Current Draw	< 12.5 mA

Table 3.2: Summary of EM9304 current consumption at 3 V for different operating modes.

Power Profile of Sensor in Literature

As an example of expected results, we look at the power profile of a sensor node in [52], represented in Figure 3.7. It shows the energy consumption of a wireless sensor node (WSN). The sensor measures temperature and acceleration, and processes the data to compute the speed of rotation. Then, it sends the result twice per second in BLE packets via advertisement. We expect to see similar patterns for BLE advertisements, data processing and sensing. However, the frequency of operation and power consumption will depend on our application. The FL2 takes measurements of glucose levels every minute [53].

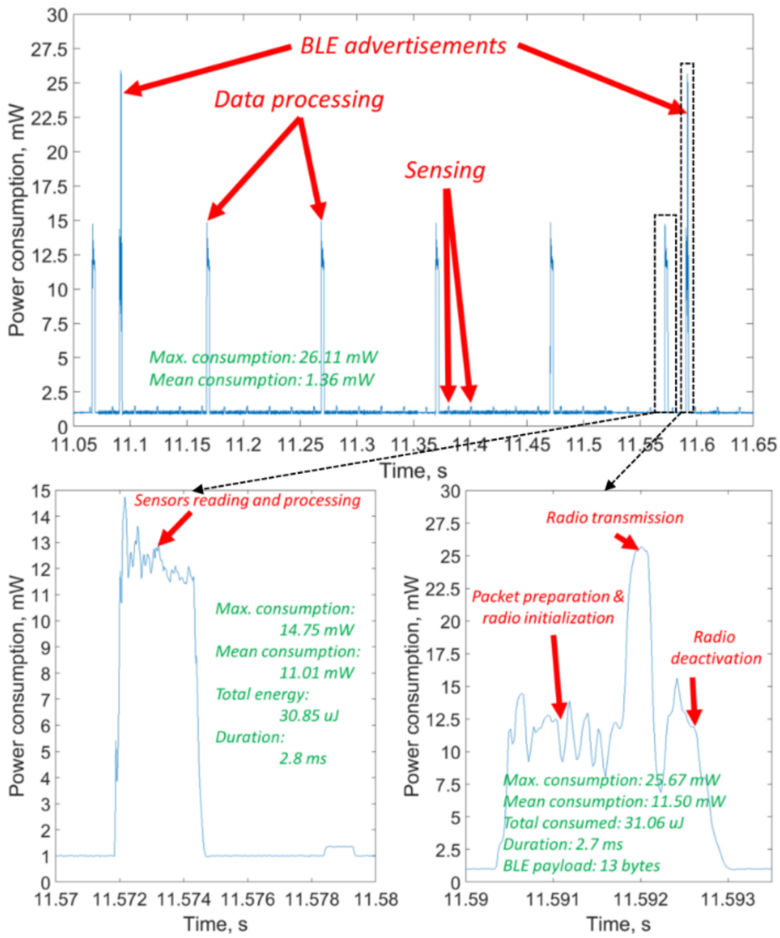

Figure 3.7: Power profile of a WSN in literature [52]. The sensor sends the result twice per second via BLE. We observe three operating modes: BLE advertisements, data processing and sensing.

Experimental Setup

We proceed as if we were using the sensor on a patient. However, instead of inserting it into the skin, we simply trigger the applicator and recover the sensor. Then we drill a small hole into the sensor casing to remove the battery. After this, we solder two wires to the cathode and anode terminals.

To mimic ISF, as described in [27, 28], we prepare a 10 mM phosphate buffered saline (PBS) solution with a pH between 7.2 and 7.4. Glucose is added to reach a concentration of 90 mg/dL (equivalent to 5 mM), which represents a normal ISF glucose level, ah shown in Figure 3.8.

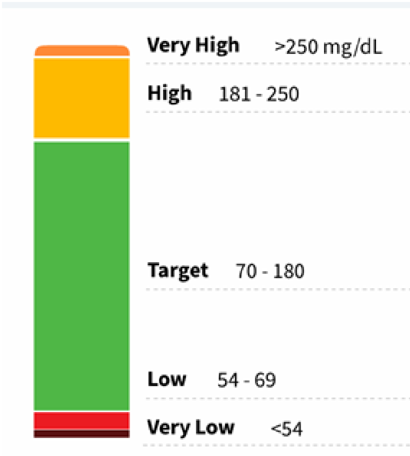

Figure 3.8: Glucose levels in ISF [54]. The target level for healthy patient is between 70 and 180 mg/dL. Our PBS solution has a glucose concentration of 90 mg/dL.

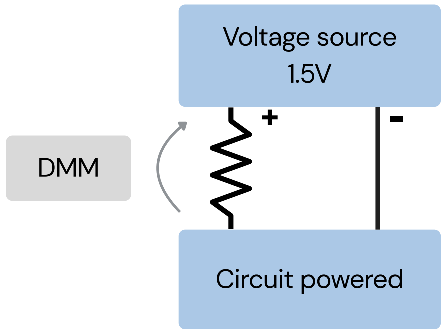

Figure 3.9: Experimental setup schematic. The sensor is powered by a 1.5V source. A known resistor is used as a shunt to measure the voltage drop across it and derive the current consumption of the load.

The sensor is powered using a 1.5 V source through a shunt resistor. Then it is placed into the PBS solution, ensuring that only the needle is immersed. To prevent liquid going into the casing, the solution is covered by a parafilm. The schematic of the experimental setup is shown in Figure 3.9.

As illustrated in Figure 3.10, we measure the voltage drop across the shunt resistor. We choose to measure the voltage instead of the current directly to ensure that the sensor is continuously powered.

The measured voltage drop across the resistor allows us to compute the current using Ohm's law, $I = \frac{V}{R}$, and the power consumption as $P = \frac{V^2}{R}$.

Careful resistor selection is critical for accurate measurements. If the resistance is too small, the voltage drop may fall below the oscilloscope's noise floor, leading to inaccurate readings. If too big, the sensor may not receive enough voltage to operate.

The standard discharge current of the battery is 50 µA at a nominal voltage of 1.55 V [55]. We determined that a maximum acceptable voltage drop is 100 mV. With a 5.8 Ω resistor and a peak current of approximately 15 mA (EM9304 operation in Table 3.2), the resulting voltage drop is around 87 mV.

At the nominal current of 50 µA, the expected voltage drop is:

$$V = R \cdot I = 5.8\,\Omega \cdot 50\,\mu\text{A} = 290\,\mu\text{V}$$

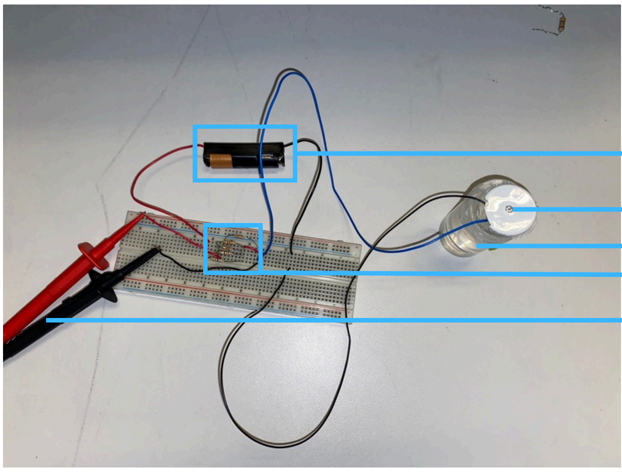

Figure 3.10: A picture of the experimental setup shows the FL2 in a PBS solution with added glucose. The sensor is powered by a 1.5V battery. Shunt resistors are placed to measure the voltage drop using the DMM probes.

To increase the resistance if necessary, we place multiple resistors in parallel that we can remove. This would help to see lower current events.

We use a Keithley DMM7510 and follow the application note [56] to measure ultra low power in WSN application.

Power Profile Results

We start by determining the minimum resolution necessary to observe the different operating modes and to measure an accurate average power. By downsampling a 100μs resolution sample under normal conditions, we compare the effect of different resolutions, see Figure 3.11. The average power over the 100 second sample is not significantly affected by the resolution until 10ms. At 10ms resolution, the signal pattern becomes unclear and the average power decreases by 2μW compared to 78μW at higher resolutions.

We use a minimum resolution of 1ms for our measurements. There is a trade-off between resolution and the duration of the measurement. We want sufficient resolution, but longer measurement durations generate more data points, and handling large volumes of data can become challenging.

Before presenting the power profiling results, we have a few comments and observations. We measured lower glucose levels than expected, but still sufficient to avoid triggering alarms. We explain this to a key factor we did not consider: the **temperature**. Because temperature affects the speed of chemical reactions, it may have slowed the RedOx reaction, resulting in lower glucose level readings.

We did not observe any change in power consumption when alarms were triggered, either due to distance or glucose levels. This is likely because the alarm processing is handled by the smartphone application rather than the sensor device.

We also did not observe any change in power consumption while scanning the device, likely due to the passive nature of NFC communication. Therefore, we focus on the BLE operating modes, including the power profile with and without [1] pairing the sensor to the

[1] We will also write 'without connection' for the situation where the sensor and the smartphone are not

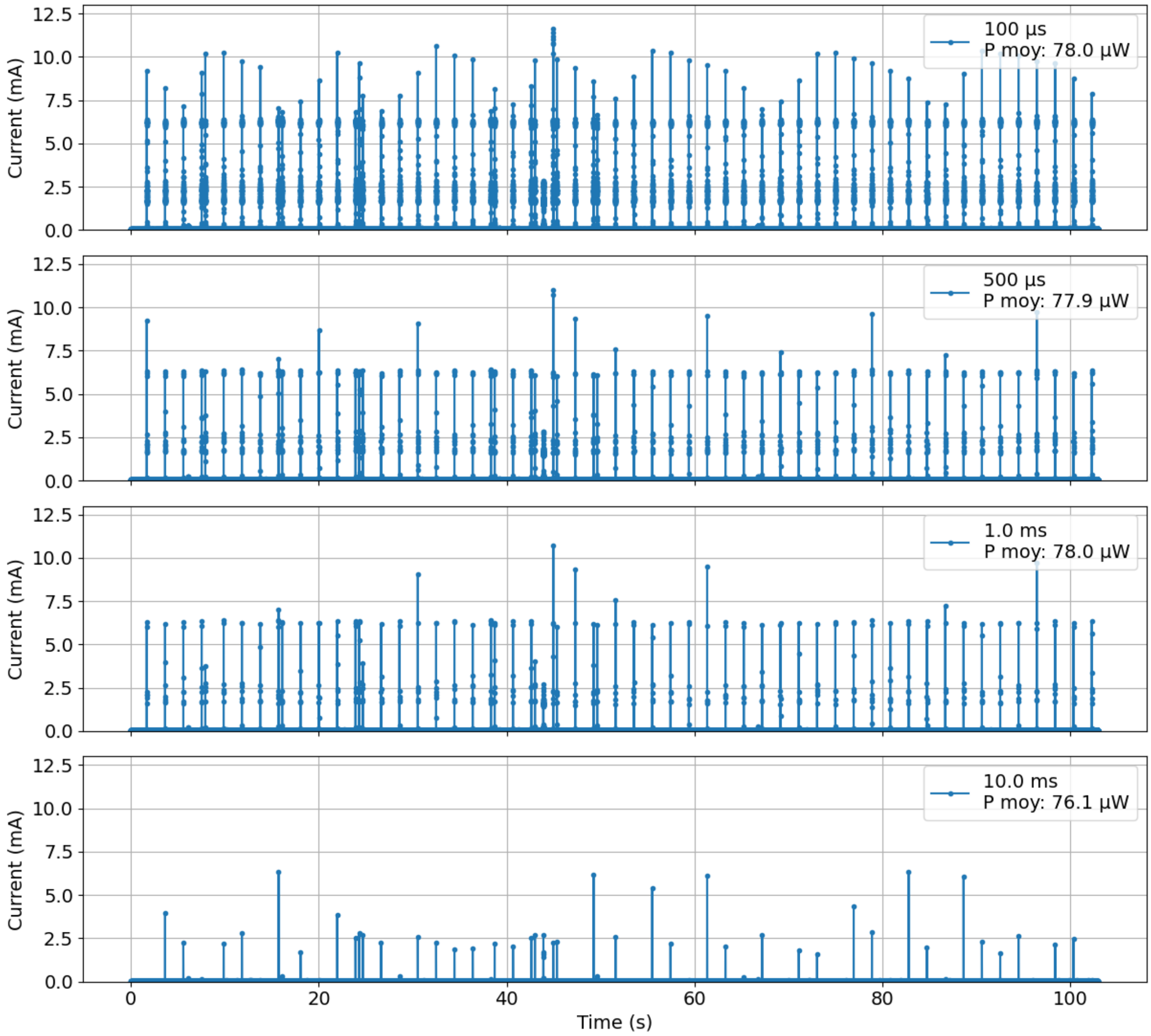

Figure 3.11: 100s of measure without any alarm or scan. Same measurement downsample at different resolution.

smartphone, as well as the effect of distance on power consumption.

The operating modes under normal conditions (good glucose levels, no alarms, no disconnection) are extracted from Figure 3.7 and the power consumption data of the components. We hypothesise about the operating modes, as shown in Figure 3.12a. The FL2 measures glucose levels every minute [53], and large TX peaks occur every 60 seconds (also confirmed in longer measurement samples), so it supports our hypothesis. According to the datasheet summarised in Table 3.2, TX peaks are expected to be the most power-consuming events (around 5.2mA at 0.4dBm), followed by RX peaks (3mA), as observed in 3.12a. The average current required to power the sensor is 49.7μA, which closely matches the 50μA standard discharge current of the battery in the FL2 (see Section 3.4.1).

The operating modes without BLE connection are shown in Figure 3.12b over a

paired. It refers to the experimental setup, where we simply turn off the Bluetooth of the smartphone to trigger the reconnection mode.

10-minute period. These are based on the same hypothesis as normal conditions shown in Figure 3.12a. A large peak appears every 2 minutes, likely a reconnection attempt, a TX peak. Medium-sized peaks, possibly signal processing, appear every minute (both before and between large peaks). The overall mean current without BLE is lower than with BLE, 42.8μA.

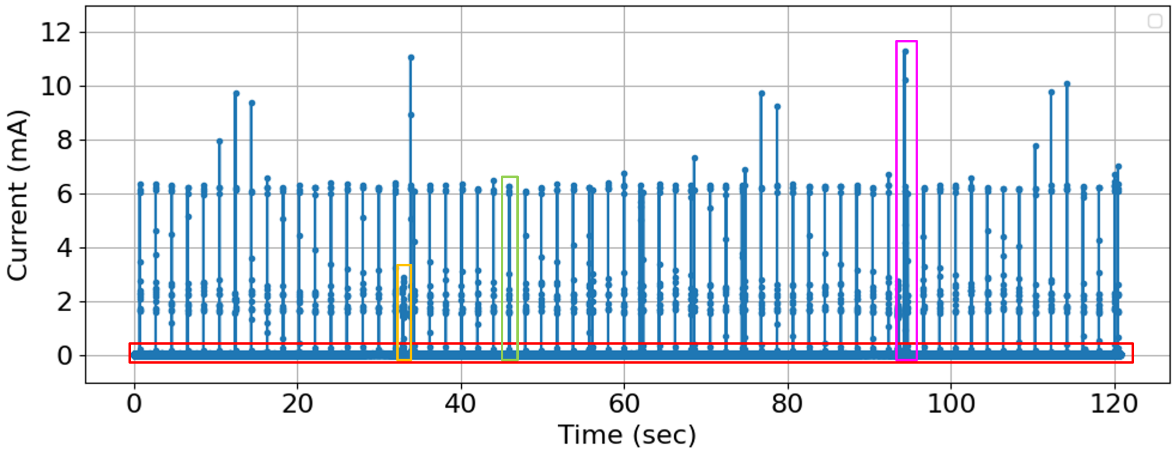

(a) Sensor normal operation (2 min, 500μs resolution). Pink: BLE transmission (TX), Green: BLE reception (RX), Yellow: signal processing, Red: sleep and sensing. Mean current = 49.7μA.

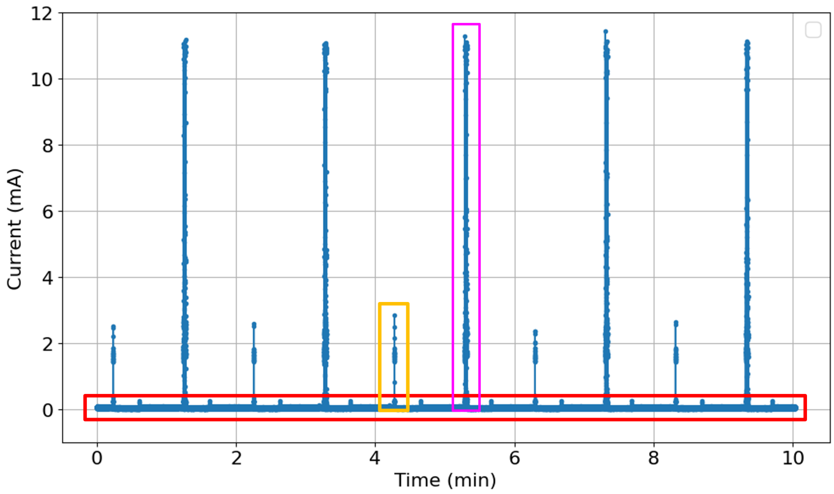

(b) BLE disconnection (10 min, 1ms resolution). Pink: BLE advertisements (TX), Yellow: signal processing, Red: sleep and sensing. Mean current = 42.8μA.

Figure 3.12: Typical operating behavior with and without BLE connection, showing different operational modes indicated by color.

Then, to characterise their current consumption with and without BLE connection, **we zoom in on the operating modes** TX, RX, signal processing, and sleep & sensing.

We analyse the BLE TX peaks, which appear every minute and are greater than 10mA, when the device is paired. The pattern is shown in Figure 3.13a. Since the 500μs resolution does not provide sufficient detail for this measurement, we use a higher resolution of 100μs. We estimate the power consumption during BLE transmission to be 3.9mA. When the smartphone connection is lost, the sensor sends advertisement packets every two minutes to re-establish the connection, as shown in Figure 3.13b. The current consumption is 0.4mA but with a longer duration of 2 seconds.

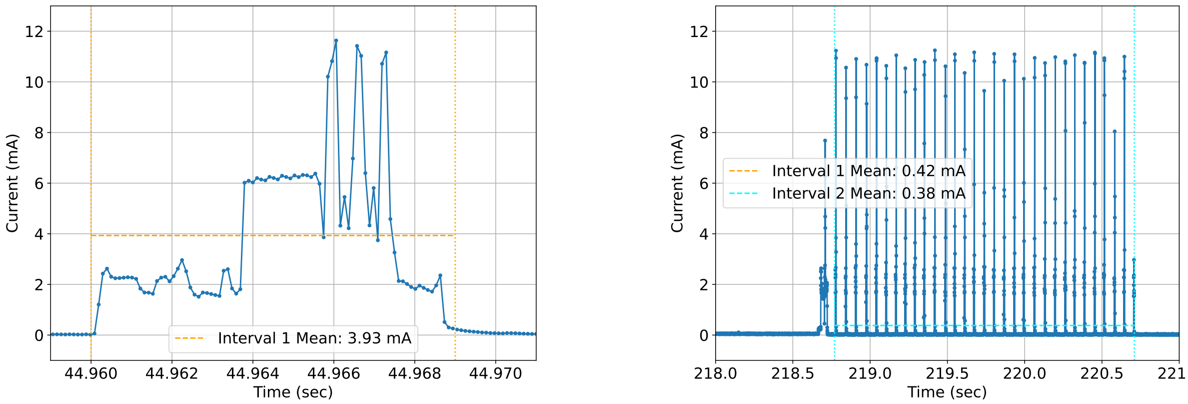

(a) BLE TX peak at $100\mu s$ resolution. The average current during transmission is 3.9mA.

(b) BLE advertisement peaks, Resolution $500\mu s$. 2 intervals are chosen with a mean power of 0.4mA and one of them is shown.

Figure 3.13: BLE transmission (TX): (left) with established connection; (right) advertisement peaks during reconnection attempts.

BLE RX peaks are shown in Figure 3.14, and are observed when the connection is established. They occur approximately every 2 seconds and are smaller than TX peaks, ranging from 7 to 10mA. These peaks disappear when the connection is lost, suggesting that they correspond to data received from the smartphone.

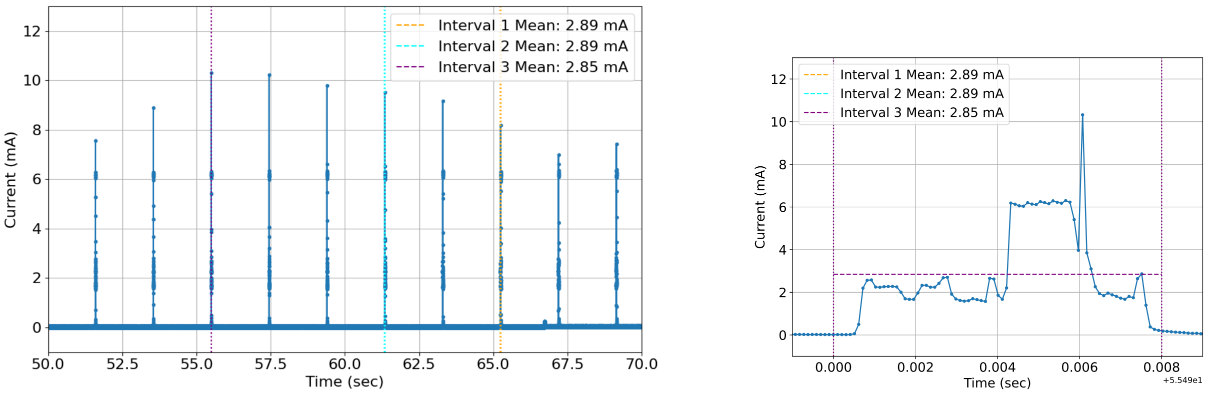

(a) BLE RX peaks at $100\mu s$ resolution. Each peak has an average current of 2.9mA.

(b) Zoom on one RX peak at $100\mu s$ resolution. RX peaks have always this shape.

Figure 3.14: BLE reception (RX) peaks observed when the device is paired.

Next, we observe signal processing peaks in Figure 3.15. Figure 3.15a shows signal processing activity when the device is connected via BLE, while Figure 3.15b shows it when the device is disconnected. The resolution differs between figures in 3.15, which may affect the comparison of mean currents.

Finally, Figure 3.16 shows the sleep and sensing modes. Figure 3.16a illustrates the behavior with an established BLE connection, while Figure 3.16b illustrates what happens when the connection is lost. RX peaks significantly influence the mean current values when the device is connected. We observe a periodic pattern lasting one minute: for the first 23 seconds, the mean current is lower, and for the remaining 37 seconds, it is higher. We refer to these phases as sleep and sensing, respectively. Due to the low current levels,

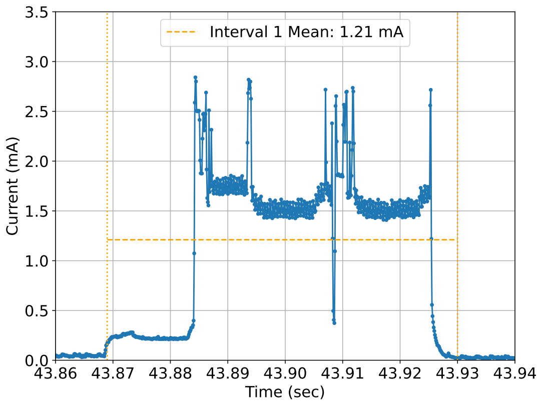

(a) Signal processing with BLE connection, 100μs resolution. The pattern is clearly visible on this high resolution measurement.

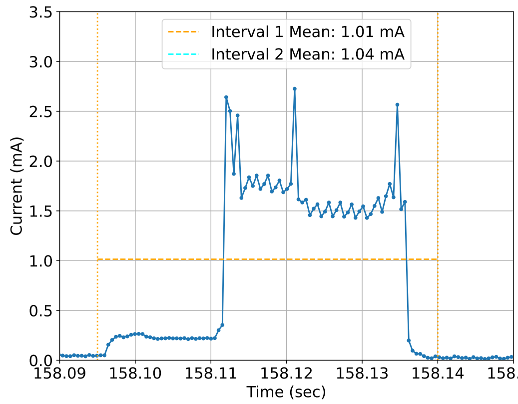

(b) Signal processing without BLE connection, 500μs resolution. Two intervals mean but one is shown.

Figure 3.15: Signal processing peaks with and without BLE connection.

the measurements are notably noisy. We hypothesise that the current during the sleep phase is around 30μA and approximately 50μA during the sensing phase.

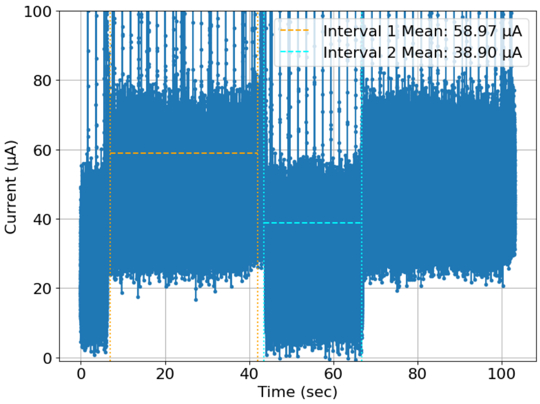

(a) Sleep and sensing with BLE connection, 100μs resolution. RX peaks increase the average power.

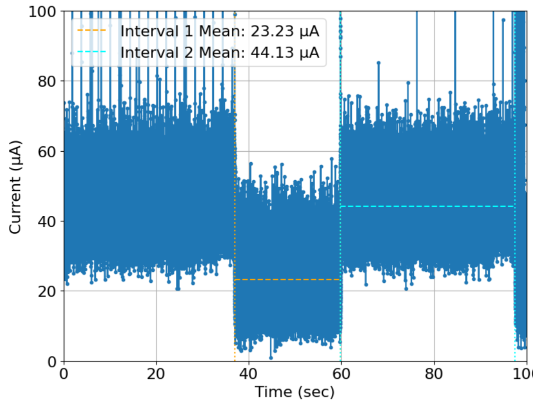

(b) Sleep and sensing after BLE disconnection, 500μs resolution. RX peaks are present in the first 35s, disconnection occurs afterward.

Figure 3.16: Sleep and sensing modes. Similar mean currents are observed, though RX peaks strongly affect the average current measured when connected. The measurements are noisy, likely due to the low level of current observed.

Using all the graphs, we **compare the power consumption for different operating modes**. We approximate the energy consumed by each operating mode with BLE connection (Table 3.3) and without connection (Table 3.4). Based on these values, we observe that the mean current consumption is 55.8μA with connection and 49.4μA without connection. These values are slightly higher than the ones extracted from the Figures, which were 49.7μA and 42.8μA respectively. The difference is likely due to the approximations made in the Tables. These include imprecise timing, estimated current values, and assumptions about the TX, RX, and signal processing durations, which are assumed to be much shorter than the one-minute cycle.

Operating mode	Average current [μA]	Time [s]	Occurrence in 1 min	Energy [μJ]
BLE TX	3900	0.01	1	58.5
BLE RX	2900	0.008	30	1044
Signal processing	1200	0.06	1	108
Sensing	50	37	1	2775
Sleep	30	23	1	1035

Table 3.3: Current consumption and energy consumed with BLE connection for the different operating modes. It is extracted from the experimental measurements. The mean power over one minute is 83.7µW (or 55.8µA in current).

Operating mode	Average current [μA]	Time [s]	Occurrence in 1 min	Energy [μJ]
BLE TX	400	1.9	0.5	570
BLE RX	/	/	/	/
Signal processing	1000	0.045	1	67.5
Sensing	50	37	1	2775
Sleep	30	23	1	1035

Table 3.4: Current consumption and energy consumed without BLE connection for the different operating modes. It is extracted from the experimental measures. The mean power over one minute is 74.1µW (or 49.4µA in current).

Figure 3.17 summarises the Tables to show the proportion of power consumed during a one-minute cycle. The power consumption remains the same in sleep and sensing modes, with or without a Bluetooth connection. These modes are the main source of consumption, representing around 75% of the total consumption. When connected, RX represents a fifth of the total power, while TX represents only about 1%. In contrast, when disconnected, the RX mode disappears, and the TX consumes more than one-fifth of the total power. The communication mode that uses the most power moves from RX communication to the reconnection protocol.

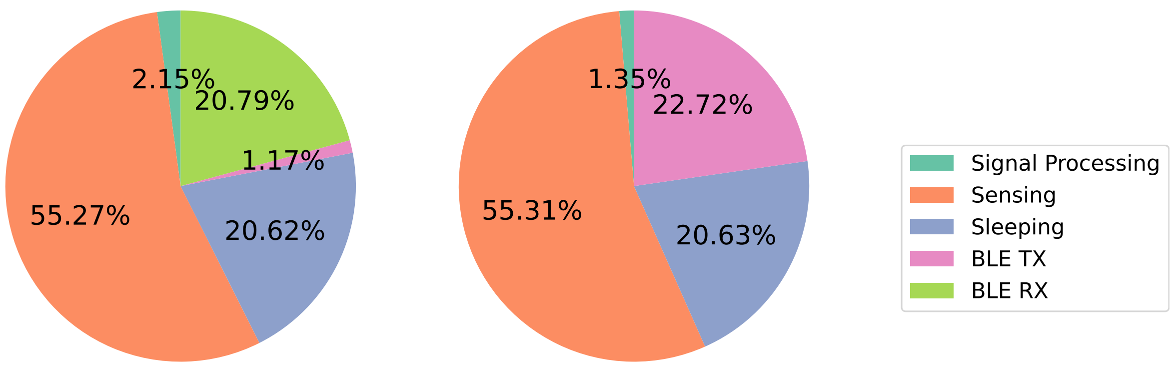

(a) With Bluetooth pairing (b) Without Bluetooth pairing

Figure 3.17: Energy consumed by the different operating modes identified in our measurements. The main contributor are the sensing and sleep modes. The signal processing is the least energy-consuming mode. Consumption of the transmission and reception depend on the pairing status of the sensor.

Then, we analyse **the impact of the distance on the current consumption**. To better understand the disconnection process, we gradually increased the distance between the sensor and the phone until disconnection occurred, while observing the resulting current consumption. Every 30 seconds, the distance was increased by 1 meter. Overall, current consumption increased with the distance. However, since the operating modes are one-minute cycles, the average power increases only when considering one interval against two, see Figure 3.18.

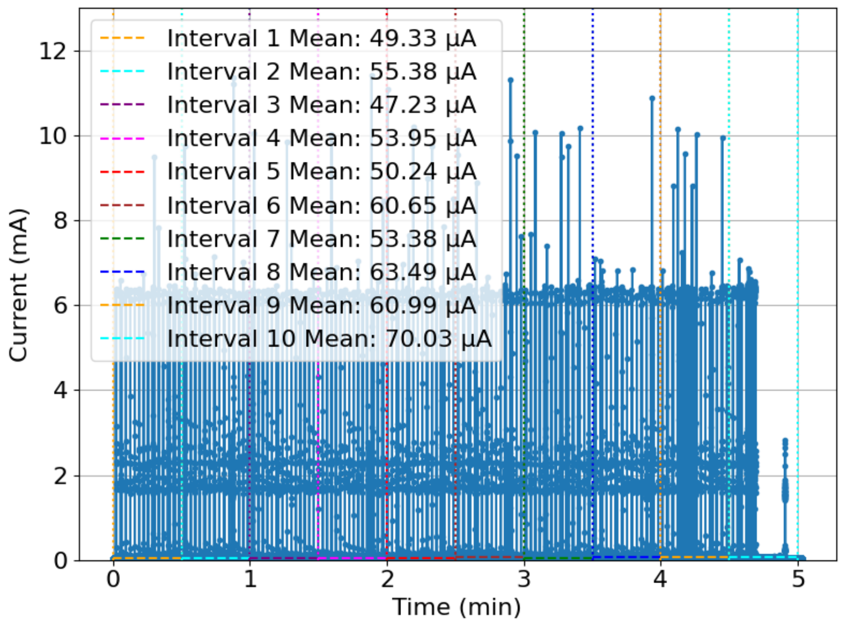

Figure 3.18: Disconnection limit, Resolution $500\mu s$. The phone is moved 1 meter further every 30 seconds until disconnection occurs. Current consumption increases as the disconnection limit is approached.

This analysis highlights **several key points regarding power consumption.** The mode without BLE connection consumes less power overall. The largest portion of power consumption comes from the sensing and sleep modes, which last the longest. Neither alarms nor scanning noticeably affect power usage, only the BLE connection has a significant impact. When the smartphone is near the disconnection limit, power consumption rises. In the worst-case scenario, assuming a constant current draw of $70\mu A$, the 28mAh battery in the FL2 would last about 16.6 days. This is closer to the 14 days lifespan announced by Abbott, providing an explanation on the safety margin.

Hypothesis

Thanks to the battery power profiling, we now have a good understanding of which components influence the battery lifetime the most and how to manage this to extend the lifetime of the entire CGM.

This strategy keeps the reusable applicator from Strategy 2. The casing and electronics also remain unchanged, but are used for a longer period. We assume the needle is not the component limiting the lifetime. Finally, the new battery must still fit onto the PCB and maintain approximately the same height and weight constraints to avoid making the CGM too big or heavy.

The new battery selected [57] has a capacity of 60 mAh with a standard discharge current of 110 μA, compared to the 28 mAh capacity and 50 μA discharge current of the FL2 battery. Since the average consumption of the FL2 has been estimated to approximately

50μA in the last section, the new lifetime can be calculated using Peukert's Law. By applying the same safety margin used for FL2 (66%), we estimate the battery to last approximately 930 hours ($\approx$ 39 days). As a result, only 9.36 devices would be needed each year, compared to the previous 26. The increase in battery weight (from 0.39 g to 0.75 g) is considered negligible for transport impacts.

All the changes are represented in Figure 3.19 and detailed numbers are provided in Table B.9.

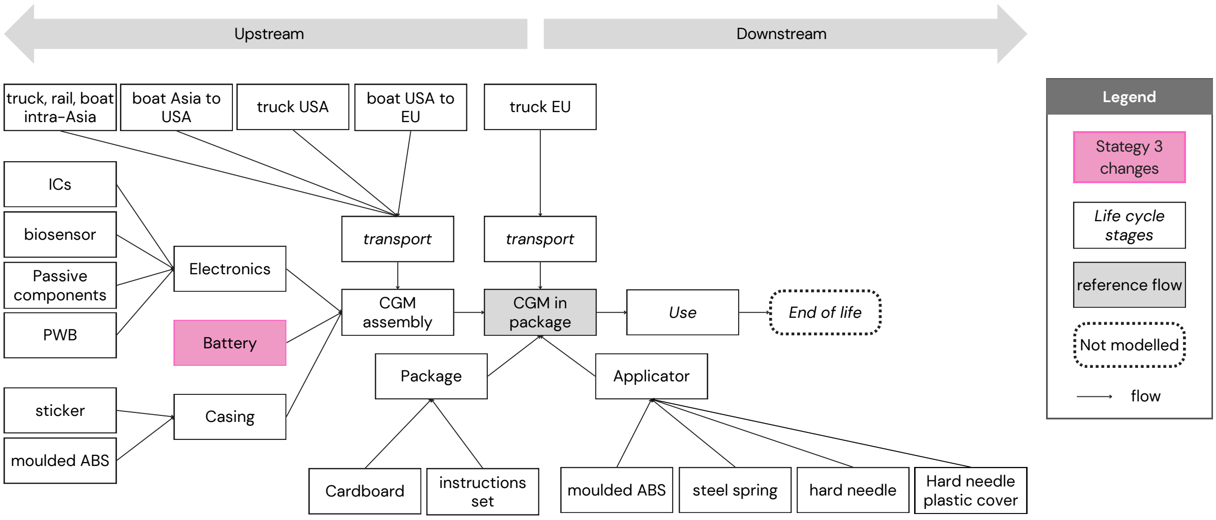

Figure 3.19: Strategy 3: foreground model with related changes. The extended lifetime is achieved by replacing the battery by a new one with a bigger energy capacity. The changes in the foreground model are on the battery side only but the number of devices per year changes as well. 9.36 devices instead of 26 are needed each year.

Peukert's Law

Peukert's law describes the relationship between the rate at which a battery is discharged and its effective capacity [58]. Essentially, higher discharge rates reduce the available capacity in a non-linear way. It was initially developed for lead-acid batteries but also applies to silver oxide batteries as they exhibit similar behaviour [59]. We use this law as an approximation for the battery lifetime. The general form of Peukert's law is:

$$t = H\left(\frac{C}{IH}\right)^k \tag{3.1}$$

where:

t is the actual discharge time (in hours),

H is the rated discharge time (in hours),

C is the rated capacity at that discharge rate (in ampere-hours),

I is the actual discharge current (in amperes),

k is Peukert's constant (dimensionless).

To determine Peukert's constant, we use values provided in the battery datasheet [57], which lists capacities at various discharge rates. The constant can be calculated with the following equation:

$$\frac{C}{C_0} = \left(\frac{t}{t_0}\right)^{\frac{k-1}{k}} \tag{3.2}$$

where:

C and C_0 are capacity values (in ampere-hours),

t and t_0 are the corresponding discharge times (in hours).

Using this relationship, we determine a Peukert's constant of 1.32. Applying this value in Equation 3.1, we calculate that the new battery would last approximately 1544 hours ($\approx$ 69 days) at a discharge rate of 50 μA as illustrated by Figure 3.20. With a 66% safety margin, the estimated effective battery life is 39 days.

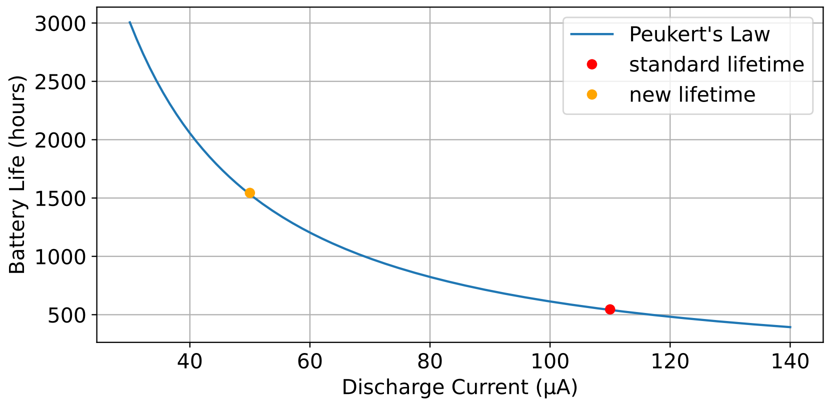

Figure 3.20: Effect of discharge current on battery life (Peukert's Law). The new battery lifetime is adapted from the expected mean discharge current of 50 μA.

3.4 Strategy 4: Reusable IC Module

Although Strategy 3 significantly reduces environmental impacts by extending the device's lifetime, the two main hotspots, the ICs and battery, remain unchanged, as shown in Figure 4.4e.

Instead of increasing the lifetime, another option would be to make the battery replaceable while reusing the ICs. **Strategy 4** achieves this by splitting the original PCB into two parts: one disposable and one reusable. This would enable the ICs to be used multiple times and reduce their impact.

To evaluate the feasibility of this design, we first need a better understanding of the working principle of the original PCB. This is detailed in the following electrical schematic. More specifically, we need to identify which components must be replaced every two weeks and which can be reused.

3.4.1 Electrical Schematic

Based on teardowns of the FL2 device (Figure 3.21) and supported by our own experiments, we analysed the operating principle of the CGM and created an electrical schematic

(Figure 3.23) to illustrate its functionality. Our methodology involved carefully tracing the PCB pathways using a magnifying glass, verifying electrical continuity between traces with a multimeter, and consulting component datasheets to determine the most probable function of each connection. The following explanation is based on informed assumptions and may not accurately reflect the actual design.

As discussed in Section 1.2, the sensor contains three electrodes: a WE, a RE, and a CEl, each connected to the analog interface and surrounded by guard rings [26].

The PCB also includes two ICs, both powered by a 1.5 V battery:

- **EM9304:** A BLE companion or System-on-Chip (SoC), used for Bluetooth communication such as transmitting alarms [50].
- **RF430:** An RFID/NFC sensor transponder that integrates an NFC interface, ultra-low-power MCU, non-volatile FRAM, analog to digital converter (ADC), a temperature sensor, and communication interfaces (SPI/I^{2}C). It is used for scanning via NFC and interfacing with the analog sensing circuit [49].

The sensing system works as follows: a small current in the nanoampere range (see Figure 3.22) that varies with the glucose concentration in the ISF is created at the working electrode via a redox reaction. This current is converted into a voltage via a resistor, then sent through the ADC in the RF430 for digital conversion and amplification using its integrated programmable-gain amplifier (PGA).

Additional technical components and signals in the system include:

- A thermistor connected to the RF430, likely used for body temperature reference and/or calibration.
- **VDDB:** The battery supply voltage, ranging between 1.45 V and 1.65 V.
- **VDD2X:** A voltage doubler output (typically ≈2.9 V) generated by a charge pump using flying capacitors (CP1 and CP2) to step up the 1.5 V battery voltage.
- **VBAT1:** Battery voltage input for the DC-DC converter, requiring a minimum of 2.6 V and supporting up to 3.6 V.
- **ANT1 & ANT2:** Antenna input and output for NFC communication.
- **ADC0:** Connected to the WE as the primary analog input.
- **ADC1/TMP1 & ADC2/TMP2:** Additional ADC inputs, likely connected to the thermistor for temperature sensing or bias.
- **SVSS:** The sensor's analog ground reference, typically around 125 mV, used for accurate ADC operation as it enables amplification of small voltages.
- **TST1 & TST2:** Internal ground references.
- **XIN & XOUT:** Inputs and outputs for the 48 MHz crystal oscillator, required by the RF transceiver for accurate frequency channelling. This oscillator may also act as a clock source.

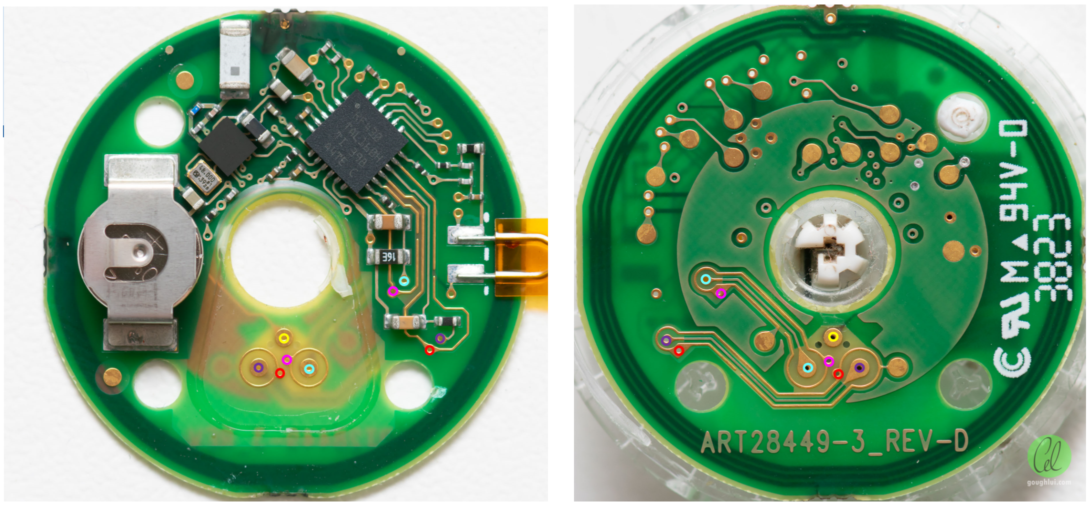

(a) front view (b) back view

Figure 3.21: PCB view of the Freestyle Libre 2, from [48]. The coloured circles annotation indicates a connection between the views. On the front view, the ICs, battery and other electronic components are visible. The three circles below the central hole correspond to the connection with the three electrodes.

- **ANT:** A single-ended antenna for Bluetooth communication, operating at 2.4 GHz. RF components (capacitors and inductors) are included for harmonic filtering and impedance matching.
- **VCC and VBAT2:** Additional analog supply voltages directly connected to the battery.
- **AVSS_PA:** Ground connection for the power amplifier (PA).

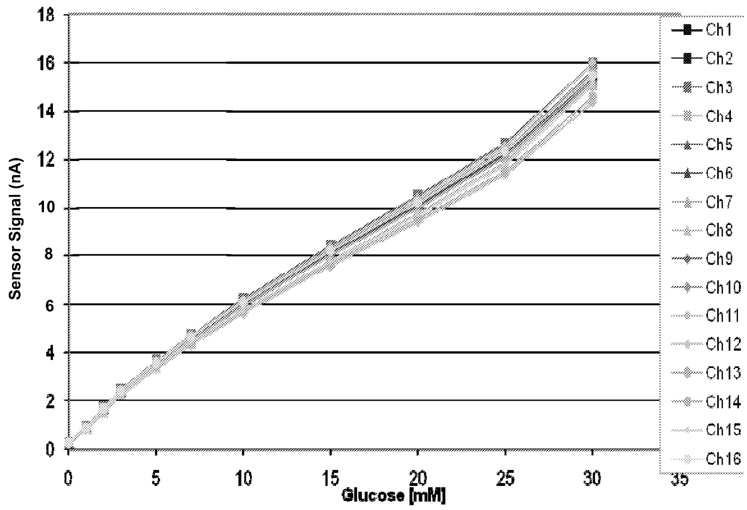

Figure 3.22: Response of the sensor depending on the current signal, from Abbott's patent [26]. The relation between the measured current and the glucose level allows to transform the concentration in a solution in an electrical signal. The current is in the nanoampere range.

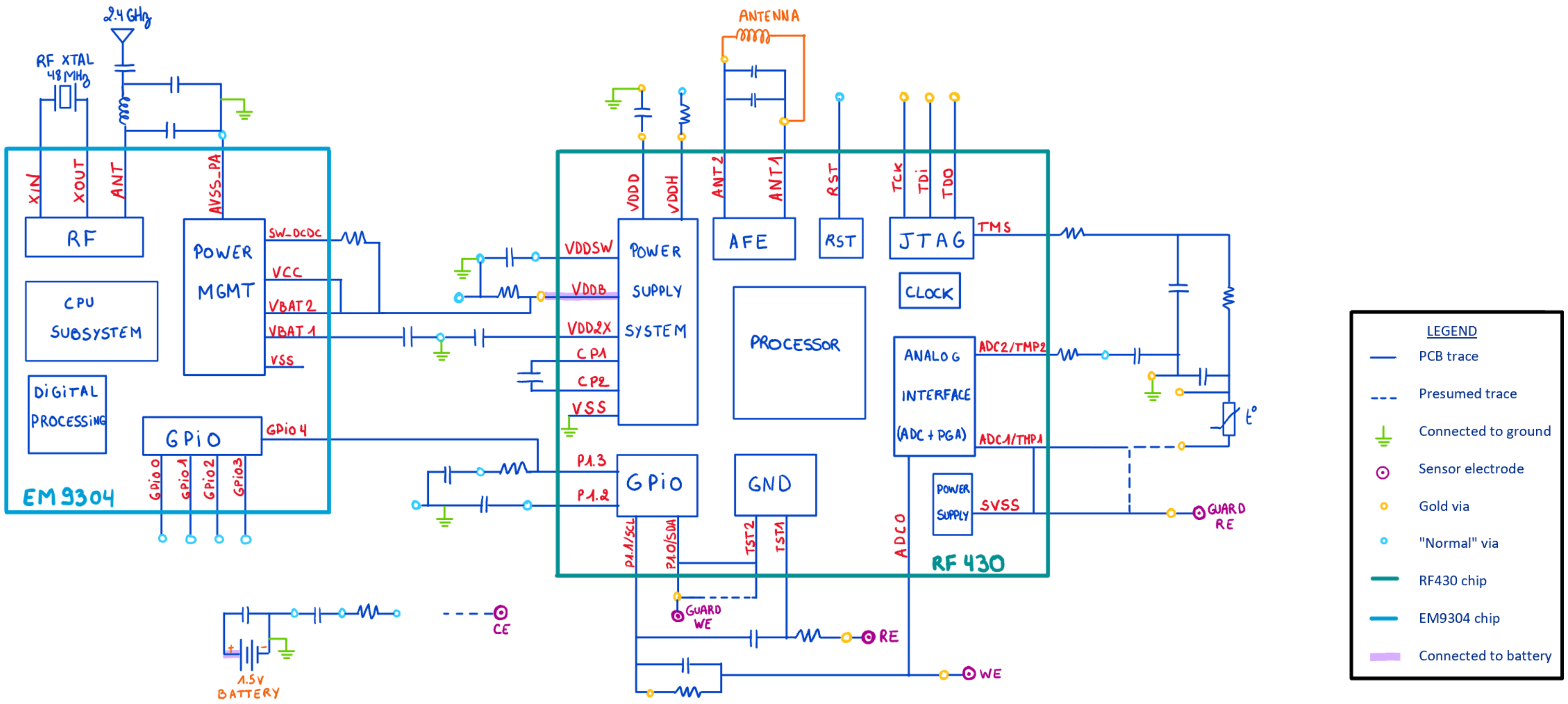

Figure 3.23: Electrical schematic of the PCB inside the FL2 based on datasheets [49, 50] and our own observations of the circuit. The two ICs and their connections with passive components and battery are illustrated.

Hypothesis

Strategy 4 keeps the reusable applicator from Strategy 2 and the same battery. The analysis carried out in the previous section has given us a better understanding of the PCB, allowing us to determine which components can be reused and how to arrange them. The main change thus involves splitting the original PCB into two modules (see Figure 3.24): a disposable module, which includes the battery and sensor needle and is replaced every 14 days, and a reusable module, which contains the two ICs and passive components and has a two-year lifetime.

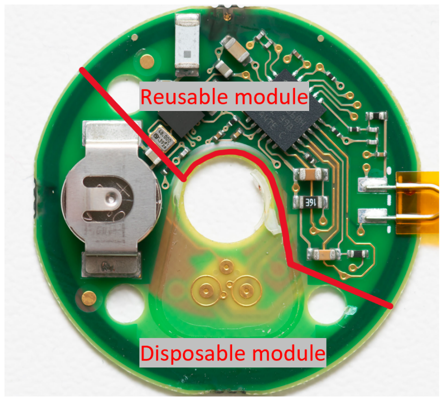

Figure 3.24: PCB split into two parts: a reusable part containing the two ICs and all the passive electronic components, and a disposable module including the battery and the sensor needle.

The disposable part represents approximately 40% of the original PCB size, while the reusable part represents the remaining 60%. The total PCB size may increase by up to 20% and requires additional soldering and a connector to link the two boards.

For this two-part design, the plastic casing is expected to increase by 10% to 50%. However, since only the disposable module with the sensor needle requires an applicator, the applicator size remains unchanged. Regarding transport, a package containing the disposable PCB module and hard needle is sent every two weeks, while a package containing the reusable applicator and reusable PCB module is delivered once every two years.

All the changes are represented in Figure 3.25, and the detailed values are provided in Table B.10.

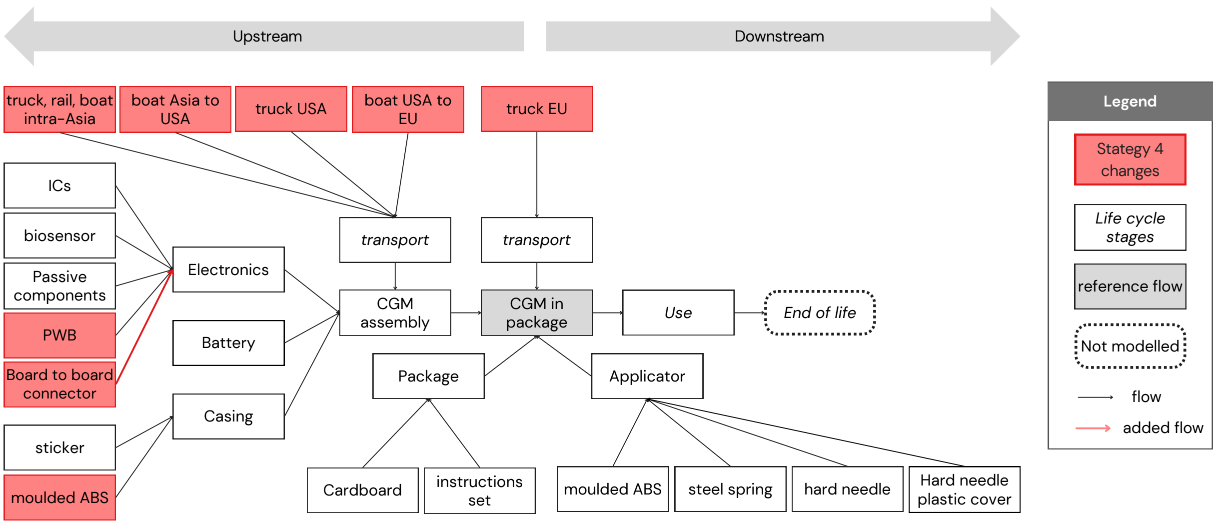

Figure 3.25: Strategy 4: foreground model with related changes. The electronics are split into two PWB: one is reusable and the other is disposable. The connection between those modules is guaranteed by a board to board connector. The amount of plastic in the casing is expected to increase. The transport are split into two categories: once every two years for the reusable parts and once every two weeks for the disposable ones.

3.5 Strategy 5: Rechargeable Battery

As shown in Figure 4.4f, reusing the ICs for two years significantly reduces their environmental impact, shifting the main hotspot to the battery. This raises the question: why not make the entire CGM reusable except for the sensor needle? The battery is one of the main issue because of its limited lifetime so a good option is to replace it with a rechargeable battery.

Inductive charging allows the battery to be charged wirelessly, without the need to open the casing, thus preserving the waterproofing and durability of the CGM. The user can simply place the CGM on a compatible inductive charger to recharge the battery. The following section explains the working principle of inductive charging technology.

3.5.1 Inductive Charger

First, we explain the different technologies used for wireless battery charging and identify the one most suitable for our application. Next, we describe the working principles and limitations of a basic inductive charger. Then, we select a compatible battery for our rechargeable FL2 design. Finally, we present a commercially available charger that is compatible with this new design.

Wireless Charger Technologies

There are three types of wireless power transfer: inductive coupling, electromagnetic radiation, and magnetic resonant coupling [60]. Magnetic resonant coupling and inductive coupling are the most relevant technologies for our design. Inductive coupling is used in applications such as electric toothbrushes and charging pads for cell phones, while implantable devices and WSNs are typically powered by magnetic resonant coupling [60]. Their features are summarised in Table 3.5.

Feature	**Inductive coupling**	**Magnetic resonant coupling**
Operating Principle	Power transfer via magnetic field between two closely spaced coils (Faraday's Law).	Power transfer via resonant magnetic fields between two coils, operating at the same frequency.
Efficiency	Up to ~90% with strong coupling (e.g., coupling factor = 0.7).	High efficiency over greater distances due to resonance.
Distance Sensitivity	Short distances (few cm).	Longer distances (few m).
Alignment Sensitivity	Highly sensitive to coil alignment and proximity.	Less sensitive to alignment due to resonant energy transfer.
Frequency Range	Typically lower frequencies (kHz to low MHz).	Operates in higher frequencies (MHz range).
Advantages	High efficiency when properly aligned.	Better tolerance to misalignment and distance.
Challenges	Precise alignment, high coupling and very close proximity required	More complex design.

Table 3.5: Comparison between inductive coupling and magnetic resonant coupling technologies [60, 61, 62, 63, 64].

We use near-field power transmission because there is a huge loss of power with distance in free space, described by the equation $P_{rad} = \frac{P_S \lambda^2}{4\pi R^2}$ [64].

The output power target determines the choice of wireless power transfer (WPT) technology. For power levels above 1kW, inductive-based systems are typically chosen, while for low power levels under 1W, resonant designs are preferred [61]. Consequently, in our design, we will use magnetic resonance coupling.

Simple Topology: Working Principles and Limitations

The working principles is illustrated by a simple topology of magnetic resonant coupling, as shown in Figure 3.26. The power source supplies an oscillator, which generates a varying magnetic field in the primary coil. A voltage is induced in the secondary coil and converted to DC to power the load.

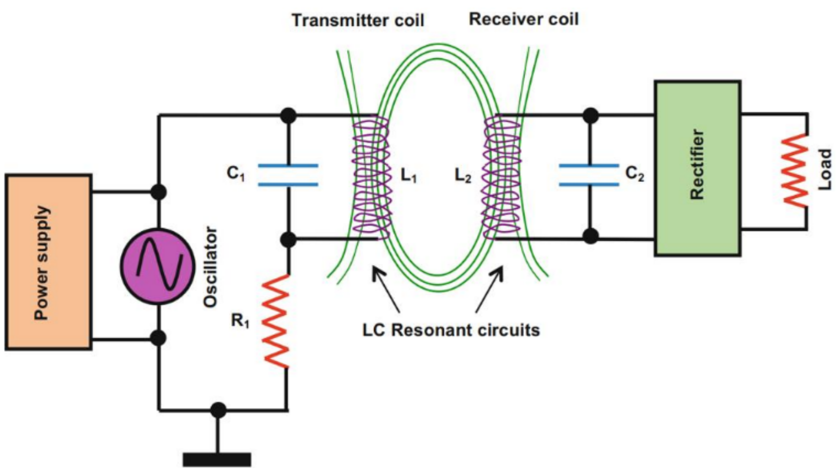

Figure 3.26: Typical resonant circuit topology [64]. An oscillator powered by a source generates an alternating magnetic field in the primary coil. The resulting voltage induced in the secondary coil is converted to DC to power the load.

To illustrate the working principle, we use an LTSpice simulation, shown in Figure 3.27. Our implementation is based on the Qi standard design from [65]. The Qi standard is the reference for WPT and was established by the Wireless Power Consortium in 2010 [61]. It is used to design generic transmitter side chargers compatible with different receivers.

In our simulation for the transmitter, we use a 5V power supply, typical of USB chargers [66]. We apply directly an oscillating voltage and do not implement a full oscillator circuit. The operating frequency is 100kHz, as the example presented in [65] and commonly used in state-of-the-art designs [61]. Typical values for the primary side capacitor and inductor are 100nF and $24\mu H$, respectively, for the TX type A1 (low power Qi standard) [65]. The resonant frequency of the LC tank at the transmitter side is calculated as $f = \frac{1}{2\pi\sqrt{LC}} = 102.7,$kHz, which is within the conventional operating range of 100 to 200kHz for Qi transmitters [61].

On the receiver side, we first select a coil that can be integrated into the FL2. According to [67], the size of the CGM is 35mm in diameter and 5mm thick. On DigiKey, two coils of similar size could be integrated into the device [68, 69]. We chose the first one

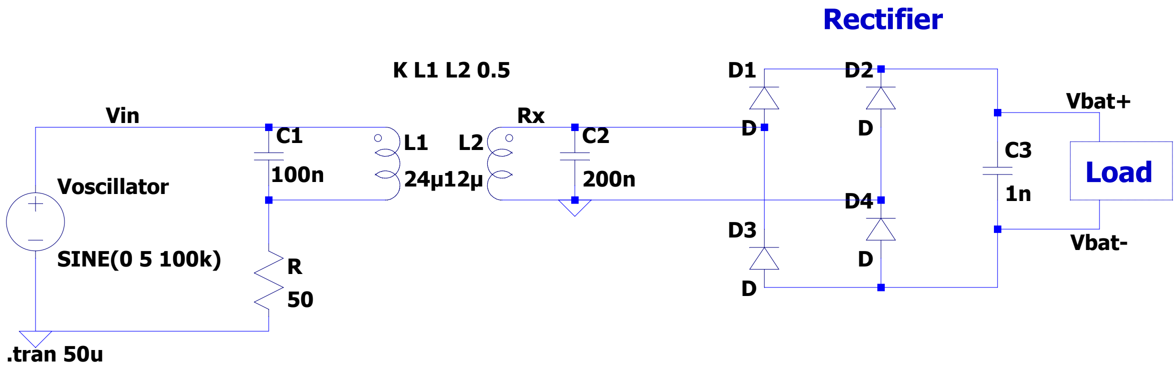

(a) LTSpice resonant circuit inspired by Qi standard design. The circuit is composed of an oscillating supply voltage, two LC tanks, a rectifier and a load.

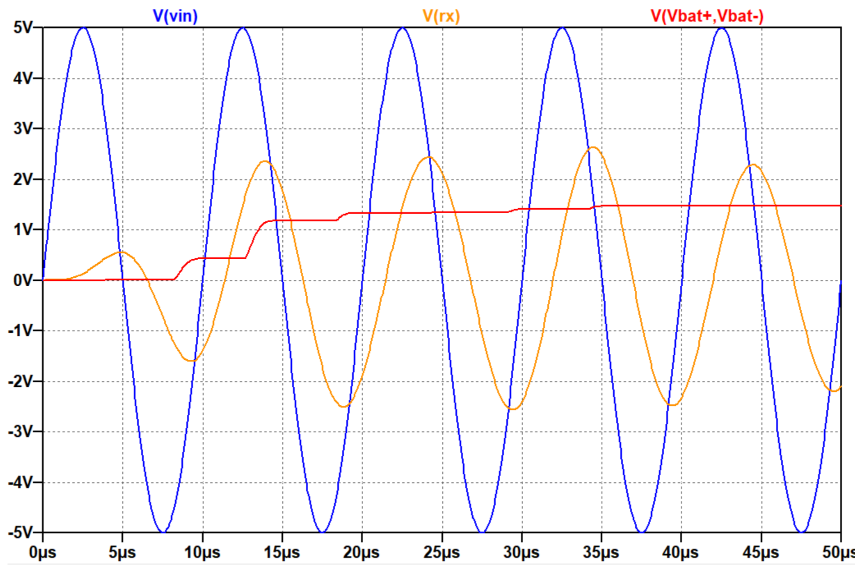

(b) LTSpice resonant circuit simulation. From the input oscillation, the receiver LC tank sees an attenuated and shifted oscillation. The rectifier transforms this AC voltage into DC voltage with an attenuation due to diode voltage drop.

Figure 3.27: Simple resonant circuit and its simulation results in LTSpice. Design inspired by Qi standard.

because we prefer adding 1mm to the diameter rather than 1mm to the thickness. The selected inductor has an inductance of $12\mu H$ and dimensions 36mm x 36mm x 0.8mm. The operating frequency of the RX is generally lower than the transmitter frequency [61]. However, in our simulation, better results are obtained when both resonate at the same frequency of 102.7kHz. The corresponding receiver capacitor is $C = \frac{1}{L(2\pi f)^2} = 200nF$.

The coupling factor influences the voltage gain between the primary and secondary sides, expressed as $\frac{V_2}{V_1} \propto k\sqrt{\frac{L_{22}}{L_{11}}}$ [65]. Typical coupling coefficients range between 0.2 and 0.7 [65]. We assume 0.5, knowing that better coupling can be achieved by design methods to mitigate misalignment.

The simplest rectifier we can implement is a full-bridge diode rectifier. Its efficiency is low due to voltage drops across the diodes, but other rectifier designs exist to improve efficiency [61].

The final resonant circuit is shown in Figure 3.27a, with the observed signals in Figure 3.27b. The input is a 5V sine wave, the receiver coil voltage is attenuated and phase-shifted, and the voltage at the load tends to a DC voltage of approximately 1.5V, reduced by the diode voltage drop.

This simple design has **limitations**. It does not take into account critical features necessary for safety and proper working operation of a wireless charger, as explained in [70]:

- The charger pad should direct magnetic flux toward the receiver and avoid exposing surrounding objects.
- It should not interfere with or corrupt data on credit cards or other smart cards.
- It should not heat up nearby metallic objects or trigger explosions in flammable devices.
- The system should be able to identify and verify receiver compatibility before transferring any energy. This requires bidirectional communication and monitoring of load conditions such as battery status.
- The charger pad should be designed to guide the receiver into the correct position either mechanically (with a specific shaped holder) or magnetically (using a magnet).

Rechargeable Battery

When choosing a battery for a wearable device, safety is a concern, as the device is often worn directly on the skin and the battery could pose a fire or explosion risk. Li-ion batteries present higher safety risks compared to other rechargeable batteries such as lead-acid, Ni-Cd, or Ni-MH [71]. However, Li-ion batteries currently offer the best performance in size and energy capacity. They are small, lightweight, and can power applications for longer period, as illustrated in Figure 3.28.

Although lithium-metal, lithium-oxygen, and lithium-sulfur batteries theoretically offer better performance, they are still under research and not yet used. As noted in [72], lithium-ion batteries also play an important role in implantable devices due to their high energy density.

However, since we assume that more frequent charging is acceptable for our application, and considering both user safety and potential regulatory requirements (such as FDA approval), we choose to use NiMH rechargeable batteries.

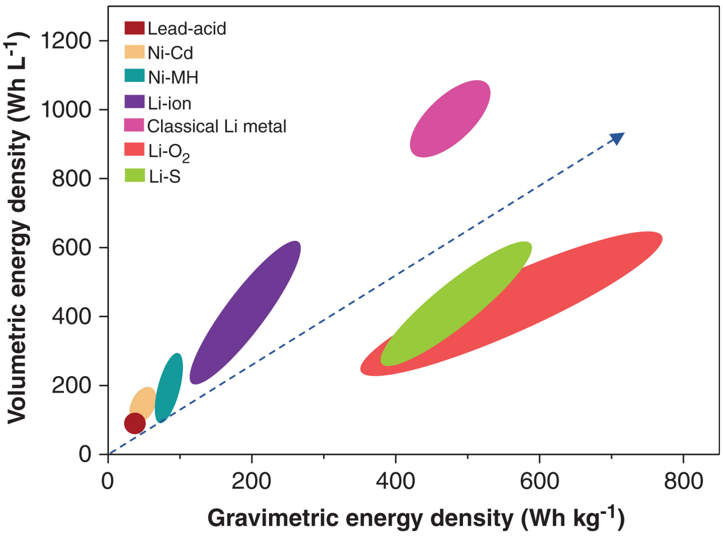

Figure 3.28: Batteries energy density by volume and mass [71]. The best commercially available battery in terms of both gravimetric and volumetric energy density is the Li-ion battery. However, Li-ion batteries pose a higher risk of fire and explosion. nickel-metal hydride (NiMH) is a safer alternative, although it offers lower performance.

Commercial Charger

In our case, a more complex circuit is needed to safely integrate the charger into the design of the CGM. The most suitable design we found is a low-power wireless charger developed for hearing aids. It operates within the same power range: 1.5V with a charge current up to 25mA, according to the datasheet [73]. It is also optimised for wearable devices where miniaturisation of the receiver coil and circuit is essential. The design also includes Zinc-Air battery detection and NiMH battery monitoring to ensure safe operation [73].

In the complete charger application shown in Figure 3.29, we observe the TX and RX coils with parallel capacitors forming LC resonant circuits on both sides. The transmitter oscillator is implemented using the LTC6990, which drives a MOSFET with a 50% duty cycle. The resonant frequency on the transmitter side is 315kHz, while the receiver resonates at a lower frequency: $f_{RX} = \frac{1}{2\pi\sqrt{13\mu H * 33nF}} = 243kHz$. The LTC4123 safely charges a NiMH battery with a rectified current of up to 25mA [73].

Figure 3.30a shows the Spice schematic of the NiMH battery charger using the IC model provided by the manufacturer. The simulation results in Figure 3.30b shows the voltages on the transmitter and receiver sides, as well as the voltage across the battery, which is constant as it charges rapidly due to the small battery capacity.

We used the datasheet [73] to establish the bill of materials required to integrate the complete charger into our LCA strategy.

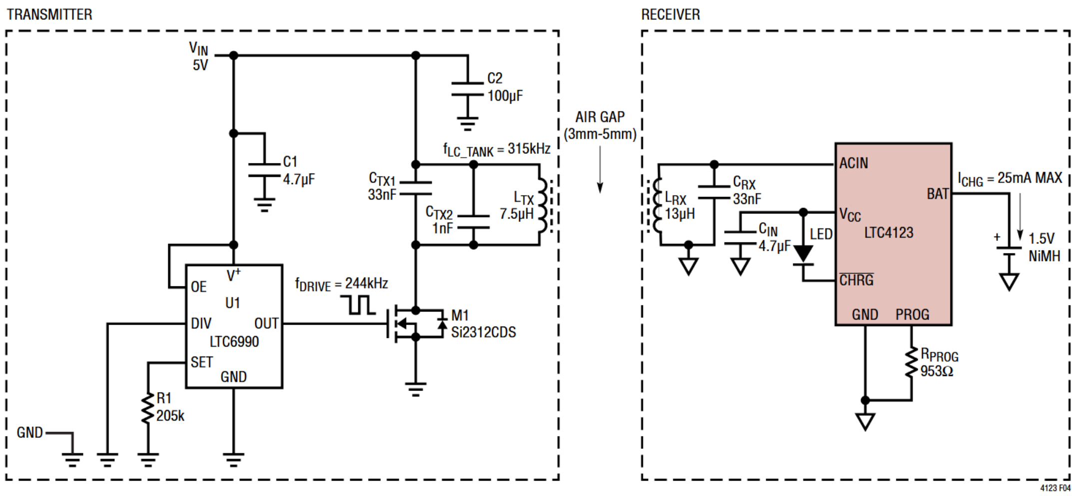

Figure 3.29: NiMH wireless battery charger circuit for typical application [73]. Both transmitter and receiver are represented with an air gap between the LC TX and LC RX tanks. The LTC6990 is the oscillator. The LTC4123 is the IC at receiver side that powers the battery with a rectified power.

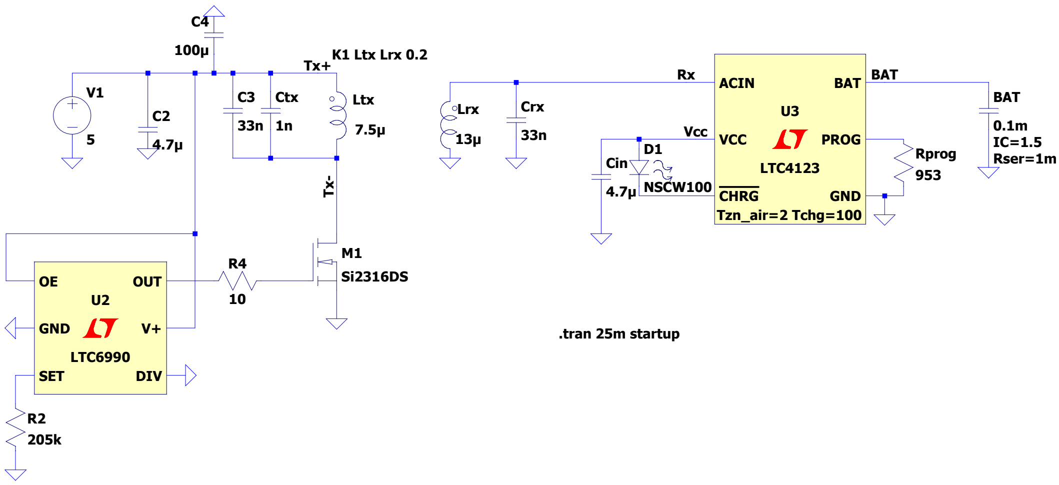

(a) SPICE schematic of the NiMH wireless battery charger circuit for a typical application [73]. The IC models are provided by the manufacturer.

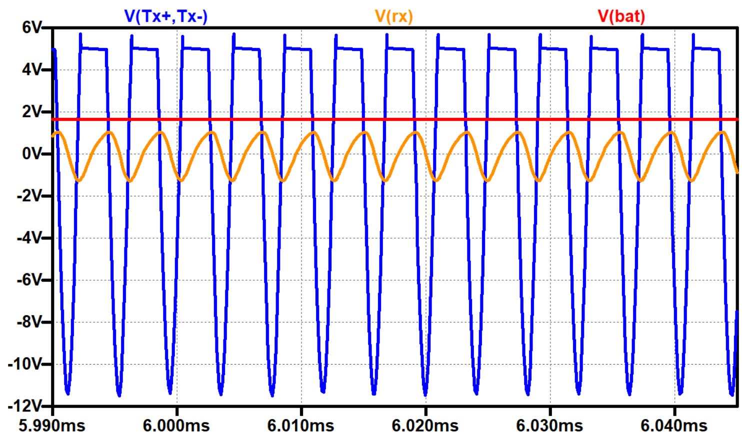

(b) Plot of simulation curves for the NiMH wireless battery charger circuit [73]. The battery voltage is constant as the battery is modelled by a capacitor that is charged in a few milliseconds.

Figure 3.30: SPICE simulation of a typical NiMH wireless battery charger circuit using the LTC4123. The schematic and simulation results are presented.

Hypothesis

This strategy keeps the reusable applicator from Strategy 2. The FL2 silver oxide battery is now replaced with a 1.2V, 74mAh NiMH rechargeable battery [74]. Since commercially available rechargeable coin cell options are limited, we assume that this new battery is suitable for CGM applications. We don't know the standard discharge current of the battery either, but we assume that it is in the same range as the average current consumed by the FL2 (50μA) and that a full charge will last at least two weeks. This would allow the CGM to be used for 14 days before it needs to be recharged.

To enable inductive charging, two additional circuits are added: a transmitter (charger) and a receiver. Both are based on the commercial charger analysed in the previous section. The transmitter includes its own PCB, plastic casing, and a USB connector for power input. We assume that users already possess a micro-USB cable, so none is included. The receiver components are added to the CGM's PCB without increasing its size, although additional soldering is required. We also assume that energy consumption from the receiver circuit is negligible.

The user alternates between two CGM devices, switching every two weeks and replacing the biosensor needle, while charging the other CGM in parallel. Due to the slightly greater height of the NiMH battery, the casing is adjusted accordingly, but the applicator remains unchanged. The new device packaging is bigger (estimated at two to four times the size of the reference box) but is shipped only once every two years. The transports are adapted consequently.

All changes are represented in Figure 3.31, with detailed values provided in Table B.13.

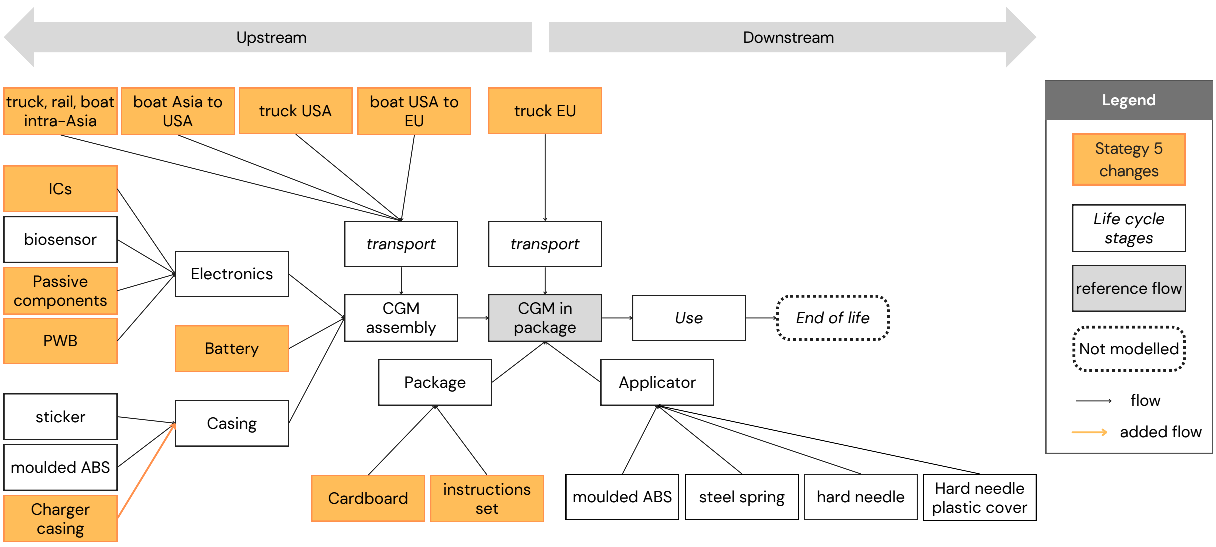

Figure 3.31: Strategy 5: foreground model with related changes. The electronic components of the wireless charger are added. The battery of the new design is a rechargeable NiMH battery compatible with the wireless charger. The transmitter side of the charger has a plastic casing. The package and transport are adapted to ship two CGMs and one charger every two years.

Chapter 4

Ecodesign Results and Interpretation

In this section, the results of all ecodesign strategies are analysed and discussed. Figure 4.1 illustrates how these strategies come together to form a progressive roadmap. First, Strategy 0 will be analysed. Second, the main roadmap strategies will be examined. Since the goal is to evaluate the environmental benefits in all impact categories for each design change, all results are normalised with respect to the reference case. This allows for direct comparison between strategies and a clearer view of the progressive reduction in environmental impacts.

Figure 4.2 presents the results for Strategy 0 across multiple impact categories. The results of the main roadmap strategies are then summarised in Figure 4.3, while Figure 4.4 shows the contribution of different components of the life-cyle model to identify environmental hotspots. Lastly, Figure 4.5 provides absolute values for some impact categories to offer a more detailed perspective.

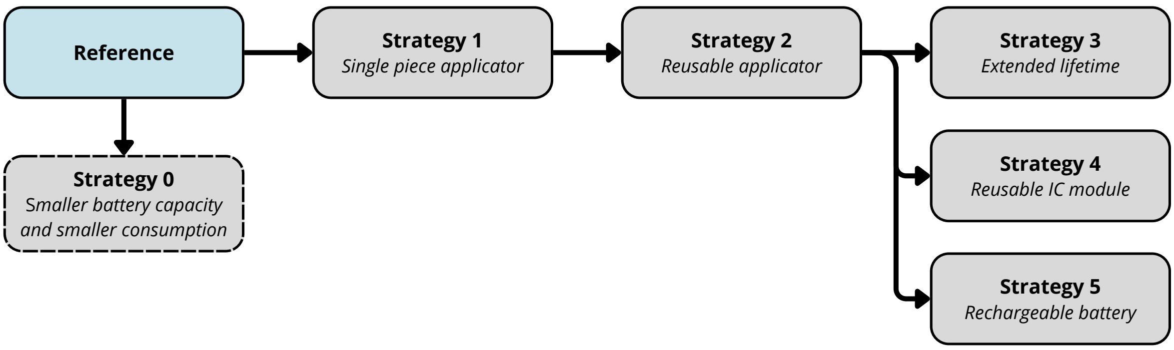

Figure 4.1: Ecodesign roadmap: Strategy 0 is shown with a dashed outline because it was a first attempt based on strong assumptions about reduced device energy consumption. The main roadmap starts with Strategies 1 and 2. Strategies 3, 4, and 5 are alternative approaches based on Strategy 2.

4.1 Strategy 0

As mentioned earlier, strategy 0 was an initial test and does not represent a realistic scenario. It was conducted because of a common belief that reducing energy consumption alone is enough to significantly reduce the environmental impact of an electronic device. The goal was to evaluate the effect of using a smaller battery but was based on a strong assumption of power consumption reduction without any changes to the device.

Despite this optimistic assumption, the reductions in most impact categories are rather small, generally less than 10% as illustrated in Figure 4.2b. Some improvements are slightly better in categories such as ECOTOX, freshwater eutrophication (FEU), and especially MRD, where the impact is almost divided by a factor of two, as shown in Figure 4.2a. It was an expected result as the mass of silver oxide cathode is reduced by more than 50%.

(a) Impact categories normalised to the reference case. The arrows illustrate the impact reductions for the most affected categories.

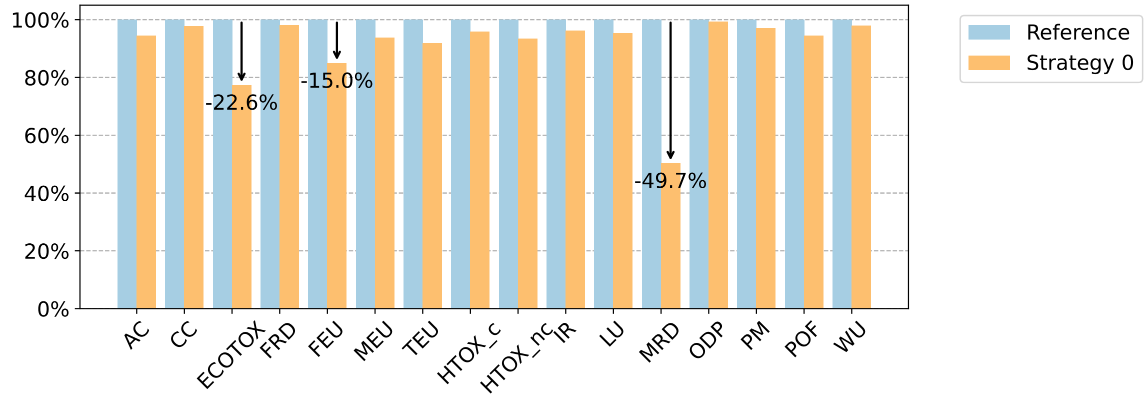

(b) Values in percentage of impact categories normalised to the reference case.

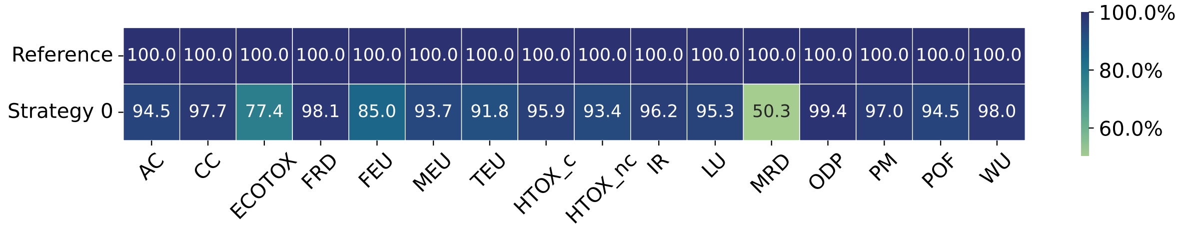

Figure 4.2: Environmental impacts of strategy 0 normalised to reference case. Overall, the environmental impacts improvements are small, except for the MRD. As this study aims to reduce an environmental burden over most categories, it is not a strategy considered in our ecodesign roadmap.

4.2 Main Roadmap

In the reference case as illustrated in Figure 4.4a, the main environmental hotspots across 13 out of 16 impact categories are the applicator, the ICs, and the transport. Hence, focusing on these components will decrease most impacts. For the remaining three categories, ECOTOX, FEU, and MRD, the battery constitutes a significant or even dominant share of the total impact. Therefore, strategies that do not address the battery will not have significant effects on these categories, as illustrated by Figure 4.5. It is thus important to directly target it in more advanced ecodesign strategies.

Strategy 0 served as an initial trial to demonstrate that only reducing the battery size is not enough. In contrast, Strategy 1 already achieves good impact reductions, with over 20% improvement in 10 out of 16 categories (see Figure 4.3), mainly due to the plastic reduction.

Despite the positive results of Strategy 1, the applicator still represents an important share of the environmental impacts (Figure 4.4c). This motivates further improvements through the implementation of a reusable applicator in Strategy 2. Nine impact categories drop below 50%, without any changes to the CGM itself. The relative impacts of the applicator become almost negligible, and transport-related emissions are also reduced due to lighter and reusable components, as shown in Figure 4.4d. However, the MRD category shows minimal improvement, as it is still dominated by the battery. At this stage, the ICs emerge as the primary hotspots in most impact categories, followed by the battery.

To address this, Strategy 3 aims to extend the lifetime of the CGM device. In particular, with a larger battery capacity, the device needs to be replaced less frequently, extending the use of the ICs and electronics. While this requires a larger battery to support a longer usage period, there is a trade-off between the environmental impact of the increased battery size and the benefit of reducing the frequency of replacements. Since all impacts continued to decrease, the environmental cost of a larger battery seems to be outweighed by the benefits of extending its usage time and reusing the electronics. Indeed, strategy 3 achieves reductions of over 70% in 11 categories (Figure 4.4e), and a 27% reduction in the MRD category.

Strategy 4 offers an alternative approach that focuses on reusing the ICs and associated electronics. It introduces a two-piece design, allowing part of the PCB to be reused. Some indicators show greater reductions compared to Strategy 3, ranging from a few additional percent to more than 25% percent for ozone depletion potential (ODP). Others, such as ECOTOX, marine eutrophication (MEU), land use (LU), and MRD, show deteriorations of 1 to 15%. This is likely due to the need for additional electronic components, such as two separate PCBs and a connector and because the battery is used for only 14 days again, see Figure 4.5. Moreover, as shown in Figure 4.4f, the impact contribution of the ICs becomes negligible. The main hotspots shift again, from the ICs in Strategy 2 to the battery and packaging, which are now the most important, as shown in Figure 4.4f).

Finally, Strategy 5 explores the most ambitious scenario: using a rechargeable battery to make the entire CGM device reusable. This strategy leads to the best overall performance, with all impact indicators reduced below 10%. This is primarily due to replacing the silver oxide battery with a NiMH rechargeable alternative with much lower environmental footprint. Moreover, almost all components are now reusable for two years, except for the sterilised needles for the sensor and applicator . While the number of electronic components due to the charger increases, their contribution to overall impacts is small. Interestingly, the impact distribution in Figure 4.4g is similar to the one of the reference case. This suggests that we are approaching the limit of possible impact reduction. Indeed, a minimum amount of plastic and electronic materials appears to be essential to fulfil the functional unit. A discussion on how far the environmental impacts actually need to be reduced is provided in Chapter 5.

(a) Barplot labels.

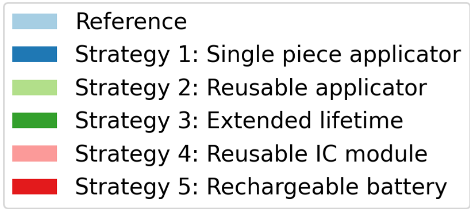

(b) Barplot part 1: impact categories normalised to the reference case. The first half of impact categories are presented. The bars for strategies 3, 4 and 5 are spaced because they are non cumulative with each other but cumulative with the first and second strategy.

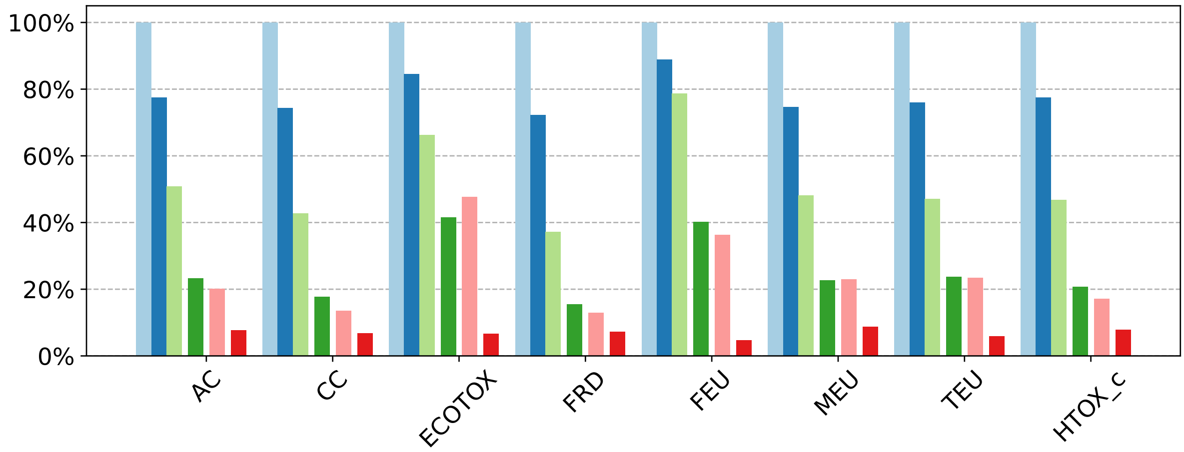

(c) Barplot part 2: impact categories normalised to the reference case. The second half of impact categories are presented. The bars for strategies 3, 4 and 5 are spaced because they are non cumulative with each other but cumulative with the first and second strategy.

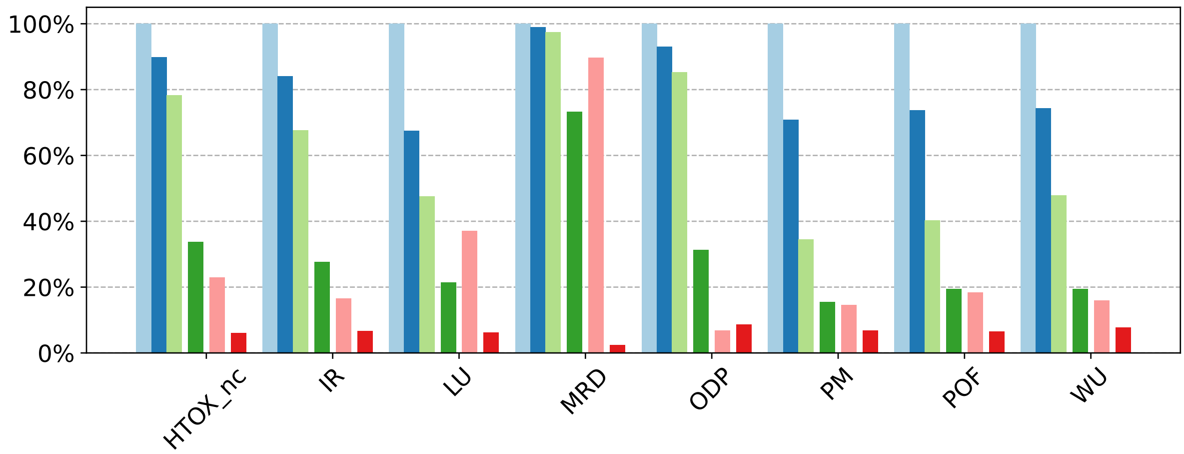

(d) The heatmap presents the same information as contained in Figures ??. It gives a color vision and the values in percentage by impact categories for the strategies normalised to the reference case.

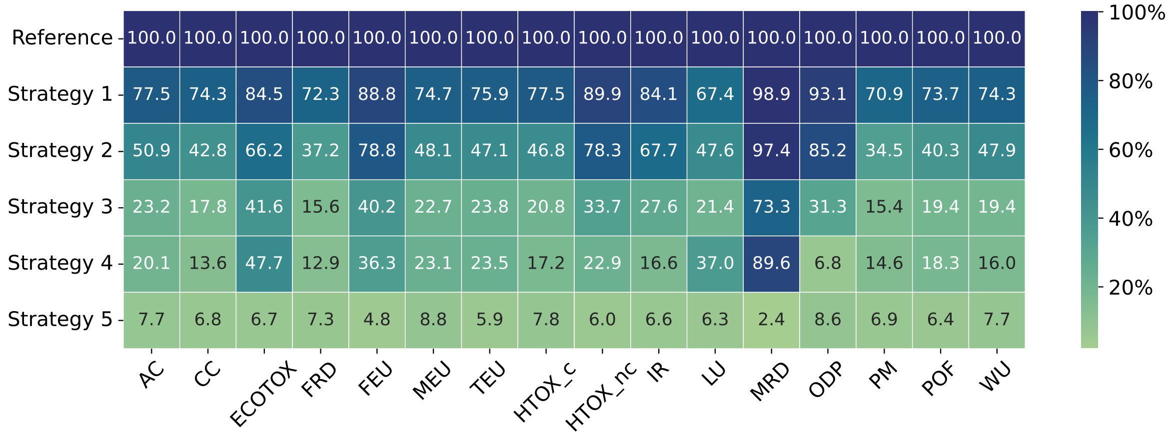

Figure 4.3: Environmental impacts normalised to reference case for all impact categories. The different strategies of the roadmap are compared in terms of improvement from the reference LCA.

Figure 4.4: Environmental impacts normalised with the total characterisation result. The reference, strategy 0 and the five other strategies are presented. The five strategies that make up our roadmap demonstrate how the targeted reduction in hotspot contributions are progressively achieved.

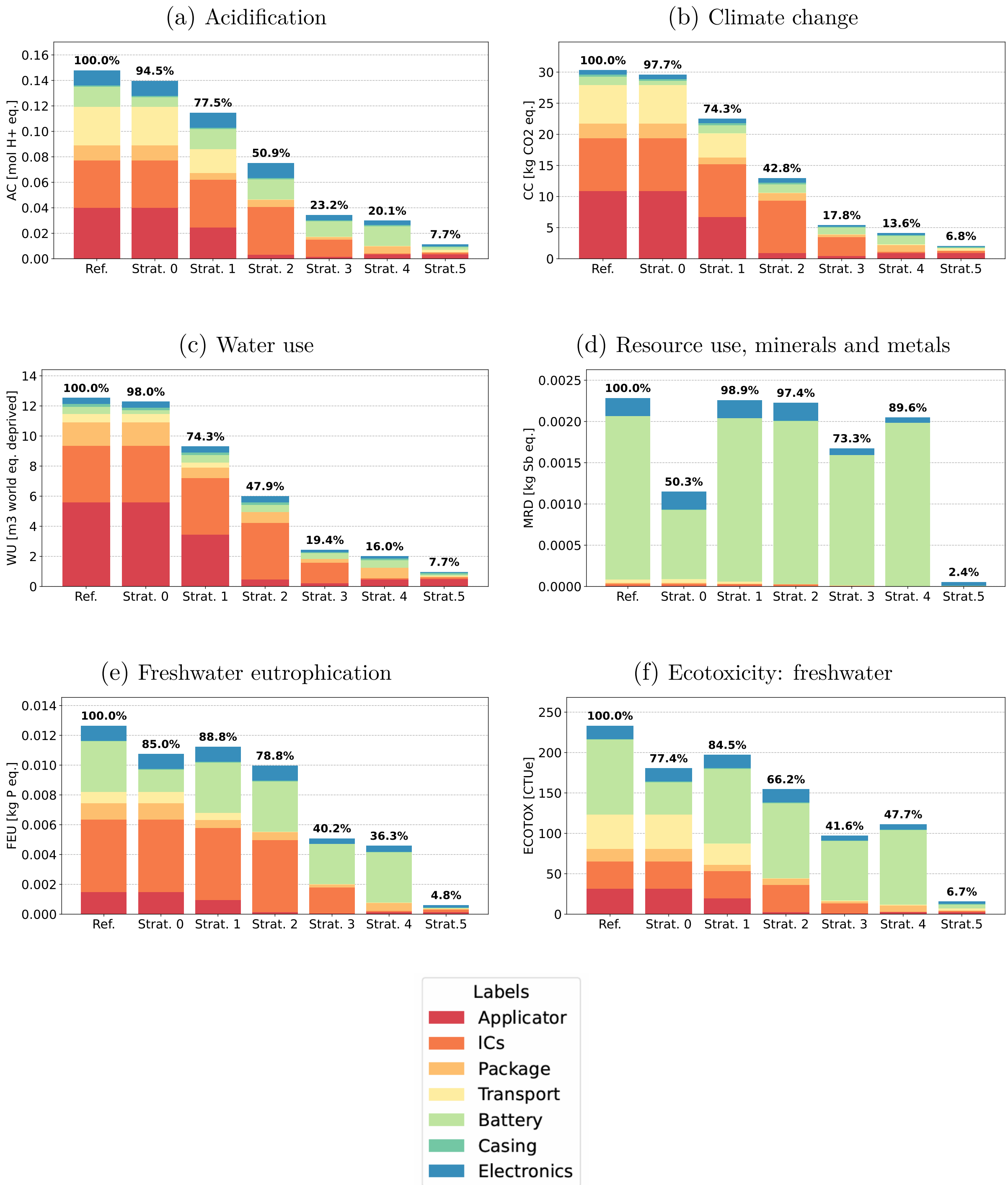

Figure 4.5: Detailed contribution analysis per impact categories with absolute values. Percentages are shown for comparison with reference and measure the reduction achieved compared to the reference case.

Chapter 5

Discussion

This chapter discusses the results of the roadmap presented in Chapter 4. It begins with details about the methodology and data management. Then, it addresses difficulties with EoL modelling and explains why this phase was excluded from the scope of this study. Next, uncertainties in the results are detailed, comparing constant and non-constant reference flows. Another point of view is presented by normalising results relative to planetary boundaries. Finally, external factors influencing the adoption of our strategies are discussed.

Methodology

In our methodology, we use a dataset that includes all material and non-material processes involved in building our product system. Due to the large volume of data, we carefully analysed the results to identify potential errors in our modelling. Despite these checks, the possibility remains that one element was mistakenly set in our Excel file, representing the full LCI. However, as the results aligned with our expectations, we believe that major errors were avoided.

We also try to represent uncertainty and potential design changes as realistically as possible, supported by experimental data and measurements from real products. Nevertheless, some values were chosen speculatively and may not correspond to the design of a future product. Therefore, the results should be interpreted with nuance and considered within the context of this study, taking into account our design choices.

End-of-Life Modelling

Life cycle stages of LCA considered in this study do not include the EoL phase and stop at the use stage. Indeed, EoL modelling for digital equipment is often excluded or given limited consideration, and remains poorly documented [75]. This review [75], highlights the lack of systematic and detailed analyses of the EoL stage for digital equipment. The challenges we faced in modelling this phase is the high level of uncertainty linked to e-waste treatment, which varies significantly by region and is described with limited data [75]. For these reasons, we excluded this phase from the scope of our study. Further in [75], recycling is included in most studies covering the EoL phase, but reported recycling rates were very different, ranging from 8 to 100%. It is difficult to determine the actual share of environmental impacts from the EoL phase, because most studies make methodological choices that tend to minimise its contribution [75].

The battery used in FL2 is a silver oxide battery, identified as one of the hotspots in our LCA. These batteries pose EoL issues in addition to the significant environmental burden associated with their production. As explained in [76], the extraction of metals, such as silver, uses corrosive chemicals, associated with contamination risks for water and soil. Battery disposal presents further concerns: incineration releases toxic gases that pose a health issue, while land filling can lead to groundwater contamination due to heavy metals like silver.

As a result, we chose to limit the scope of our study due to the lack of data, while recognising that it does not account for certain significant impacts.

Uncertainties

All the results in the previous chapter (4) were obtained with default values. However, these default values do not reflect the variation in design parameters. Based on our experience with other designs and experimental data, we were unable to determine all parameters with full certainty. To account for this uncertainty, we used distributions (triangular or uniform) instead of fixed values to represent a range of possible values in the LCI.

The results with constant reference flow are represented in Figure 5.1. Although some variation is observed, it does not affect the conclusion we have established in the previous section. The distribution remains close to the mean values. Interestingly, strategies 3, 4, and 5 show more compact distributions than the others. This may seem counterintuitive, as these strategies build cumulatively on strategy 2. However, since the impacts of transport, the battery, and other major sources of uncertainty are reduced, their contribution to overall uncertainty also decreases.

However, Figure 5.1 does not take into account all uncertainties. One of the most influential parameters is the number of sensors used per year. When this parameter is no longer fixed, it directly applies a scaling factor to the results, leading to a much wider distribution. As shown in Figure 5.2, uncertainty under a non-constant reference flow is significantly more spread out. The number of CGMs is modelled using a triangular distribution ranging from 26 to 37, with a default value of 31. This variation reflects real usage, where sensors may be replaced more frequently in normal condition due to failures or user-related issues (e.g. accidental detachment).

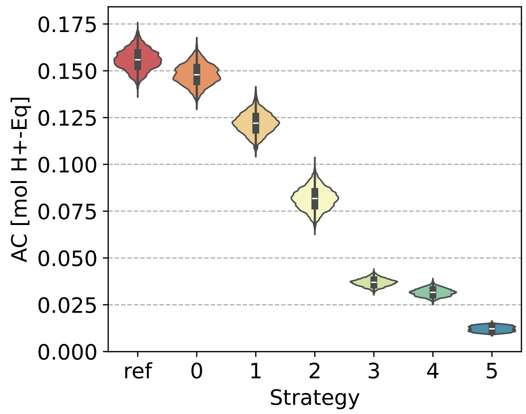

(a) Uncertainties at constant reference flow, acidification (AC)

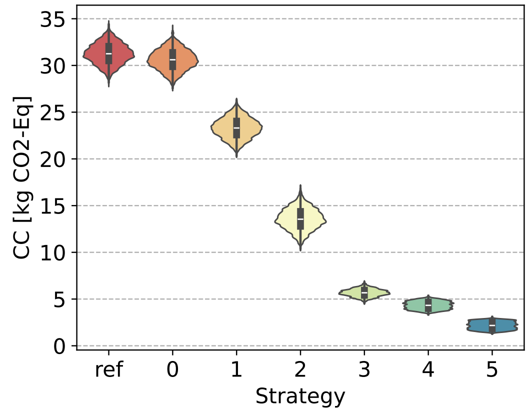

(b) Uncertainties at constant reference flow, CC

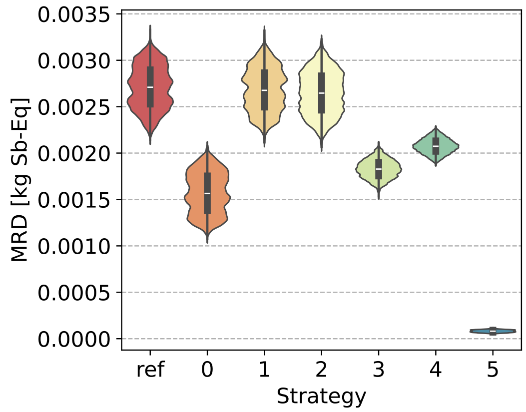

(c) Uncertainties at constant reference flow, MRD

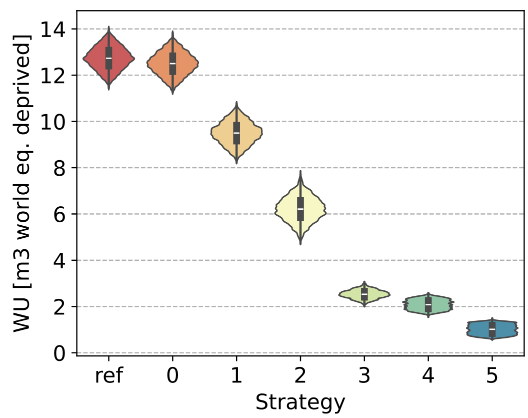

(d) Uncertainties at constant reference flow, WU

Figure 5.1: Uncertainties in strategies at constant reference flow for different impact categories. We observe relatively compact distribution except for MRD.

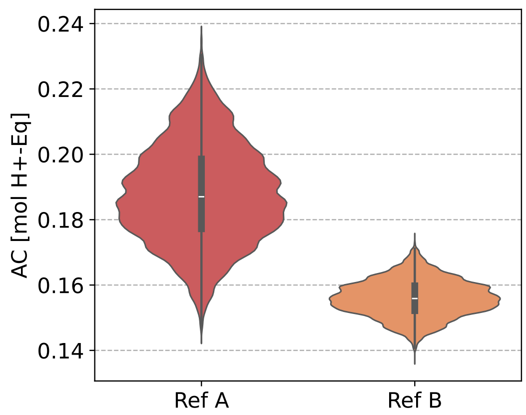

(a) Reference with (A) and without (B) uncertainty on the reference flow, AC

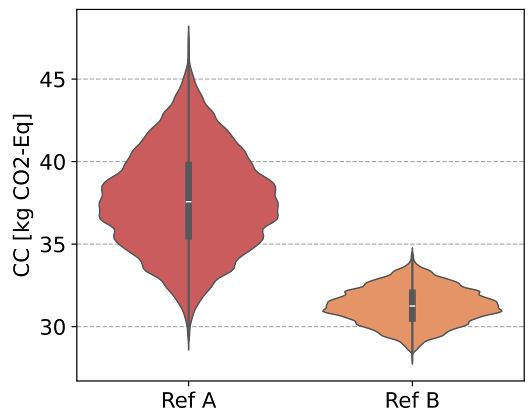

(b) Reference with (A) and without (B) uncertainty on the reference flow, CC

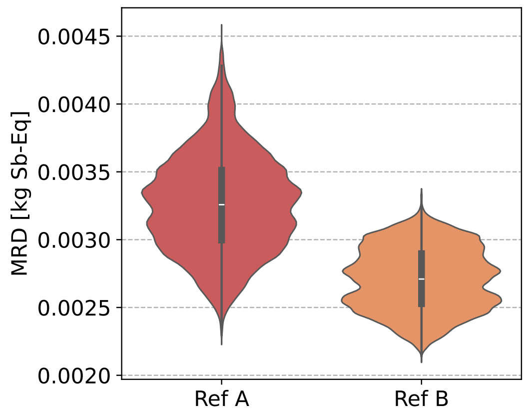

(c) Reference with (A) and without (B) uncertainty on the reference flow, MRD

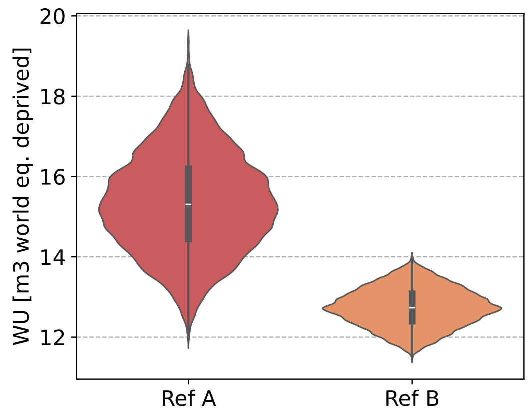

(d) Reference with (A) and without (B) uncertainty on the reference flow, WU

Figure 5.2: Comparison of the uncertainties with constant (B) and non-constant (A) reference flow for the reference strategy. Larger uncertainties, with higher impact values are observed in case (A). As we set that the distribution on the number of CGM ranges from 26 and 37, the case (B) represent the fixed 26 value case and is supposed to be shrink to lower values compared to (A).

Planetary Boundaries

A LCA can be interpreted using different methods. In our study, we use normalisation relative to the reference FL2. This means results are expressed as a comparison to the initial design. However, this restricts the scope of interpretation to product scale. To asses the environmental impact on a larger scale, normalisation against planetary boundaries (PB) can be used. This expresses the sensor's impact in relation to what is environmentally acceptable at the planetary level.

The PB *"help identify whether production and consumption are environmentally sustainable in absolute terms, namely compared to the Earth's ecological limits and carrying capacity"* [77]. Figure 5.3 presents the results normalised against PB adapted to Environmental Footprint (EF) metrics for comparing LCIA results, following the methodology from [77]. While the normalisation factors are based on EF2.0 rather than the updated EF 3.1, they are still used because the mapping of the PB to the EF indicators remains relevant. It is assumed that PB have not significantly changed in recent years and that the impact categories between EF2.0 and EF 3.1 are consistent. To express PB on a per capita basis, we divide the global limits by the estimated world population in May 2025 [78]. Equality allocation is assumed, meaning that all the population has equal rights to the environment and therefore the PB are distributed equally.

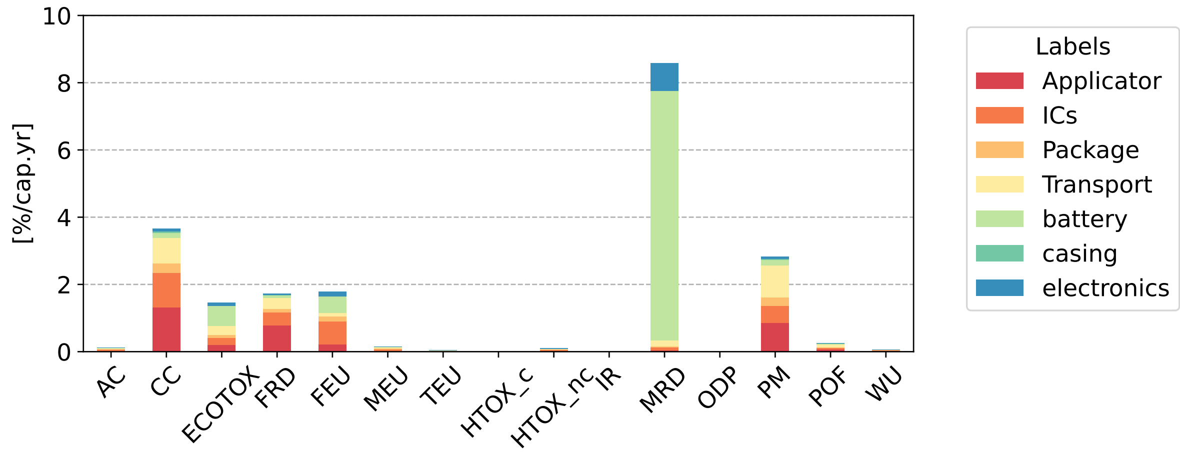

Figure 5.3: Environmental impacts of reference case normalised to planetary boundaries in % per capita per year. Nine impact categories are almost invisible. However, CC and particularly MRD stand out, with contribution dominated by the battery, ICs and applicator.

In Figure 5.3, nine impact categories are nearly invisible. Therefore, they are negligible relative to the limits of planetary resource. It suggests that, for most categories, CGMs contributions are small. Consequently, ecodesign efforts may not be justified based on these impacts alone. However, two categories stand out, specifically the CC and the MRD.

The CC impact reaches nearly 4% of the annual per capita limit. This is largely due to the applicator and packaging, which are mainly composed of cardboard and plastics. The MRD impact is more significant, exceeding 8 % of the annual per capita limit. This is primarily due to the battery and electronic components.

With this in mind, we mention that the study could have taken a different perspective. It could have focused on reducing the most significant planetary boundary hotspots. While CGMs are not major contributors in most categories, environmental impacts should still be a part of design decisions. Small changes can already bring meaningful improvements at the device level. Although, batteries and electronics remain major contributors at a larger scale.

Strategies Adoption

Due to our device-centered perspective, some key external factors influencing the adoption of our strategies were not addressed. For instance, the economic considerations of manufacturers, patient willingness to pay, and patient quality of life directly affect the feasibility and implementation of our roadmap.

Firstly, economic viability is essential from a manufacturer's perspective. If the strategy does not ensure financial returns, it is unlikely to be implemented. Financial return is linked to both the number of users and the price of the device. However, both factors depend on the insurance reimbursement plan. Pricing a medical device is complex, and assessing whether it exceeds reimbursement of health care insurance thresholds adds further uncertainty. We are in a context where an ageing population and higher living standards drive demand, while new treatments and technologies are increasing healthcare costs [79]. However, as explained in [79], high prices do not necessarily correspond to large health gains. This raises a key question: would health insurance reimburse a (maybe more expensive) CGM from our roadmap based on the health gains it offers? In addition, regulatory approval from CE and FDA plays an important role, since it directly impacts reimbursement eligibility.

Then, patient willingness to pay must be considered. Would patients pay for a device with a longer lifetime or less environmental impact? Health economics addresses this question through the concept of willingness to pay. In adults with type 1 diabetes using multiple daily injections and experiencing poor glycemic control, CGM is cost-effective at a $ 100,000/QALY threshold on a lifetime analysis [80]. The QALY, or quality adjusted life year, represents one year with best possible quality of life [81]. For example, if a design improves patient health by 0.5 QALY, it would be cost-effective below a $ 50,000 threshold.

Lastly, patient quality of life is an aspect that is not addressed in our strategies. Studies show that CGMs significantly improve diabetes patients quality of life. They reduce diabetes distress and increase hypoglycemic confidence in type 1 diabetes [82]. Nonetheless, for widespread adoption, device usability factors matter. Ease of use, maintenance frequency, device lifespan, and battery management can limit patient acceptance. For example, frequent battery replacements may be challenging for elderly patients. Similarly, the need to recharge the device regularly could discourage use.

Further Improvements

The main improvements for future work would be to study the environmental impact of CGMs on a larger scale. Extra healthcare support and infrastructure are needed when CGM is not used. Since complications are avoided with CGM, it creates indirect positive impacts of CGM usage and it should be included. The analysis should go beyond product-to-product comparisons. It should add economic evaluations to the results to take into account reimbursement and market feasibility. EoL modelling should be added, with careful selection of accurate data on e-waste treatment and recycling. Uncertainty analysis should be completed, especially regarding the non-constant reference flow of sensors. Finally, the roadmap should be updated to reflect patient usability and willingness to pay, as these factors influence the feasibility of adopting strategies.

Conclusion

With the growing number of people with diabetes, the demand for CGMs is increasing, and so is the environmental impact of their frequent disposal. Furthermore, as these devices are single-use, they generate a significant amount of waste. This thesis aimed to identify the main environmental hotspots associated with these devices and explore ecodesign strategies to reduce their impact.

An LCA was performed on a reference product, the commercially available FL2, revealing that the plastic applicator, ICs, and battery are the most impactful components. Although total environmental impacts remain relatively low when normalised to planetary boundaries in a later analysis, certain categories such as MRD and CC show higher contributions (8% and 4%, respectively), justifying further investigation.

Based on this reference, several ecodesign strategies were proposed. Initially, the applicator was the main focus, first by using less plastic and then by introducing a reusable design. These changes alone resulted in significant reductions in environmental impacts without modifying the device itself. Subsequent strategies focused on extending the product lifetime and reusing ICs while keeping the reusable applicator. Ultimately, wireless recharging using a NiMH battery allowed the entire device to be reused (except for the single-use needles). This final strategy achieved the biggest reductions, with all impact indicators reduced by at least a factor of ten compared to the reference case.

The results of all the implemented strategies represent a best-case scenario because they are based on the assumption of a constant reference flow with a maximum lifetime (14 days). In reality, the number of devices used may be higher, thereby amplifying the overall environmental burden. Nevertheless, the findings emphasise the importance and feasibility of incorporating ecodesign principles into the development of medical devices, as even small changes can bring significant environmental benefits.

This study focused exclusively on environmental impacts, without addressing the social or economic dimensions that can influence the feasibility and adoption of these strategies. Although some proposed changes may face practical limitations, intermediary solutions balancing sustainability, usability, and cost could be identified through further research.

Future work could involve incorporating uncertainty analysis with a variable reference flow and broadening the scope to include the health benefits of CGMs, such as improved disease management and the prevention of severe complications. Such global assessments would provide a better understanding of the overall value and sustainability of this technology.

This work paves the way for future efforts to reconcile innovation in diabetes care and medical devices in general with the urgent need for environmental responsibility, an issue that is becoming increasingly important.

Appendix A

LCIA methods

Region	Name	Approach	Description
Europe	CML-IA	midpoint	CML impact assessment (IA) by the Institute of Environmental Sciences of University of Leiden in Netherlands. Developed in 1992 and last updated in 2016.
	EF v3.1	midpoint	Method maintained by the EC, stands for environmental footprint. EF v3.0 was updated to v3.1 in July 2022. Often considered as state of the art because updated recently, includes latest IPCC 2021 characterisation factors (CF) and is method of choice for Product Environmental Footprint (PEF) studies[40]
Global	IMPACT World +	midpoint & endpoint	update and compilation of IMPACT 2002+, LUCAS, and EDIP methods.
	ReCiPe 2016	midpoint & endpoint	Contains both 18 midpoint (problem oriented) and 3 endpoint (damage oriented) impact categories. Available for 3 different perspectives: individualist (I), hierarchist (H), and egalitarian (E).
	EDP 2018	mid	Ecosystem damage potential,developed by Swiss Federal institute of technology (ETH) in 1997
North America	TRACI 2.1	midpoint	TRACI stand for **T**ool for the **R**eduction and **A**ssessment of **C**hemical and other environmental **I**mpacts. Published by the U.S Environmental agency in 2002 and updated to v2.1 in 2012.

Table A.1: LCIA Methods comparison [41][83]

Appendix B

Strategies

B.1 Reference

An open-source repository is available for the reference LCA model at `https://github.com/auwattiez/Comparative-LCA-of-CGM-and-FPBT-devices`. The repository includes the complete LCA model, all numerical data, Python scripts, and detailed data sources for each parameter distribution. This ensures full transparency and reproducibility of the results, while also facilitating future adaptations or extensions of the model. The reference script can be adapted for each ecodesign strategy by simply replacing the reference values with those provided in the tables in the following sections.

B.2 Strategy 0

battery	standard capacity (mAh)	standard discharge current (μA)	diameter (mm)	height (mm)	weight (g)
reference	28	50	6.8	2.6	0.39
new (strategy 0)	16	30	5.8	2.15	0.23

Table B.1: Comparison of battery from Strategy 0 with reference case

The new values of battery flows were determined using the following calculations:

$$\text{aire\_up} = \pi\frac{d^2}{4} + \pi dh \tag{B.1}$$

$$\text{aire\_down} = \pi\frac{d^2}{4} \tag{B.2}$$

$$\text{powder weight} = \text{battery weight} - \text{protection up \& down weight} \tag{B.3}$$

	ref	strat 0	scaling	scaled flow
aire_up [mm^2]	91.86	65.6	0.714	external protection up
aire_down [mm^2]	36.32	26.42	0.73	external protection down, other plastic element
powder weight [g]	0.1516	0.06548	0.42	zinc powder, silver oxide powder
battery capacity [mAh]	28	16	$\frac{16}{28}$	manufacturing energy

Table B.2: scaling for battery components

foreground name	unit	qty ref	qty 0	Min	Max	distrib
blue plastic	g	9.65	9.65	-	-	fixed
dark grey plastic	g	9.67	9.67	-	-	fixed
lighter grey plastic	g	17.5	17.5	-	-	fixed
light grey plastic	g	14.54	14.54	-	-	fixed
transparent plastic	g	8.72	8.72	-	-	fixed
inner plastic part 1	g	2.38	2.38	-	-	fixed
inner plastic part 2	g	5.73	5.73	-	-	fixed
inner plastic part 3	g	0.27	0.27	-	-	fixed
inner plastic part 4	g	1.33	1.33	-	-	fixed
spring	g	1.31	1.31	-	-	fixed
hard needle	g	0.049	0.049	-	-	fixed

(a) Applicator subassembly

foreground name	unit	qty ref	qty 0	Min	Max	distrib
sticker	g	0.17	0.17	-	-	fixed
casing top	g	0.6	0.6	-	-	fixed
casing bottom	g	1.08	1.08	-	-	fixed
transparent soft plastic	g	0.085	0.085	-	-	fixed
opaque hard plastic	g	0.11	0.11	-	-	fixed
amperometric transdermal glucose biosensor	unit	1	1	-	-	fixed

(b) CGM

foreground name	unit	qty ref	qty 0	Min	Max	distrib
yellow box	g	18.6	18.6	-	-	fixed
instructions set	g	4.02	4.02	-	-	fixed
protective foil	g	0.78	0.78	-	-	fixed
whole package	g	85	85	-	-	fixed

(c) Package

foreground name	unit	qty ref	qty 0	Min	Max	distrib
IC1 frontend	mm^2 die	5.52	5.52	-	-	fixed
IC2 frontend	mm^2 die	5.3095	5.3095	-	-	fixed
IC1 backend	g	0	0	-	-	fixed
IC2 backend	g	0.0403	0.0403	-	-	fixed

(d) ICs

foreground name	unit	qty ref	qty 0	Min	Max	distrib
battery connector	g	0.08	0.156	-	-	fixed
antenna	g	0.0168	0.0168	-	-	fixed
SMD capacitors 0603	g	0.00462	0.00462	÷2	x2	triangle
SMD capacitors 1005	g	0.0032	0.0032	÷2	x2	triangle
SMD capacitors 1608	g	0.0243	0.0243	÷2	x2	triangle
SMD resistor 0603	g	0.00105	0.00105	÷2	x2	triangle
SMD resistor 1005	g	0.0016	0.0016	÷2	x2	triangle
SMD resistor 1608	g	0.004	0.004	÷2	x2	triangle
SMD soldering - calculated from EIME table	g	0.0395	0.0395	÷2	x2	triangle
SMD soldering - visually estimated	g	0.02	0.02	÷2	x2	uniform
printed wiring board (PWB)	cm^2	5.074963	5.074963	-	-	fixed

(e) electronics

foreground name	unit	qty ref	qty 0	Min	Max	distrib
zinc powder	g	0.0319	0.0135	-10%	+10%	triangle
silver oxide powder	g	0.1197	0.0507	-10%	+10%	triangle
external protection - up	g	0.11	0.07854	-10%	+10%	triangle
external protection - down	g	0.087	0.06351	-10%	+10%	triangle
other plastic element (membrane)	g	0.03078	0.02247	-10%	+10%	triangle
manufacturing energy	Wh	4.34	2.48	x1	x1.5	uniform

(f) battery

foreground name	dist. (km)	unit	qty ref	qty 0	Min	Max	distrib
Intra-Asia travels (truck)	1000	g	0.5	0.5	÷2	x2	uniform
Intra-Asia travels (train)	1000	g	0.5	0.5	÷2	x2	uniform
Intra-Asia travels (boat)	2000	g	0.5	0.5	÷2	x2	uniform
Asia to US port	10000	g	0.5	0.5	-20%	+20%	triangle
US port to US production lines	2500	g	0.5	0.5	÷2	x2	triangle
US production lines to US port	2500	g	78.5	78.5	÷2	x2	triangle
US port to England port	6000	g	78.5	78.5	-20%	+20%	triangle
England port to England manufacturing facility	150	g	78.5	78.5	-20%	+20%	triangle
England mfg facility to Wisbaden	850	g	78.5	78.5	x1	+20%	triangle
Wisbaden to delivery warehouse (Merkala)	480	g	103.5	103.5	x1	+20%	triangle
Delivery warehouse to end-user (BE)	250	g	146	146	x1	+20%	triangle

(g) transport

Table B.3: Values of all the flows for strategy 0. Changes are represented in blue

B.3 Strategy 1

foreground name	unit	qty ref	qty 1	Min	Max	distrib
blue plastic	g	9.65	8.598	-	-	fixed
dark grey plastic	g	9.67	0	-	-	fixed
lighter grey plastic	g	17.5	0	-	-	fixed
light grey plastic	g	14.54	11.65	-	-	fixed
transparent plastic	g	8.72	18.56	-	-	fixed
inner plastic part 1	g	2.38	2.55	-	-	fixed
inner plastic part 2	g	5.73	0	-	-	fixed
inner plastic part 3	g	0.27	0	-	-	fixed
inner plastic part 4	g	1.33	0	-	-	fixed
spring	g	1.31	1.31	-	-	fixed
hard needle	g	0.049	0.049	-	-	fixed

(a) Applicator subassembly

foreground name	unit	qty ref	qty 1	Min	Max	distrib
sticker	g	0.17	0.17	-	-	fixed
casing top	g	0.6	0.6	-	-	fixed
casing bottom	g	1.08	1.08	-	-	fixed
transparent soft plastic	g	0.085	0.085	-	-	fixed
opaque hard plastic	g	0.11	0.11	-	-	fixed
amperometric transdermal glucose biosensor	unit	1	1	-	-	fixed

(b) CGM

foreground name	unit	qty ref	qty 1	Min	Max	distrib
yellow box	g	18.6	9.58	-	-	fixed
instructions set	g	4.02	4.02	-	-	fixed
protective foil	g	0.78	0	-	-	fixed
whole package	g	85	43.775	-	-	fixed

(c) Package

foreground name	unit	qty ref	qty 1	Min	Max	distrib
IC1 frontend	mm^2 die	5.52	5.52	-	-	fixed
IC2 frontend	mm^2 die	5.3095	5.3095	-	-	fixed
IC1 backend	g	0	0	-	-	fixed
IC2 backend	g	0.0403	0.0403	-	-	fixed

(d) ICs

foreground name	unit	qty ref	qty 1	Min	Max	distrib
battery connector	g	0.08	0.08	-	-	fixed
antenna	g	0.0168	0.0168	-	-	fixed
SMD capacitors 0603	g	0.00462	0.00462	÷2	x2	triangle
SMD capacitors 1005	g	0.0032	0.0032	÷2	x2	triangle
SMD capacitors 1608	g	0.0243	0.0243	÷2	x2	triangle
SMD resistor 0603	g	0.00105	0.00105	÷2	x2	triangle
SMD resistor 1005	g	0.0016	0.0016	÷2	x2	triangle
SMD resistor 1608	g	0.004	0.004	÷2	x2	triangle
SMD soldering - calculated from EIME table	g	0.0395	0.0395	÷2	x2	triangle
SMD soldering - visually estimated	g	0.02	0.02	÷2	x2	uniform
PWB	cm^2	5.074963	5.074963	-	-	fixed

(e) electronics

foreground name	unit	qty ref	qty 1	Min	Max	distrib
zinc powder	g	0.0319	0.0319	-10%	+10%	triangle
silver oxide powder	g	0.1197	0.1197	-10%	+10%	triangle
external protection - up	g	0.11	0.11	-10%	+10%	triangle
external protection - down	g	0.087	0.087	-10%	+10%	triangle
other plastic element (membrane)	g	0.037078	0.037078	-10%	+10%	triangle
manufacturing energy	Wh	4.34	4.34	x1	x1.5	uniform

(f) battery

foreground name	dist. (km)	unit	qty ref	qty 1	Min	Max	distrib
Intra-Asia travels (truck)	1000	g	0.5	0.5	÷2	x2	uniform
Intra-Asia travels (train)	1000	g	0.5	0.5	÷2	x2	uniform
Intra-Asia travels (boat)	2000	g	0.5	0.5	÷2	x2	uniform
Asia to US port	10000	g	0.5	0.5	-20%	+20%	triangle
US port to US production lines	2500	g	0.5	0.5	÷2	x2	triangle
US production lines to US port	2500	g	78.5	50.5	÷2	x2	triangle
US port to England port	6000	g	78.5	50.5	-20%	+20%	triangle
England port to England manufacturing facility	150	g	78.5	50.5	-20%	+20%	triangle
England mfg facility to Wisbaden	850	g	78.5	50.5	x1	+20%	triangle
Wisbaden to delivery warehouse (Merkala)	480	g	103.5	64.5	x1	+20%	triangle
Delivery warehouse to end-user (BE)	250	g	146	84.5	x1	+20%	triangle

(g) transport

Table B.4: Values of all the flows for strategy 1. Changes are represented in blue

B.4 Strategy 2

foreground name	unit	qty 1	qty 2	Min	Max	distrib	# of uses
blue plastic	g	8.598	51.1656	-10%	+10%	uniform	52
dark grey plastic	g	0	0	-	-	fixed	52
lighter grey plastic	g	0	0	-	-	fixed	52
light grey plastic	g	11.65	0	-	-	fixed	52
transparent plastic	g	18.56	0	-	-	fixed	52
inner plastic part 1	g	2.55	0	-	-	fixed	52
inner plastic part 2	g	0	0	-	-	fixed	52
inner plastic part 3	g	0	0	-	-	fixed	52
inner plastic part 4	g	0	0	-	-	fixed	52
spring	g	1.31	1.31	-	-	fixed	52
hard needle	g	0.049	0.049	-	-	fixed	1
hard needle plastic cover	g	0	5	1	10	uniform	1

(a) Applicator subassembly

foreground name	unit	qty 1	qty 2	Min	Max	distrib	# of uses
sticker	g	0.17	0.17	-	-	fixed	1
casing top	g	0.6	0.6	-	-	fixed	1
casing bottom	g	1.08	1.08	-	-	fixed	1
transparent soft plastic	g	0.085	0.085	-	-	fixed	1
opaque hard plastic	g	0.11	0.11	-	-	fixed	1
amperometric transdermal glucose biosensor	unit	1	1	-	-	fixed	1

(b) CGM

foreground name	unit	qty 1	qty 2	Min	Max	distrib	# of uses
yellow box (CGM+needle)	g	9.58	9.58	-20%	+20%	uniform	1
applicator box	g	0	9.58	-10%	+30%	uniform	52
instructions set	g	4.02	4.02	-	-	fixed	0.98
protective foil	g	0	0	-	-	fixed	1
whole package (CGM+needle)	g	43.775	43.775	-20%	+20%	uniform	1
whole package applicator	g	0	43.775	-10%	+30%	uniform	52

(c) Package

foreground name	unit	qty 1	qty 2	Min	Max	distrib	# of uses
IC1 frontend	mm^2 die	5.52	5.52	-	-	fixed	1
IC2 frontend	mm^2 die	5.3095	5.3095	-	-	fixed	1
IC1 backend	g	0	0	-	-	fixed	1
IC2 backend	g	0.0403	0.0403	-	-	fixed	1

(d) ICs

foreground name	unit	qty 1	qty 2	Min	Max	distrib	# of uses
battery connector	g	0.08	0.08	-	-	fixed	1
antenna	g	0.0168	0.0168	-	-	fixed	1
SMD capacitors 0603	g	0.00462	0.00462	÷2	x2	triangle	1
SMD capacitors 1005	g	0.0032	0.0032	÷2	x2	triangle	1
SMD capacitors 1608	g	0.0243	0.0243	÷2	x2	triangle	1
SMD resistor 0603	g	0.00105	0.00105	÷2	x2	triangle	1
SMD resistor 1005	g	0.0016	0.0016	÷2	x2	triangle	1
SMD resistor 1608	g	0.004	0.004	÷2	x2	triangle	1
SMD soldering - calculated from EIME table	g	0.0395	0.0395	÷2	x2	triangle	1
SMD soldering - visually estimated	g	0.02	0.02	÷2	x2	uniform	1
PWB	cm^2	5.074963	5.074963	-	-	fixed	1

(e) electronics

foreground name	unit	qty 1	qty 2	Min	Max	distrib	# of uses
zinc powder	g	0.0319	0.0319	-10%	+10%	triangle	1
silver oxide powder	g	0.1197	0.1197	-10%	+10%	triangle	1
external protection - up	g	0.11	0.11	-10%	+10%	triangle	1
external protection - down	g	0.087	0.087	-10%	+10%	triangle	1
other plastic element (membrane)	g	0.037078	0.037078	-10%	+10%	triangle	1
manufacturing energy	Wh	4.34	4.34	x1	x1.5	uniform	1

(f) battery

foreground name	dist. (km)	unit	qty 1	qty 2	Min	Max	distrib	# of uses
Intra-Asia travels (truck)	1000	g	0.5	0.5	÷2	x2	uniform	1
Intra-Asia travels (train)	1000	g	0.5	0.5	÷2	x2	uniform	1
Intra-Asia travels (boat)	2000	g	0.5	0.5	÷2	x2	uniform	1
Asia to US port	10000	g	0.5	0.5	-20%	+20%	triangle	1
US port to US production lines	2500	g	0.5	0.5	÷2	x2	triangle	1
US production lines to US port (CGM+needle)	2500	g	50.5	10.5	÷2	x2	triangle	1
US production lines to US port (applicator)	2500	g	0	52.5	÷2	x2	triangle	52
US port to England port (CGM+needle)	6000	g	50.5	10.5	-20%	+20%	triangle	1
US port to England port (applicator)	6000	g	0	52.5	-20%	+20%	triangle	52
England port to England manufacturing facility(CGM+needle)	150	g	50.5	10.5	-20%	+20%	triangle	1
England port to England manufacturing facility(applicator)	150	g	0	52.5	-20%	+20%	triangle	52
England mfg facility to Wisbaden (CGM+needle)	850	g	50.5	15.5	x1	+20%	triangle	1
England mfg facility to Wisbaden (applicator)	850	g	0	52.5	x1	+20%	triangle	52
Wisbaden to delivery warehouse (Merkala)(CGM+needle)	480	g	64.5	25.5	x1	+20%	triangle	1
Wisbaden to delivery warehouse (Merkala)(applicator)	480	g	0	62.5	x1	+20%	triangle	52
Delivery warehouse to end-user (BE)(CGM+needle)	250	g	84.5	45.5	x1	+20%	triangle	1
Delivery warehouse to end-user (BE)(applicator)	250	g	0	82.5	x1	+20%	triangle	52

(g) transport

Table B.5: Values of all the flows for strategy 2 with values from strategy 1 for reference. Changes are represented in blue

Added flow	**Ecoinvent (EI) activity name**	**loc**
hard needle plastic cover	*UCLouvain custom*: process_moulded_ABS	GLO
applicator box	market for corrugated board box	RER
whole package applicator	market for corrugated board box	RER
US production lines to US port (applicator)	transport, freight, lorry, all sizes, EURO6 to generic market for transport, freight, lorry, unspecified	RoW
US port to England port (applicator)	transport, freight, sea, container ship	GLO
England port to England manufacturing facility(applicator)	market group for transport, freight, light commercial vehicle	RER
England mfg facility to Wisbaden (applicator)	transport, freight, lorry, all sizes, EURO6 to generic market for transport, freight, lorry, unspecified	RER
Wisbaden to delivery warehouse (Merkala)(applicator)	market group for transport, freight, light commercial vehicle	RER
Delivery warehouse to end-user (BE)(applicator)	market group for transport, freight, light commercial vehicle	RER

Table B.6: EI activities chosen for added flows in strategy 2

B.5 Strategy 3

battery	name	standard capacity (mAh)	standard discharge current (μA)	diameter (mm)	height (mm)	weight (g)
reference	SR926W	28	50	6.8	2.6	0.39
new (strategy 3)	SR927W	60	110	9.5	2.7	0.75

Table B.7: Comparison of the batteries with reference case

The new values of battery flows were determined with the same equations (B.1) as strategy 0 :

	ref	strat 0	scaling	scaled flow
aire_up [mm^2]	91.86	151.46	1.65	external protection up
aire_down [mm^2]	36.32	70.88	1.95	external protection down, other plastic element
powder weight [g]	0.1516	0.3388	2.23	zinc powder, silver oxide powder
battery capacity [mAh]	28	60	$\frac{60}{28}$	manufacturing energy

Table B.8: scaling for battery components

Furthermore, since the new lifetime of the CGM is 39 days, only 9.36 sensors/year are needed instead of 26. CGMs from strategy 3 are thus used 26/9.36 = 2.78 times more than the reference ones.

foreground name	**unit**	**qty 2**	**qty 3**	**Min**	**Max**	**distrib**	**# of uses**
blue plastic	g	51.1656	51.1656	-10%	+10%	uniform	52
dark grey plastic	g	0	0	-	-	fixed	52
lighter grey plastic	g	0	0	-	-	fixed	52
light grey plastic	g	0	0	-	-	fixed	52
transparent plastic	g	0	0	-	-	fixed	52
inner plastic part 1	g	0	0	-	-	fixed	52
inner plastic part 2	g	0	0	-	-	fixed	52
inner plastic part 3	g	0	0	-	-	fixed	52
inner plastic part 4	g	0	0	-	-	fixed	52
spring	g	1.31	1.31	-	-	fixed	52
hard needle	g	0.049	0.049	-	-	fixed	2.78
hard needle plastic cover	g	5	5	1	10	uniform	2.78

(a) Applicator subassembly

foreground name	unit	qty 2	qty 3	Min	Max	distrib	# of uses
sticker	g	0.17	0.17	-	-	fixed	2.78
casing top	g	0.6	0.6	-	-	fixed	2.78
casing bottom	g	1.08	1.08	-	-	fixed	2.78
transparent soft plastic	g	0.085	0.085	-	-	fixed	2.78
opaque hard plastic	g	0.11	0.11	-	-	fixed	2.78
amperometric transdermal glucose biosensor	unit	1	1	-	-	fixed	2.78

(b) CGM

foreground name	unit	qty 2	qty 3	Min	Max	distrib	# of uses
yellow box (CGM+needle)	g	9.58	9.58	-20%	+20%	uniform	2.78
applicator box	g	9.58	9.58	-10%	+30%	uniform	52
instructions set	g	4.02	4.02	-	-	fixed	2.64
protective foil	g	0	0	-	-	fixed	1
whole package (CGM+needle)	g	43.775	43.775	-20%	+20%	uniform	2.78
whole package applicator	g	43.775	43.775	-10%	+30%	uniform	52

(c) Package

foreground name	unit	qty 2	qty 3	Min	Max	distrib	# of uses
IC1 frontend	mm^2 die	5.52	5.52	-	-	fixed	2.78
IC2 frontend	mm^2 die	5.3095	5.3095	-	-	fixed	2.78
IC1 backend	g	0	0	-	-	fixed	2.78
IC2 backend	g	0.0403	0.0403	-	-	fixed	2.78

(d) ICs

foreground name	unit	qty 2	qty 3	Min	Max	distrib	# of uses
battery connector	g	0.08	0.156	-	-	fixed	2.78
antenna	g	0.0168	0.0168	-	-	fixed	2.78
SMD capacitors 0603	g	0.00462	0.00462	÷2	x2	triangle	2.78
SMD capacitors 1005	g	0.0032	0.0032	÷2	x2	triangle	2.78
SMD capacitors 1608	g	0.0243	0.0243	÷2	x2	triangle	2.78
SMD resistor 0603	g	0.00105	0.00105	÷2	x2	triangle	2.78
SMD resistor 1005	g	0.0016	0.0016	÷2	x2	triangle	2.78
SMD resistor 1608	g	0.004	0.004	÷2	x2	triangle	2.78
SMD soldering - calculated from EIME table	g	0.0395	0.0395	÷2	x2	triangle	2.78
SMD soldering - visually estimated	g	0.02	0.02	÷2	x2	uniform	2.78
PWB	cm^2	5.074963	5.074963	-	-	fixed	2.78

(e) electronics

foreground name	unit	qty 2	qty 3	Min	Max	distrib	# of uses
zinc powder	g	0.0319	0.071	-10%	+10%	triangle	2.78
silver oxide powder	g	0.1197	0.267	-10%	+10%	triangle	2.78
external protection - up	g	0.11	0.1815	-10%	+10%	triangle	2.78
external protection - down	g	0.087	0.1697	-10%	+10%	triangle	2.78
other plastic element (membrane)	g	0.037078	0.06	-10%	+10%	triangle	2.78
manufacturing energy	Wh	4.34	9.3	x1	x1.5	uniform	2.78

(f) battery

foreground name	dist. (km)	unit	qty 2	qty 3	Min	Max	distrib	# of uses
Intra-Asia travels (truck)	1000	g	0.5	0.5	÷2	x2	uniform	2.78
Intra-Asia travels (train)	1000	g	0.5	0.5	÷2	x2	uniform	2.78
Intra-Asia travels (boat)	2000	g	0.5	0.5	÷2	x2	uniform	2.78
Asia to US port	10000	g	0.5	0.5	-20%	+20%	triangle	2.78
US port to US production lines	2500	g	0.5	0.5	÷2	x2	triangle	2.78
US production lines to US port (CGM+needle)	2500	g	10.5	10.5	÷2	x2	triangle	2.78
US production lines to US port (applicator)	2500	g	52.5	52.5	÷2	x2	triangle	52
US port to England port (CGM+needle)	6000	g	10.5	10.5	-20%	+20%	triangle	2.78
US port to England port (applicator)	6000	g	52.5	52.5	-20%	+20%	triangle	52
England port to England manufacturing facility(CGM+needle)	150	g	10.5	10.5	-20%	+20%	triangle	2.78
England port to England manufacturing facility(applicator)	150	g	52.5	52.5	-20%	+20%	triangle	52
England mfg facility to Wisbaden (CGM+needle)	850	g	15.5	15.5	x1	+20%	triangle	2.78
England mfg facility to Wisbaden (applicator)	850	g	52.5	52.5	x1	+20%	triangle	52
Wisbaden to delivery warehouse (Merkala)(CGM+needle)	480	g	25.5	25.5	x1	+20%	triangle	2.78
Wisbaden to delivery warehouse (Merkala)(applicator)	480	g	62.5	62.5	x1	+20%	triangle	52
Delivery warehouse to end-user (BE)(CGM+needle)	250	g	45.5	45.5	x1	+20%	triangle	2.78
Delivery warehouse to end-user (BE)(applicator)	250	g	82.5	82.5	x1	+20%	triangle	52

(g) transport

Table B.9: Values of all the flows for strategy 3 with values from strategy 2 for reference. Changes are represented in blue

B.6 Strategy 4

foreground name	unit	qty 2	qty 4	Min	Max	distrib	# of uses
blue plastic	g	51.1656	51.1656	-10%	+10%	uniform	52
dark grey plastic	g	0	0	-	-	fixed	52
lighter grey plastic	g	0	0	-	-	fixed	52
light grey plastic	g	0	0	-	-	fixed	52
transparent plastic	g	0	0	-	-	fixed	52
inner plastic part 1	g	0	0	-	-	fixed	52
inner plastic part 2	g	0	0	-	-	fixed	52
inner plastic part 3	g	0	0	-	-	fixed	52
inner plastic part 4	g	0	0	-	-	fixed	52
spring	g	1.31	1.31	-	-	fixed	52
hard needle	g	0.049	0.049	-	-	fixed	1
hard needle plastic cover	g	5	5	1	10	uniform	1

(a) Applicator subassembly

foreground name	unit	qty 2	qty 4	Min	Max	distrib	# of uses
sticker	g	0.17	0.17	-	-	fixed	1
casing top (ICs module)	g	0.6	0.468	-20%	+20%	uniform	52
casing top (battery + needle module)	g	0	0.312	-20%	+20%	uniform	1
casing bottom (ICs module)	g	1.08	0.8424	-20%	+20%	uniform	52
casing bottom (battery + needle module)	g	0	0.5616	-20%	+20%	uniform	1
transparent soft plastic	g	0.085	0.085	-	-	fixed	1
opaque hard plastic	g	0.11	0.11	-	-	fixed	1
amperometric transdermal glucose biosensor	unit	1	1	-	-	fixed	1

(b) CGM

foreground name	unit	qty 2	qty 4	Min	Max	distrib	# of uses
yellow box (CGM+needle)	g	9.58	9.58	-20%	+20%	uniform	1
applicator box	g	9.58	9.58	-10%	+30%	uniform	52
instructions set	g	4.02	4.02	-	-	fixed	0.98
protective foil	g	0	0	-	-	fixed	1
whole package (CGM+needle)	g	43.775	43.775	-20%	+20%	uniform	1
whole package applicator	g	43.775	43.775	-10%	+30%	uniform	52

(c) Package

foreground name	unit	qty 2	qty 4	Min	Max	distrib	# of uses
IC1 frontend	mm^2 die	5.52	5.52	-	-	fixed	1
IC2 frontend	mm^2 die	5.3095	5.3095	-	-	fixed	1
IC1 backend	g	0	0	-	-	fixed	1
IC2 backend	g	0.0403	0.0403	-	-	fixed	1

(d) ICs

foreground name	unit	qty 2	qty 4	Min	Max	distrib	# of uses
battery connector	g	0.08	0.08	-	-	fixed	1
antenna	g	0.0168	0.0168	-	-	fixed	1
SMD capacitors 0603	g	0.00462	0.00462	÷2	x2	triangle	1
SMD capacitors 1005	g	0.0032	0.0032	÷2	x2	triangle	1
SMD capacitors 1608	g	0.0243	0.0243	÷2	x2	triangle	1
SMD resistor 0603	g	0.00105	0.00105	÷2	x2	triangle	1
SMD resistor 1005	g	0.0016	0.0016	÷2	x2	triangle	1
SMD resistor 1608	g	0.004	0.004	÷2	x2	triangle	1
SMD soldering - calculated from EIME table	g	0.0395	0.0395	÷2	x2	triangle	1
SMD soldering - visually estimated	g	0.02	0.02	÷2	x3	uniform	1
PWB (ICs module)	cm^2	5.074963	3.3495	-10%	+10%	uniform	52
PWB (battery + needle module)	cm^2	0	2.233	-10%	+10%	uniform	1
PWB connector male	g	0	0.0083	-	-	fixed	1
PWB connector female	g	0	0.015	-	-	fixed	52

(e) electronics

foreground name	unit	qty 2	qty 4	Min	Max	distrib	# of uses
zinc powder	g	0.0319	0.0319	-10%	+10%	triangle	1
silver oxide powder	g	0.1197	0.1197	-10%	+10%	triangle	1
external protection - up	g	0.11	0.11	-10%	+10%	triangle	1
external protection - down	g	0.087	0.087	-10%	+10%	triangle	1
other plastic element (membrane)	g	0.037078	0.037078	-10%	+10%	triangle	1
manufacturing energy	Wh	4.34	4.34	x1	x1.5	uniform	1

(f) battery

foreground name	dist. (km)	unit	qty 2	qty 4	Min	Max	distrib	# of uses
Intra-Asia travels (truck) (battery)	1000	g	0.5	0.4	÷2	x2	uniform	1
Intra-Asia travels (truck) (ICs+electronics)	1000	g	0	0.1	÷2	x2	uniform	52
Intra-Asia travels (train) (battery)	1000	g	0.5	0.4	÷2	x2	uniform	1
Intra-Asia travels (train) (ICs+electronics)	1000	g	0	0.1	÷2	x2	uniform	52
Intra-Asia travels (boat) (battery)	2000	g	0.5	0.4	÷2	x2	uniform	1
Intra-Asia travels (boat) (ICs+electronics)	2000	g	0	0.1	÷2	x2	uniform	52
Asia to US port (battery)	10000	g	0.5	0.4	-20%	+20%	triangle	1
Asia to US port (ICs+electronics)	10000	g	0	0.1	-20%	+20%	triangle	52
US port to US production lines (battery)	2500	g	0.5	0.4	÷2	x2	triangle	1
US port to US production lines (ICs+electronics)	2500	g	0	0.1	÷2	x2	triangle	52
US production lines to US port ((battery + needle module)+needle)	2500	g	10.5	4.4	÷2	x2	triangle	1
US production lines to US port (applicator+ICs module)	2500	g	52.5	58.6	÷2	x2	triangle	52
US port to England port ((battery + needle module)+needle)	6000	g	10.5	4.4	-20%	+20%	triangle	1
US port to England port (applicator+ICs module)	6000	g	52.5	58.6	-20%	+20%	triangle	52
England port to England manufacturing facility ((battery + needle module)+needle)	150	g	10.5	4.4	-20%	+20%	triangle	1
England port to England manufacturing facility (applicator+ICs module)	150	g	52.5	58.6	-20%	+20%	triangle	52
England mfg facility to Wisbaden ((battery + needle module)+needle)	850	g	15.5	9.4	x1	+20%	triangle	1
England mfg facility to Wisbaden (applicator+ICs module)	850	g	52.5	58.6	x1	+20%	triangle	52
Wisbaden to delivery warehouse (Merkala)((battery + needle module)+needle)	480	g	25.5	19.4	x1	+20%	triangle	1
Wisbaden to delivery warehouse (Merkala) (applicator+ICs module)	480	g	62.5	68.6	x1	+20%	triangle	52
Delivery warehouse to end-user (BE)((battery + needle module)+needle)	250	g	45.5	39.4	x1	+20%	triangle	1
Delivery warehouse to end-user (BE)(applicator+ICs module)	250	g	82.5	88.6	x1	+20%	triangle	52

(g) transport

Table B.10: Values of all the flows for strategy 4 with values from strategy 2 for reference. Changes are represented in blue

Added flow	**EI activity name**	**loc**
casing top (battery + needle module)	*UCLouvain custom*: process_moulded_ABS	GLO
casing bottom (battery + needle module)	*UCLouvain custom*: process_moulded_ABS	GLO
PWB (battery + needle module)	printed wiring board production, for surface mounting, Pb free surface	GLO
PWB connector male	market for electric connector, peripheral component interconnect buss	GLO
PWB connector female	market for electric connector, peripheral component interconnect buss	GLO
Intra-Asia travels (truck) (ICs+electronics)	transport, freight, lorry, all sizes, EURO5 to generic market for transport, freight, lorry, unspecified	RoW
Intra-Asia travels (train) (ICs+electronics	transport, freight train, diesel	CN
Intra-Asia travels (boat) (ICs+electronics)	transport, freight, sea, container ship	GLO
Asia to US port (ICs+electronics)	transport, freight, sea, container ship	GLO
US port to US production lines (ICs+electronics)	transport, freight, lorry, all sizes, EURO6 to generic market for transport, freight, lorry, unspecified	RoW

Table B.11: EI activities chosen for added flows in strategy 4

B.7 Strategy 5

battery	name	nominal voltage	standard capacity (mAh)	standard discharge current (μA)	diameter (mm)	height (mm)	weight (g)
reference	SR926W	1.55	28	50	6.8	2.6	0.39
new (strategy 5)	NiMH	1.2	74	?	11.5	6	≈ 2

Table B.12: Comparison of the batteries with reference case

foreground name	**unit**	**qty 2**	**qty 5**	**Min**	**Max**	**distrib**	**# of uses**
blue plastic	g	51.1656	51.1656	-10%	+10%	uniform	52
dark grey plastic	g	0	0	-	-	fixed	52
lighter grey plastic	g	0	0	-	-	fixed	52
light grey plastic	g	0	0	-	-	fixed	52
transparent plastic	g	0	0	-	-	fixed	52
inner plastic part 1	g	0	0	-	-	fixed	52
inner plastic part 2	g	0	0	-	-	fixed	52
inner plastic part 3	g	0	0	-	-	fixed	52
inner plastic part 4	g	0	0	-	-	fixed	52
spring	g	1.31	1.31	-	-	fixed	52
hard needle	g	0.049	0.049	-	-	fixed	1
hard needle plastic cover	g	5	5	1	10	uniform	1

(a) Applicator subassembly

foreground name	**unit**	**qty 2**	**qty 5**	**Min**	**Max**	**distrib**	**# of uses**
sticker	g	0.17	0.17	-	-	fixed	1
casing top	g	0.6	0.69	-	-	fixed	26
casing bottom	g	1.08	1.24	-	-	fixed	26
charger plastic casing	g	0	50	20	70	uniform	52
transparent soft plastic	g	0.085	0.085	-	-	fixed	1
opaque hard plastic	g	0.11	0.11	-	-	fixed	1
amperometric transdermal glucose biosensor	unit	1	1	-	-	fixed	1

(b) CGM

foreground name	unit	qty 2	qty 5	Min	Max	distrib	# of uses
yellow box	g	9.58	55.8	x2/3	x4/3	uniform	52
instructions set	g	4.02	4.02	-	-	fixed	52
protective foil	g	0	0	-	-	fixed	1
whole package	g	43.775	255	x2/3	x4/3	uniform	52

(c) Package

foreground name	unit	qty 2	qty 5	Min	Max	distrib	# of uses
IC1 frontend	mm^2 die	5.52	5.52	-	-	fixed	26
IC2 frontend	mm^2 die	5.3095	5.3095	-	-	fixed	26
IC3 frontend RX	mm^2 die	0	1.5	1	2	uniform	26
IC4 frontend TX	mm^2 die	0	2.25	1.5	3	uniform	52
IC1 backend	g	0	0	-	-	fixed	26
IC2 backend	g	0.0403	0.0403	-	-	fixed	26
IC3 backend RX	g	0	0.00756	-20%	+20%	triangle	26
IC4 backend TX	g	0	0.01133	-20%	+20%	triangle	52

(d) ICs

foreground name	unit	qty 2	qty 5	Min	Max	distrib	# of uses
battery connector	g	0.08	0.156	-	-	fixed	26
antenna	g	0.0168	0.0168	-	-	fixed	26
SMD capacitors 0603	g	0.00462	0.00462	÷2	x2	triangle	26
SMD capacitors 1005	g	0.0032	0.0032	÷2	x2	triangle	26
SMD capacitors 1608	g	0.0243	0.0243	÷2	x2	triangle	26
SMD capacitors TX + RX	g	0	0.0458	-	-	fixed	26
SMD resistor 0603	g	0.00105	0.00105	÷2	x2	triangle	26
SMD resistor 1005	g	0.0016	0.0016	÷2	x2	triangle	26
SMD resistor 1608	g	0.004	0.004	÷2	x2	triangle	26
SMD resitors TX + RX	g	0	0.0013	-	-	fixed	26
SMD soldering - calculated from EIME table	g	0.0395	0.0395	÷2	x2	triangle	26
SMD soldering - visually estimated	g	0.02	0.07	÷2	x2	uniform	26
PWB	cm^2	5.074963	5.074963	-	-	fixed	26
PWB TX	cm^2	0	5.074963	÷2	x2	triangle	52
MOSFET TX	g	0	0.008	-	-	fixed	52
ferrite RX	g	0	0.5	x2/3	x4/3	uniform	26
ferrite TX	g	0	1.25	x2/3	x4/3	uniform	52
antenna RX	g	0	0.2	÷2	x2	triangle	26
antenna TX	g	0	0.55	÷1.5	x1.5	triangle	52
USB socket TX	g	0	0.209	-	-	fixed	52

(e) electronics

foreground name	unit	qty 2	qty 5	Min	Max	distrib	# of uses
zinc powder	g	0.0319	0	-10%	+10%	triangle	1
silver oxide powder	g	0.1197	0	-10%	+10%	triangle	1
external protection - up	g	0.11	0	-10%	+10%	triangle	1
external protection - down	g	0.087	0	-10%	+10%	triangle	1
other plastic element (membrane)	g	0.037078	0	-10%	+10%	triangle	1
manufacturing energy	Wh	4.34	0	x1	x1.5	uniform	1
NiMH battery	g	0	2	-	-	fixed	26
NiMH recharge energy	Wh	0	0.0888	-	-	fixed	1

(f) battery

foreground name	dist. (km)	unit	qty 2	qty 5	Min	Max	distrib	# of uses
Intra-Asia travels (truck)	1000	g	0.5	2.1	÷2	x2	uniform	52
Intra-Asia travels (train)	1000	g	0.5	2.1	÷2	x2	uniform	52
Intra-Asia travels (boat)	2000	g	0.5	2.1	÷2	x2	uniform	52
Asia to US port	10000	g	0.5	2.1	-20%	+20%	triangle	52
US port to US production lines	2500	g	0.5	2.1	÷2	x2	triangle	52
US production lines to US port	2500	g	52.5	57.9	÷2	x2	triangle	52
US port to England port	6000	g	52.5	57.9	-20%	+20%	triangle	52
England port to England manufacturing facility	150	g	52.5	57.9	-20%	+20%	triangle	52
England mfg facility to Wisbaden	850	g	52.5	317.9	x1	+20%	triangle	52
Wisbaden to delivery warehouse (Merkala)	480	g	62.5	377.7	x1	+20%	triangle	52
Delivery warehouse to end-user (BE)	250	g	82.5	437.7	x1	+20%	triangle	52

(g) transport

Table B.13: Values of all the flows for strategy 5 with values from strategy 2 for reference. Changes are represented in blue

Added flow	EI activity name	loc
charger plastic casing	*UCLouvain custom*: process_moulded_ABS	GLO
IC3 frontend RX	*UCLouvain custom*: process_IC_frontend	GLO
IC4 frontend TX	*UCLouvain custom*: process_IC_frontend	GLO
IC3 frontend RX	*UCLouvain custom*: process_IC_backend	GLO
IC4 frontend TX	*UCLouvain custom*: process_IC_backend	GLO
SMD capacitors TX + RX	market for capacitor, for surface-mounting	GLO
SMD resistors TX + RX	market for resistor, surface-mounted	GLO
PWB TX	printed wiring board production, for surface mounting, Pb free surface	GLO
MOSFET TX	market for transistor, surface-mounted	GLO
ferrite RX	market for ferrite	GLO
ferrite TX	market for ferrite	GLO
antenna RX	*UCLouvain custom*: process_antenna	GLO
antenna TX	*UCLouvain custom*: process_antenna	GLO
USB socket TX	market for electric connector, peripheral type buss	GLO
NiMH battery	market for battery, NiMH, rechargeable, prismatic	GLO
NiMH recharge energy	market for electricity, low voltage	BE

Table B.14: EI activities chosen for added flows in strategy 5

Bibliography

[1] *Diabetes Facts and Figures | International Diabetes Federation*. URL: https://idf.org/about-diabetes/diabetes-facts-figures/ (visited on 09/04/2025).

[2] *IDF Diabetes Atlas 2025*. en-GB. URL: https://diabetesatlas.org/resources/idf-diabetes-atlas-2025/ (visited on 15/04/2025).

[3] David Olczuk and Ronny Priefer. 'A history of continuous glucose monitors (CGMs) in self-monitoring of diabetes mellitus'. In: *Diabetes & Metabolic Syndrome: Clinical Research & Reviews* 12.2 (Apr. 2018), pp. 181–187. ISSN: 1871-4021. DOI: 10.1016/j.dsx.2017.09.005. URL: https://www.sciencedirect.com/science/article/pii/S187140211730303X (visited on 07/04/2025).

[4] Olesya Didyuk et al. 'Continuous Glucose Monitoring Devices: Past, Present, and Future Focus on the History and Evolution of Technological Innovation'. EN. In: *Journal of Diabetes Science and Technology* 15.3 (May 2021). Publisher: SAGE Publications Inc, pp. 676–683. ISSN: 1932-2968. DOI: 10.1177/1932296819899394. URL: https://doi.org/10.1177/1932296819899394 (visited on 21/03/2025).

[5] Sebastian F Petry et al. 'Quantification of Different Types of Waste and Batteries Associated With the Widespread Usage of Continuous Glucose Monitoring Systems'. EN. In: *Journal of Diabetes Science and Technology* (Dec. 2024). Publisher: SAGE Publications Inc, p. 19322968241305161. ISSN: 1932-2968. DOI: 10.1177/19322968241305161. URL: https://doi.org/10.1177/19322968241305161 (visited on 21/03/2025).

[6] Rodolfo J. Galindo and Grazia Aleppo. 'Continuous glucose monitoring: The achievement of 100 years of innovation in diabetes technology'. eng. In: *Diabetes Research and Clinical Practice* 170 (Dec. 2020), p. 108502. ISSN: 1872-8227. DOI: 10.1016/j.diabres.2020.108502.

[7] Clara Bender et al. 'The History, Evolution and Future of Continuous Glucose Monitoring (CGM)'. en. In: *Diabetology* 6.3 (Mar. 2025). Number: 3 Publisher: Multidisciplinary Digital Publishing Institute, p. 17. ISSN: 2673-4540. DOI: 10.3390/diabetology6030017. URL: https://www.mdpi.com/2673-4540/6/3/17 (visited on 21/03/2025).

[8] *1Q24 Diabetes Technology Industry Roundup – CGM sales of $2.7 billion, rising 23%; record insulin pump sales of $1.1 billion, rising 18% | Close Concerns*. URL: https://www.closeconcerns.com/knowledgebase/r/9b39b3ad (visited on 21/03/2025).

[9] Yiqun Liu et al. 'Transdermal amperometric biosensors for continuous glucose monitoring in diabetes'. In: *Talanta* 253 (Feb. 2023), p. 124033. ISSN: 0039-9140. DOI: 10.1016/j.talanta.2022.124033. URL: https://www.sciencedirect.com/science/article/pii/S0039914022008293 (visited on 03/03/2025).

[10] Lutz Heinemann and Edward Krisiunas. 'Diabetes Technology and Waste: A Complex Problem Piling Up!' In: *Journal of Diabetes Science and Technology* 13.5 (Mar. 2019), pp. 815–816. ISSN: 1932-2968. DOI: 10.1177/1932296819836395. URL: https://www.ncbi.nlm.nih.gov/pmc/articles/PMC6955464/ (visited on 09/04/2025).

[11] Javier Cifuentes-Faura. ‘European Union policies and their role in combating climate change over the years’. en. In: *Air Quality, Atmosphere & Health* 15.8 (Aug. 2022), pp. 1333–1340. ISSN: 1873-9326. DOI: 10.1007/s11869-022-01156-5. URL: https://doi.org/10.1007/s11869-022-01156-5 (visited on 10/04/2025).

[12] Manfred Lenzen et al. ‘The environmental footprint of health care: a global assessment’. English. In: *The Lancet Planetary Health* 4.7 (July 2020). Publisher: Elsevier, e271–e279. ISSN: 2542-5196. DOI: 10.1016/S2542-5196(20)30121-2. URL: https://www.thelancet.com/journals/lanplh/article/PIIS2542-5196(20)30121-2/fulltext#fig3 (visited on 07/04/2025).

[13] *The European Green Deal - European Commission*. URL: https://commission.europa.eu/strategy-and-policy/priorities-2019-2024/european-green-deal_en (visited on 22/04/2025).

[14] *Circular economy action plan - European Commission*. URL: https://environment.ec.europa.eu/strategy/circular-economy-action-plan_en (visited on 22/04/2025).

[15] *Ecodesign for Sustainable Products Regulation - European Commission*. URL: https://commission.europa.eu/energy-climate-change-environment/standards-tools-and-labels/products-labelling-rules-and-requirements/ecodesign-sustainable-products-regulation_en (visited on 22/04/2025).

[16] *eco-design — European Environment Agency*. URL: https://www.eea.europa.eu/help/glossary/eea-glossary/eco-design (visited on 05/05/2025).

[17] Michael Z. Hauschild et al., eds. *Life Cycle Assessment: Theory and Practice*. en. Cham: Springer International Publishing, 2018. ISBN: 978-3-319-56474-6 978-3-319-56475-3. DOI: 10.1007/978-3-319-56475-3. URL: https://link.springer.com/10.1007/978-3-319-56475-3 (visited on 09/04/2025).

[18] Irl B. Hirsch. ‘Introduction: History of Glucose Monitoring’. In: *Compendia* 2018.1 (Aug. 2018), p. 1. ISSN: 2771-6872. DOI: 10.2337/db20181-1. URL: https://doi.org/10.2337/db20181-1 (visited on 21/03/2025).

[19] *Eversense 365 Receives FDA Clearance: The World’s First One Year CGM*. en. URL: https://www.senseonics.com/investor-relations/news-releases/2024/09-17-2024-120118174 (visited on 25/04/2025).

[20] Srivastava Rahul et al. ‘FreeStyle® Libre™ Flash Glucose Monitoring System: A Novel Diagnostic Technique for Monitoring Diabetes’. en. In: *International Journal of Contemporary Medicine, Surgery and Radiology* 3.3 (Sept. 2018). ISSN: 25654802, 25654810. DOI: 10.21276/ijcmsr.2018.3.3.11. URL: https://www.ijcmsr.com/uploads/1/0/2/7/102704056/ijcmsr_120_v2_1.pdf (visited on 03/03/2025).

[21] Jayachidambaram Ambalavanan et al. ‘Diabetes technology: A primer for clinicians’. en. In: *Cleveland Clinic Journal of Medicine* 91.6 (June 2024). Publisher: Cleveland Clinic Journal of Medicine Section: Review, pp. 353–360. ISSN: 0891-1150, 1939-2869. DOI: 10.3949/ccjm.91a.23073. URL: https://www.ccjm.org/content/91/6/353 (visited on 03/03/2025).

[22] *Everything you need to know about the Freestyle Libre 2 System*. URL: https://www.freestylelibre.com.au/media/pdf-downloads/13367_FSL_Tips_Tricks_Booklet_Updated_A5_v7B.pdf?srsltid=AfmBOorScU5K4MfbedSiaqOVJO_9A-6TZfB75_YNcNaofQUTWtlXrCob (visited on 19/04/2025).

[23] Augustin Wattiez et al. *Exploring the Direct and Indirect Environmental Impacts of Mobile Health A Case Study on Continuous Glucose Monitoring*.

[24] Mohammad Mansour et al. 'Wearable devices for glucose monitoring: A review of state-of-the-art technologies and emerging trends'. In: *Alexandria Engineering Journal* 89 (Feb. 2024), pp. 224–243. ISSN: 1110-0168. DOI: 10.1016/j.aej.2024.01.021. URL: https://www.sciencedirect.com/science/article/pii/S1110016824000231 (visited on 03/03/2025).

[25] Ali Esmaeilian et al. 'Innovations in Self-Powered glucose Biosensors: From energy harvesting to Continuous, Non-Invasive monitoring'. In: *Inorganic Chemistry Communications* 174 (Apr. 2025), p. 114076. ISSN: 1387-7003. DOI: 10.1016/j.inoche.2025.114076. URL: https://www.sciencedirect.com/science/article/pii/S138770032500190X (visited on 04/03/2025).

[26] Udo Hoss et al. 'Analyte Sensors and Methods of Making and Using the Same'. US20170188908A1. July 2017. URL: https://patents.google.com/patent/US20170188908A1/en?oq=US2017188908A1 (visited on 07/03/2025).

[27] Federico Ribet et al. 'Real-time intradermal continuous glucose monitoring using a minimally invasive microneedle-based system'. en. In: *Biomedical Microdevices* 20.4 (Dec. 2018), p. 101. ISSN: 1572-8781. DOI: 10.1007/s10544-018-0349-6. URL: https://doi.org/10.1007/s10544-018-0349-6 (visited on 03/03/2025).

[28] Wanying Chen et al. 'An Individually Addressable Microneedle Array for Continuous Real-Time Monitoring of Glucose in Interstitial Fluid'. In: *2024 IEEE SENSORS*. ISSN: 2168-9229. Oct. 2024, pp. 1–4. DOI: 10.1109/SENSORS60989.2024.10785208. URL: https://ieeexplore.ieee.org/document/10785208 (visited on 14/05/2025).

[29] *Abbott's FreeStyle® Libre 2 iCGM Cleared in U.S. for Adults and Children with Diabetes, Achieving Highest Level of Accuracy and Performance Standards - Jun 15, 2020.* URL: https://abbott.mediaroom.com/2020-06-15-Abbotts-FreeStyle-R-Libre-2-iCGM-Cleared-in-U-S-for-Adults-and-Children-with-Diabetes-Achieving-Highest-Level-of-Accuracy-and-Performance-Standards (visited on 28/04/2025).

[30] *Libre 2 Plus Sensor.* URL: https://pro.freestyle.abbott/uk-en/freestyle-portfolio/freestyle-libre-systems/freestyle-libre-2-plus-sensor.html (visited on 28/04/2025).

[31] *Abbott's FreeStyle® Libre 3 System Receives CE Mark - Features World's Smallest, Thinnest Sensor with Best-in-Class Performance at the Same Low Cost for People with Diabetes - Sep 28, 2020.* URL: https://abbott.mediaroom.com/2020-09-28-Abbotts-FreeStyle-R-Libre-3-System-Receives-CE-Mark-Features-Worlds-Smallest-Thinnest-Sensor-with-Best-in-Class-Performance-at-the-Same-Low-Cost-for-People-with-Diabetes (visited on 28/04/2025).

[32] Shridhara Alva et al. 'Accuracy of a 14-Day Factory-Calibrated Continuous Glucose Monitoring System With Advanced Algorithm in Pediatric and Adult Population With Diabetes'. en. In: *Journal of Diabetes Science and Technology* 16.1 (Jan. 2022), pp. 70–77. ISSN: 1932-2968, 1932-2968. DOI: 10.1177/1932296820958754. URL: https://journals.sagepub.com/doi/10.1177/1932296820958754 (visited on 23/04/2025).

[33] *DexCom, Inc. - Dexcom G7 Receives FDA Clearance: The Most Accurate Continuous Glucose Monitoring System Cleared in the U.S.* URL: https://investors.dexcom.com/news/news-details/2022/Dexcom-G7-Receives-FDA-Clearance-The-Most-Accurate-Continuous-Glucose-Monitoring-System-Cleared-in-the-U.S/default.aspx (visited on 28/04/2025).

[34] *FDA Authorizes Dexcom G6 CGM - Eliminating the need for fingerstick blood testing for people with diabetes | Dexcom.* URL: https://www.dexcom.com/news/fda-authorizes-dexcom-g6 (visited on 28/04/2025).

[35] *Innovation Milestones | Medtronic*. en. Dec. 2012. URL: https://www.medtronicdiabetes.com/about-medtronic-innovation/milestone-timeline (visited on 25/04/2025).

[36] *Waste statistics*. en. URL: https://ec.europa.eu/eurostat/statistics-explained/index.php?title=Waste_statistics (visited on 10/05/2025).

[37] Mary Ann Curran. 'Overview of Goal and Scope Definition in Life Cycle Assessment'. en. In: *Goal and Scope Definition in Life Cycle Assessment*. Ed. by Mary Ann Curran. Dordrecht: Springer Netherlands, 2017, pp. 1–62. ISBN: 978-94-024-0855-3. DOI: 10.1007/978-94-024-0855-3_1. URL: https://doi.org/10.1007/978-94-024-0855-3_1 (visited on 02/05/2025).

[38] European Commission. Joint Research Centre. Institute for Environment and Sustainability. *International Reference Life Cycle Data System (ILCD) Handbook :general guide for life cycle assessment : detailed guidance*. en. LU: Publications Office, 2010. URL: https://data.europa.eu/doi/10.2788/38479 (visited on 03/05/2025).

[39] *JRC Publications Repository - Updated characterisation and normalisation factors for the Environmental Footprint 3.1 method*. URL: https://publications.jrc.ec.europa.eu/repository/handle/JRC130796 (visited on 23/04/2025).

[40] Niels Jungbluth. 'Description of life cycle impact assessment methods'. en. In: ().

[41] *ecoinvent Version 3.9.1*. URL: https://support.ecoinvent.org/ecoinvent-version-3.9.1 (visited on 10/05/2025).

[42] *Brightway LCA Software Framework — Brightway documentation*. URL: https://docs.brightway.dev/en/latest/ (visited on 10/05/2025).

[43] Steven Mitchell and Matthew Simmons. 'Devices for analyte monitoring'. en. WO2022147329A1. July 2022. URL: https://patents.google.com/patent/WO2022147329A1/fr?oq=WO2022147329A1 (visited on 10/05/2025).

[44] Michael Z. Hauschild and Mark A.J. Huijbregts, eds. *Life Cycle Impact Assessment*. en. LCA Compendium – The Complete World of Life Cycle Assessment. Dordrecht: Springer Netherlands, 2015. ISBN: 978-94-017-9743-6 978-94-017-9744-3. DOI: 10.1007/978-94-017-9744-3. URL: https://link.springer.com/10.1007/978-94-017-9744-3 (visited on 04/05/2025).

[45] *Insulin Pumps and CGMs: A Complete Guide for Diabetes Management | US MED*. URL: https://www.usmed.com/insulin-pump-and-cgm/ (visited on 14/05/2025).

[46] Mao-Sung Huang et al. 'Lancing device'. en. US8568434B2. Oct. 2013. URL: https://patents.google.com/patent/US8568434B2/en?q=(lancing+device)&oq=lancing+device&page=2 (visited on 14/05/2025).

[47] Boenmed. *Twist blood lancets technical date sheet*. URL: https://www.boenmedical.com/?products=twist-blood-lancet (visited on 14/05/2025).

[48] lui_gough. *Teardown: Abbott FreeStyle Libre 2 Flash Glucose Monitoring System Sensor*. en-US. Nov. 2024. URL: https://goughlui.com/2024/11/06/teardown-abbott-freestyle-libre-2-flash-glucose-monitoring-system-sensor/ (visited on 07/03/2025).

[49] *RF430FRL152H data sheet, product information and support | TI.com*. URL: https://www.ti.com/product/RF430FRL152H#features (visited on 07/03/2025).

[50] *EM9304 | EM Microelectronic*. URL: https://www.emmicroelectronic.com/product/standard-protocols/em9304 (visited on 23/04/2025).

[51] *DMM7510 7-1/2-Digit Graphical Sampling Multimeter*. en. URL: https://www.tek.com/en/datasheet/high-resolution-digital-multimeters/dmm7510-7-1-2-digit-graphical-sampling-multimeter (visited on 14/05/2025).

[52] Janne Janhunen et al. 'Wireless Energy Transfer Powered Wireless Sensor Node for Green IoT: Design, Implementation and Evaluation'. In: *Sensors* 19 (Dec. 2018), p. 90. DOI: 10.3390/s19010090.

[53] *How frequently does the FreeStyle Libre 2 sensor capture and store glucose readings?* en-US. URL: https://www.support.freestyle.abbott/hc/en-us/articles/14771787043863-How-frequently-does-the-FreeStyle-Libre-2-sensor-capture-and-store-glucose-readings (visited on 17/05/2025).

[54] *LibreView_Quick_Reference_Guide*. URL: https://www.freestyleprovider.abbott/content/dam/adc/freestyleprovider/countries/us-en/office-care/documents/ADC-75852_LibreView_Quick_Reference_Guide.pdf#:~:text=%EF%BF%BDDefault%20range%20is%2070-180%20mg%2FdL.%20%E2%80%A1For%20adults%20with,and%20to%20transfer%20to%20on%20ecte%20ps%20%2F%2Fdoi.org%2F10. (visited on 14/05/2025).

[55] Seiko Instruments Inc. 'Silver Oxide Battery Product Catalogue'. en. In: (2014).

[56] *Measuring Ultra-Low Power in Wireless Sensor Node Applications Using the DMM7510 7-1/2-Digit Graphical Sampling Multimeter*. en. URL: https://www.tek.com/en/documents/application-note/measuring-ultra-low-power-wireless-sensor-node-applications-using-dmm7510 (visited on 14/05/2025).

[57] *SR927 Murata Electronics | Produits de batterie | DigiKey*. URL: https://www.digikey.fr/fr/products/detail/murata-electronics/SR927/9859015?srsltid=AfmBOooidUioncYkWBJJr_ksGFSQWeHODBH2Bunh1aK8y33PHqbvaG6z (visited on 16/05/2025).

[58] *Peukert's law*. en. Page Version ID: 1259846925. Nov. 2024. URL: https://en.wikipedia.org/w/index.php?title=Peukert%27s_law&oldid=1259846925 (visited on 16/05/2025).

[59] Noshin Omar et al. 'Peukert Revisited—Critical Appraisal and Need for Modification for Lithium-Ion Batteries'. In: *Energies* 6 (Nov. 2013), pp. 5625–5641. DOI: 10.3390/en6115625.

[60] Liguang Xie et al. 'Wireless power transfer and applications to sensor networks'. In: *IEEE Wireless Communications* 20.4 (Aug. 2013). Conference Name: IEEE Wireless Communications, pp. 140–145. ISSN: 1558-0687. DOI: 10.1109/MWC.2013.6590061. URL: https://ieeexplore.ieee.org/abstract/document/6590061 (visited on 07/03/2025).

[61] Elisabetta Moisello et al. 'Recent Trends and Challenges in Near-Field Wireless Power Transfer Systems'. In: *IEEE Open Journal of the Solid-State Circuits Society* 3 (2023). Conference Name: IEEE Open Journal of the Solid-State Circuits Society, pp. 197–213. ISSN: 2644-1349. DOI: 10.1109/OJSSCS.2023.3313575. URL: https://ieeexplore.ieee.org/document/10246316 (visited on 04/03/2025).

[62] SangWook Park et al. 'Wireless power transmission characteristics for implantable devices inside a human body'. In: *2014 International Symposium on Electromagnetic Compatibility*. ISSN: 2325-0364. Sept. 2014, pp. 1190–1194. DOI: 10.1109/EMCEurope.2014.6931084. URL: https://ieeexplore.ieee.org/document/6931084/authors (visited on 12/05/2025).

[63] D.B. Ahire and Vitthal J. Gond. 'Wireless power transfer system for biomedical application: A review'. In: *2017 International Conference on Trends in Electronics and Informatics (ICEI)*. May 2017, pp. 135–140. DOI: 10.1109/ICOEI.2017.8300903. URL: https://ieeexplore.ieee.org/abstract/document/8300903 (visited on 04/03/2025).

[64] Milad Zamani and Kjeld Laursen. *Wearable and Implantable Electronic Devices*.

[65] 'Designing a Qi-compliant receiver coil for wireless power systems, Part 1'. en. In: (2012).

[66] Ishtiyaque Ahmad and B. G. Fernandes. ‘Concept of Universal USB Charger’. In: *2020 IEEE Industry Applications Society Annual Meeting*. ISSN: 2576-702X. Oct. 2020, pp. 1–5. DOI: 10.1109/IAS44978.2020.9334768. URL: https://ieeexplore.ieee.org/abstract/document/9334768?casa_token=NEIGTvaf18kAAAAA:iQPc-BR7uutxpwFhVuNPRPruXRuYP7flmuUE1E-beRZh_UYb6lMqSYXoA69PqKAtXKFA1k0-6uSSjQ (visited on 21/03/2025).

[67] *Quelle est la taille du capteur ? À quelle profondeur est-il inséré ?* fr-BE. URL: https://www.freestyle.abbott/be-fr/support/faq/question-reponse.html?q=faq-befrquestion-3 (visited on 12/05/2025).

[68] *AWCCA-36R36H08-C51-B*. en-be. URL: https://www.digikey.be/en/products/detail/abracon-llc/AWCCA-36R36H08-C51-B/5801532 (visited on 12/05/2025).

[69] *WR303050-15F5-G*. en-be. URL: https://www.digikey.be/en/products/detail/tdk-corporation/WR303050-15F5-G/4702658 (visited on 12/05/2025).

[70] S. Y. Hui. ‘Planar Wireless Charging Technology for Portable Electronic Products and Qi’. In: *Proceedings of the IEEE* 101.6 (June 2013). Conference Name: Proceedings of the IEEE, pp. 1290–1301. ISSN: 1558-2256. DOI: 10.1109/JPROC.2013.2246531. URL: https://ieeexplore.ieee.org/document/6481427 (visited on 10/03/2025).

[71] Yeru Liang et al. ‘A review of rechargeable batteries for portable electronic devices’. en. In: *InfoMat* 1.1 (2019). _eprint: https://onlinelibrary.wiley.com/doi/pdf/10.1002/inf2.12000, pp. 6–32. ISSN: 2567-3165. DOI: 10.1002/inf2.12000. URL: https://onlinelibrary.wiley.com/doi/abs/10.1002/inf2.12000 (visited on 17/04/2025).

[72] Michael J. Root. ‘Medical Device Batteries’. en. In: *Batteries for Sustainability: Selected Entries from the Encyclopedia of Sustainability Science and Technology*. Ed. by Ralph J. Brodd. New York, NY: Springer, 2013, pp. 359–392. ISBN: 978-1-4614-5791-6. DOI: 10.1007/978-1-4614-5791-6_11. URL: https://doi.org/10.1007/978-1-4614-5791-6_11 (visited on 30/03/2025).

[73] *LTC4123 Datasheet and Product Info | Analog Devices*. URL: https://www.analog.com/en/products/ltc4123.html (visited on 13/05/2025).

[74] *Varta Power One ACCU plus Blau p675 NiMH Knopfzelle | Akku für Hörgeräte | 1,2V 74mAh*. URL: https://www.akku-wechsel.de/shop/akkus/knopfzellen/varta-power-one-accu-plus-blau-p675-nimh-knopfzelle-akku-fur-horgerate-1-2v-74mah.html?___store=fr&___from_store=fr (visited on 22/05/2025).

[75] Marion Ficher et al. ‘A comprehensive review of the end-of-life modeling in LCAs of digital equipment’. In: *The International Journal of Life Cycle Assessment* 30 (Sept. 2024), pp. 20–42. DOI: 10.1007/s11367-024-02367-x.

[76] Parizad Avari et al. ‘Batteries Within Diabetes Devices: A Narrative Review on Recycling, Environmental, and Sustainability Perspective’. en. In: *Journal of Diabetes Science and Technology* (Sept. 2024). Publisher: SAGE Publications Inc, p. 19322968241278374. ISSN: 1932-2968. DOI: 10.1177/19322968241278374. URL: https://doi.org/10.1177/19322968241278374 (visited on 03/03/2025).

[77] Serenella Sala et al. ‘Environmental sustainability of European production and consumption assessed against planetary boundaries’. en. In: *Journal of Environmental Management* 269 (Sept. 2020), p. 110686. ISSN: 03014797. DOI: 10.1016/j.jenvman.2020.110686. URL: https://linkinghub.elsevier.com/retrieve/pii/S0301479720306186 (visited on 20/05/2025).

[78] *World Population Clock: 8.2 Billion People (LIVE, 2025)*. en. URL: http://www.worldometers.info/world-population/ (visited on 20/05/2025).

[79] Werner Brouwer et al. ‘When is it too expensive? Cost-effectiveness thresholds and health care decision-making’. en. In: *The European Journal of Health Economics* 20.2 (Mar. 2019), pp. 175–180. ISSN: 1618-7601. DOI: 10.1007/s10198-018-1000-4. URL: https://doi.org/10.1007/s10198-018-1000-4 (visited on 22/05/2025).

[80] Wen Wan et al. ‘Cost-effectiveness of Continuous Glucose Monitoring for Adults With Type 1 Diabetes Compared With Self-Monitoring of Blood Glucose: The DIAMOND Randomized Trial’. eng. In: *Diabetes Care* 41.6 (June 2018), pp. 1227–1234. ISSN: 1935-5548. DOI: 10.2337/dc17-1821.

[81] Steven R. Kraaijeveld. ‘Continuous Glucose Monitoring as a Matter of Justice’. en. In: *HEC Forum* 33.4 (Dec. 2021), pp. 345–370. ISSN: 1572-8498. DOI: 10.1007/s10730-020-09413-9. URL: https://doi.org/10.1007/s10730-020-09413-9 (visited on 23/05/2025).

[82] William H. Polonsky et al. ‘The Impact of Continuous Glucose Monitoring on Markers of Quality of Life in Adults With Type 1 Diabetes: Further Findings From the DIAMOND Randomized Clinical Trial’. eng. In: *Diabetes Care* 40.6 (June 2017), pp. 736–741. ISSN: 1935-5548. DOI: 10.2337/dc17-0133.

[83] *SimaPro database manual: methods library*. URL: https://www.researchgate.net/publication/284902588_SimaPro_database_manual_methods_library (visited on 03/05/2025).

UNIVERSITÉ CATHOLIQUE DE LOUVAIN
École polytechnique de Louvain
Rue Archimède, 1 bte L6.11.01, 1348 Louvain-la-Neuve, Belgique | **www.uclouvain.be/epl**